

## **INFORMATION TO USERS**

This manuscript has been reproduced from the microfilm master. UMI films the text directly from the original or copy submitted. Thus, some thesis and dissertation copies are in typewriter face, while others may be from any type of computer printer.

**The quality of this reproduction is dependent upon the quality of the copy submitted.** Broken or indistinct print, colored or poor quality illustrations and photographs, print bleedthrough, substandard margins, and improper alignment can adversely affect reproduction.

In the unlikely event that the author did not send UMI a complete manuscript and there are missing pages, these will be noted. Also, if unauthorized copyright material had to be removed, a note will indicate the deletion.

Oversize materials (e.g., maps, drawings, charts) are reproduced by sectioning the original, beginning at the upper left-hand corner and continuing from left to right in equal sections with small overlaps. Each original is also photographed in one exposure and is included in reduced form at the back of the book.

Photographs included in the original manuscript have been reproduced xerographically in this copy. Higher quality 6" x 9" black and white photographic prints are available for any photographs or illustrations appearing in this copy for an additional charge. Contact UMI directly to order.

# **UMI**

**A Bell & Howell Information Company**  
300 North Zeeb Road, Ann Arbor MI 48106-1346 USA  
313/761-4700 800/521-0600



# **Workpiece Localization: Theory, Algorithms and Implementation**

A thesis submitted to  
The Hong Kong University of Science and Technology  
in partial fulfillment of the requirements for  
the degree of Doctor of Philosophy in  
Electrical and Electronic Engineering

By

Yunxian Chu

Department of Electrical and Electronic Engineering  
The Hong Kong University of Science and Technology

March, 1999

**UMI Number: 9936673**

---

**UMI Microform 9936673**  
**Copyright 1999, by UMI Company. All rights reserved.**

**This microform edition is protected against unauthorized  
copying under Title 17, United States Code.**

---

**UMI**  
**300 North Zeeb Road**  
**Ann Arbor, MI 48103**

**Workpiece Localization:  
Theory, Algorithms and Implementation**

by

Yunxian Chu

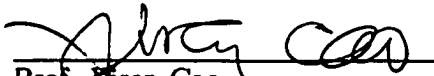
Approved by:

  
Dr. Zexiang Li

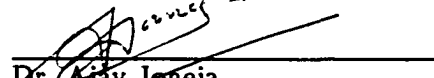
Thesis Supervisor

  
Dr. Peiyuan Qian

Thesis Examination Committee Member (Chairman)

  
Prof. Xiren Cao

Thesis Examination Committee Member

  
Dr. Ajay Joneja

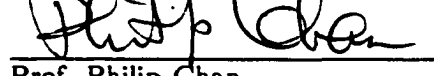
Thesis Examination Committee Member

  
Dr. Yunhui Lui

Thesis Examination Committee Member

  
Dr. Li Qiu

Thesis Examination Committee Member

  
Prof. Philip Chan

Head of Department

Department of Electrical and Electronic Engineering  
The Hong Kong University of Science and Technology

March 1999

# Workpiece Localization: Theory, Algorithms and Implementation

by

Yunxian Chu

for the Degree of Doctor of Philosophy

At The Hong Kong University of Science and Technology

in March 1999

## ABSTRACT

Workpiece localization refers to the following problem: assuming a rigid workpiece is arbitrarily fixtured to a work table, determine the position and orientation of the workpiece frame relative to some known world reference frame. In this dissertation, we develop a unified geometric theory for localization of all three types of workpieces: (1) general 3-dimensional workpieces where points from the finished surfaces fully constrain the rigid motions of the workpieces; (2) symmetric workpieces where rigid motions along the symmetry directions of the workpiece can not be determined; and (3) partially machined workpieces where points from the finished surfaces are inadequate to fully constrain the rigid motions of the workpieces. Applications of the study include workpiece setup, refixturing and dimensional inspections in a flexible manufacturing environment. The contributions of the dissertation are as follows:

First, we formulate the general 3-dimensional localization problem as a least squares problem (LSP) on the Euclidean group,  $SE(3)$ . The mathematics of LSP is analyzed in detail where necessary conditions are derived for the optimal Euclidean transformation and the optimal home surface points. We describe an iterative method for solving LSP and show how different considerations in updating the Euclidean transformations lead to different algorithms. We show the local convergence of three localization algorithms and present a method to improve the performance of these algorithms. We give simulation results showing convergence, accuracy and computational efficiency of the various geometric algorithms.

Second, we discuss the factors affecting the accuracy and reliability of the lo-

calization results. Using the F-test method in statistics, we provide an effective algorithm to analyze the reliability of workpiece localization. This allows the localization method to be applied effectively to real manufacturing tasks.

Third, we formulate the hybrid localization/envelopment problem (HLEP) as a symmetric localization problem on the homogeneous space  $SE(3)/G_0$  of the Euclidean group and a minimization problem on  $G_0$  subject to inequality constraints, where  $G_0 \subset SE(3)$  is the symmetry subgroup formed by the finished surfaces of the workpiece. We solve the envelopment problem by solving a sequence of linear programming problems where the solution from the symmetric localization problem is used as an initial condition. We also address the issue of hybrid localization/inspection/machinability. We develop a methodology for treating localization, on-line inspection and machinability of workpieces simultaneously using the geometric properties of the homogeneous space. We also analyze the localization problem of a class of workpieces with special shapes and discuss their configuration spaces. We show that this kind of localization problem can be transformed into a two-dimension problem, thus, a set of simpler algorithms can be obtained.

Finally, making use of these algorithms, we propose a computer aided setup (CAS) system and implement the system on an open architecture machining tool environment. The experimental results show the validation of the developed localization algorithms and the CAS system. Availability of the CAS system eliminates the need of having an operator fixture workpiece accurately, thus simplifying and accelerating greatly the machining cycle.

## Acknowledgments

During the years of graduate study at HKUST, I learned the fact that a PhD work is more than just a single person's work. I have been taught, advised and helped by many people around me. I want to take this opportunity to express my sincere gratitude to them.

First of all, I would like to thank my supervisor, Prof. Zexiang Li, for his guidance, advice and support during the period of my PhD study. I have benefited greatly from his outstanding insight and rigorous research attitude. His strong mathematical background, hard work and style of scientific pursuit helped me to learn how to be a good researcher and will continuously influence me in the years to come.

I would also like to give special thanks to the members of my thesis committee for their support: Prof. Peiyuan Qian(Chairman), Prof. Xiren Cao, Prof. Ajay Joneja, Prof. Yunhui Lui, and to Prof. Li Qiu.

My special thanks go to Prof. Jianghua Lu of the University of Arizona for her help in the mathematics; Prof. J.W. Hong and X.L. Tan for proposing to us the localization problems; Prof. Hanfu Chen of the Chinese Academy of Science for his helpful suggestions and discussions on recursive estimation of workpiece localization; Prof. Michael Yu Wang of University of Maryland, for his suggestions on localization problems; Prof. Tianyuan Xiao of Tsinghua University and Prof. Y.L. Xiong of Huazhong University of Science and Technology, for discussions on applications of workpiece localization; Prof. K.L. Tsui of HKUST for his helpful advice in using Jackknife method.

I would like to thank Prof. Hong Wu and Mr. Xikang Qian for their help in implementing the automatic workpiece localization system on the HKUST three-axis CNC milling machine system. Prof. Wu's deep insight on engineering problems is a source of inspiration. I benefited greatly from the frequent discussions with Dr. Jianbo Gou. I would also like to thank many friends and colleagues at HKUST, especially, Li Qingxiang, Jiang Shilong, Qin Zhiqiang, Guan Yisheng, AnHui, Yiu Yiu Kuen, Maurice Yeung, Woo Kam Tim, Tan Kan, Cai Zhihong, Bao Zhong, Huang WeiQing and Zhang Chunng for their kind help and friendship.



I would also like to thank the faculty in the Department of Electrical and Electronic Engineering for teaching me new knowledge and the staff at the Department for providing excellence service I needed.

Finally, I owe huge gratitude to my family: my parents-in-law, my mother, my husband Cao Kai and my lovely daughter Cao Wenting for their understanding, support and patience. A mere "Thank you" really can not make up for the hardships they suffered. I have never forgotten my daughter's tears when she saw me off at the airport for my leaving for Honk Kong to pursue my PhD degree. The continuous encouragement of my husband has been a source of great strength. I would like to dedicate this dissertation to my beloved husband and daughter: Cao Kai and Cao Wenting.

# Contents

<b>1</b>	<b>Introduction</b>	<b>1</b>
1.1	Workpiece Localization . . . . .	1
1.2	Applications of Workpiece Localization . . . . .	2
1.3	Previous Work . . . . .	4
1.4	Problem Statements . . . . .	5
1.5	Contributions of This Work . . . . .	8
1.6	Organization of the Dissertation . . . . .	9
<b>2</b>	<b>Geometric Analysis and Algorithms for Workpiece Localization</b>	<b>13</b>
2.1	Introduction . . . . .	13
2.2	Rigid Motions . . . . .	13
2.3	Least Squares Formulation of Localization . . . . .	17
2.4	Geometric Analysis of Least Squares Problem . . . . .	19
2.5	Optimal Home Surface Points . . . . .	22
2.6	The Geometric Algorithms for Workpiece Localization . . . . .	26
2.7	The Localization Algorithms with Global Convergence . . . . .	32
2.8	Performance Analysis of Localization Algorithms . . . . .	35
2.8.1	Robustness . . . . .	37
2.8.2	Global Convergence . . . . .	37
2.8.3	Accuracy . . . . .	39
2.8.4	Computational efficiency . . . . .	41
2.9	Conclusion . . . . .	41

<b>3 Reliability Analysis for Workpiece Localization</b>	<b>45</b>
3.1 Introduction . . . . .	45
3.2 Choice of Measurement Points . . . . .	46
3.3 Reliability Analysis with F-test Method . . . . .	48
3.3.1 Analysis of error bounds . . . . .	48
3.3.2 Translational reliability . . . . .	49
3.3.3 Rotational reliability . . . . .	51
3.3.4 Simulations . . . . .	52
3.4 Conclusion . . . . .	52
<b>4 Localization of Partially Finished Workpieces</b>	<b>55</b>
4.1 Introduction . . . . .	55
4.2 Configuration Spaces of Symmetric Features . . . . .	56
4.3 Hybrid Localization/Envelopment Problem . . . . .	60
4.3.1 Problem Formulation . . . . .	60
4.3.2 The Symmetric Localization Algorithm . . . . .	62
4.3.3 The Envelopment Algorithms . . . . .	65
4.3.4 The Hybrid Algorithms . . . . .	68
4.3.5 Simulation Results . . . . .	68
4.4 Hybrid Localization/Inspection/Machinability Problem . . . . .	72
4.4.1 Minimax Formulation of the Hybrid Problem . . . . .	74
4.4.2 The Localization/Inspection/Machinability Algorithm . . . . .	77
4.4.3 Simulation Results . . . . .	81
4.5 Comparison of the LS and Minimax Method . . . . .	82
4.6 Conclusion . . . . .	89
<b>5 Localization of Workpieces with Special Geometries</b>	<b>91</b>
5.1 Introduction . . . . .	91
5.2 Problem Formulation . . . . .	91
5.3 Geometric Algorithms . . . . .	94
5.3.1 Home Surface points . . . . .	95
5.3.2 Transformation update $g$ . . . . .	96

<i>Contents</i>	ix
5.4 Conclusion . . . . .	98
<b>6 A Computer-Aided Setup(CAS) System for Workpieces</b>	<b>99</b>
6.1 Introduction . . . . .	99
6.2 An Open Architecture CNC System . . . . .	99
6.3 Composition of the CAS System . . . . .	101
6.3.1 Probing System . . . . .	101
6.3.2 Software System . . . . .	102
6.4 Operational Principle of the CAS System . . . . .	103
6.4.1 Probing Strategy . . . . .	106
6.4.2 Error Compensation for Measurement Points . . . . .	109
6.4.3 Reliability analysis and toolpath modification . . . . .	110
6.5 Experimental Verification of the CAS System . . . . .	112
6.6 Conclusion . . . . .	115
<b>7 Conclusion and Future Work</b>	<b>117</b>
7.1 Conclusions . . . . .	117
7.2 Future Research . . . . .	119
<b>Biography</b>	<b>131</b>
<b>Publications</b>	<b>133</b>



# List of Figures

1.1	An open architecture CNC machine with CAM/CAS . . . . .	3
2.1	A rigid motion of an object in the reference frame . . . . .	14
2.2	Workpiece localization in a manufacturing environment . . . . .	18
2.3	Relationship between a transformed measurement point and a corresponding home surface point . . . . .	25
2.4	Different perpendicular points of a given transformed measurement point $\hat{y}_i$ at the same surface $S_i$ . . . . .	26
2.5	Reference points used to improve the convergence of localization algorithms . . . . .	26
2.6	Iterative sequence showing construction of a localization solution . . . . .	28
2.7	Flow chart of the global localization algorithms . . . . .	34
2.8	Shading model of a 2.5D Workpiece (A) . . . . .	36
2.9	Shading model of a turbine blade(Workpiece B) . . . . .	36
2.10	A profile of convergence by each of the algorithms, where the Hong-Tan algorithm converges in a few iterations. . . . .	38
2.11	Regions of convergence in terms of the maximal orientation errors for each of the algorithms . . . . .	38
2.12	Accuracy of estimation achieved by each of the algorithms as a function of the numbers of measurement points . . . . .	40
2.13	Transformation errors versus the number of measurement points, where the mean of the measurement noises is 0.002 and the variances of the measurement noises are $\sigma = 0.01, 0.02$ and $0.03$ , respectively . . . . .	40
2.14	Computational time versus the number of measurement points. . . . .	42

3.1	A trapezoid to be localized . . . . .	46
3.2	Upper bounds of transformation errors versus the number of measurement points. . . . .	53
4.1	Symmetric features and their configuration spaces . . . . .	59
4.2	Signed distance from a transformed measurement point to the corresponding home surface . . . . .	63
4.3	Flowchart of the hybrid localization/envelopment algorithm . . . . .	67
4.4	A workpiece having one finished surface . . . . .	69
4.5	Deviations of transformed measurement points from their CAD model surfaces . . . . .	71
4.6	A workpiece having two intersecting finished surfaces and one sculptured unfinished surface . . . . .	72
4.7	Deviation of transformed measurement points from their CAD mode surfaces with 40 points and different levels of measurement noise . . . . .	87
4.8	Deviation of transformed measurement points from their CAD mode surfaces with 90 points and different levels of measurement noise . . . . .	88
5.1	Localization of an "essentially" 2.5D workpiece . . . . .	92
6.1	Implementation of localization algorithms in a five-axis machine center environment. . . . .	100
6.2	An open architecture CNC machine system . . . . .	101
6.3	The composition diagram of CAS system . . . . .	102
6.4	Software modules of the CAS system . . . . .	103
6.5	The user-machine interface of the CAS system (Dos version) . . . . .	104
6.6	Procedure of workpiece localization . . . . .	105
6.7	The probing process . . . . .	107
6.8	The touch location and its coordinates of a probing point . . . . .	109
6.9	Error compensation for measurement points . . . . .	111
6.10	The probing system on the machine tool is measuring the workpiece bracket machined by means of the CAS system . . . . .	114
6.11	Three workpieces machined by means of the CAS system . . . . .	114

# List of Tables

2.1	Initial orientation states . . . . .	34
2.2	Transformation errors of the three algorithms at various actual transformations for Workpiece B. Unit of orientation error: degree; unit of translation error: mm. HTA: Hong-Tan algorithm, VA: Variational algorithm, TA: Tangent algorithm. . . . .	39
2.3	Computational time of the five algorithms for Workpiece A . . . . .	42
2.4	Computational time of the five algorithms for Workpiece B . . . . .	42
4.1	Solutions computed at different stages for Example 4.3.1 . . . . .	70
4.2	Solutions computed at different stages for Example 4.3.2 . . . . .	73
4.3	Solutions computed at different stages for Example 4.3.3 . . . . .	73
4.4	Solutions computed at different stages for Example 4.4.1 . . . . .	82
4.5	Solutions computed at different stages for Example 4.4.2 . . . . .	83
4.6	Localization results of a planar surface with 4 sets of points using the least squares and minimax methods, where $v_3$ is the normal of the plane, $p$ is the translation and <i>toler.</i> is the tolerance zone of the plane	84
4.7	Localization results of the workpiece with two intersecting planar surfaces and with 4 sets of points using the least squares and minimax methods, where $p_2$ is a free component . . . . .	85
4.8	Comparison of transformation errors between the Least squares and Minimax methods . . . . .	86
4.9	Comparison of tolerance zones of three surfaces between the Least squares and Minimax methods . . . . .	86



6.1 Transformations of the workpiece computed by experimental measurement points . . . . . 113

# Chapter 1

## Introduction

### 1.1 Workpiece Localization

*Workpiece localization* refers to the following problem: assuming a rigid workpiece is arbitrarily fixtured to a work table, determine the position and orientation of the workpiece frame relative to some known world reference frame. Workpiece localization plays a vital role in automation of many manufacturing processes, such as workpiece setup, refixturing, dimensional inspection and robot assembly.

Over the last twenty years, a great deal of effort has been dedicated to improve production efficiency in manufacturing through automating production processes and by eliminating as much as possible human interaction. Computer technology is the brain of manufacturing automation. The employment of computer technology has changed manufacturing processes dramatically from product design (Computer Aided Design), to manufacturing (Computer Aided Manufacturing), and to quality inspection (computer controlled Coordinate Measurement Machine(CMM)). Typically, a computer-controlled multi-axis machine tool can manufacture various complicated workpieces automatically according to tool paths generated by CAD/CAM software and the workpiece models. Also, with increasing demands for product diversity, quick product introduction, high product quality, short product cycle-time and low price, it is necessary that manufacturing systems be flexible enough to respond quickly to changes in demands and products. Use of computer technology makes quick response possible.

Although the employment of computers provides a relatively high degree of au-

tomation in design and machining processes, the use of computers in workpiece setup has received limited attention in the scientific literature and the manufacturing community. Workpiece setup, as a bridge between design and machining, is addressed in the old-fashioned way through the dedicated fixtures, and long hours of calibration. Much human interaction is required for high precision fixturing and machining. For example, for different kinds of workpieces one still need to design and manufacture different fixtures to set them up, and to use specific hard gauges to perform off-line inspection. Also, in order to machine a workpiece a machinist has to accurately set up and then re-set up the workpiece. Given the accuracy requirements of typical machining jobs this is a difficult and time-consuming task even for a highly skilled machinist with specially designed tools and gauges. In some cases, setting up a workpiece may take several hours while machining it just takes a few minutes. The problem is made worse for workpieces with sculptured surfaces where reference points are difficult to identify. It is desirable to automate workpiece setup and to perform on-line inspections.

With advances in CNC technology and availability of on-machine probing sensors, it is possible to employ computers and localization algorithms to automate the process of workpiece setup. In the next section, we will discuss how workpiece localization technology can be applied to practical manufacturing systems.

## 1.2 Applications of Workpiece Localization

Localization has its main applications in automation of the following manufacturing processes: workpiece setup, refixturing, dimensional inspection and robot assembly.

Figure 1.1 shows the diagram of an open architecture CNC machine with a CAM/CAS (computer-aided manufacturing and computer aided setup) system. The CAS system consists of a touch sensor, data process and localization algorithms. The process of the computer-aided setup is suggested as follows: First, with a workpiece arbitrarily fixtured on the machine table, a touch sensor is programmed to sample a number of points on the surfaces of the workpiece relative to the machine frame. Then, using the measurement points and the CAD model of the workpiece, the Euclidean transformation (position and orientation) of the workpiece with respect to

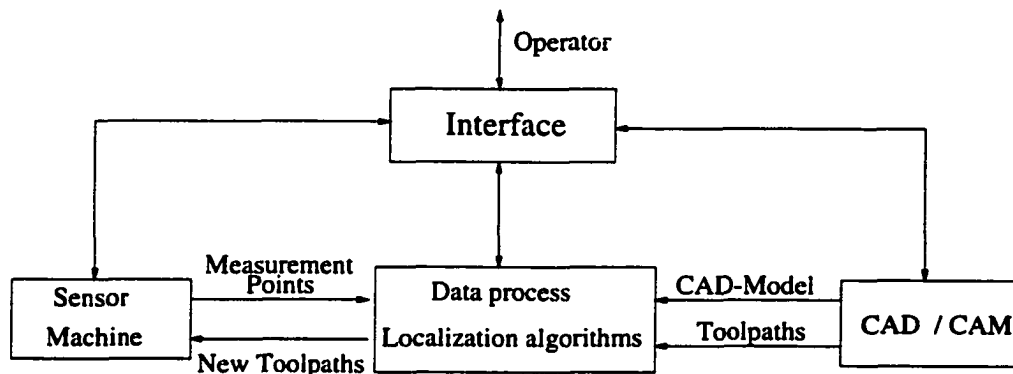


Figure 1.1: An open architecture CNC machine with CAM/CAS

the machine frame is computed by using the localization algorithms. Finally, the new Euclidean transformation is used to compensate for and optimize initially generated tool paths which will then act on the workpiece as if it were accurately fixtured to the machine table, thus achieving highly accurate cutting of inaccurately fixtured workpieces and greatly accelerating machining cycles while reducing machining cost.

In recent years, coordinate measuring machines (CMMs) have been widely utilized for dimensional inspection of workpieces [25, 35, 36]. In its operation, a workpiece is arbitrarily fixtured to the machine table, and a set of points are measured on the surfaces of the workpiece. Then the optimal transformation (translation and orientation) of the workpiece relative to the machine frame is computed using localization algorithms. The measurement points are then transformed to the CAD frame of the workpiece. Finally, the tolerance values are computed by matching the transformed points with the nominal features of the workpiece, leading to acceptance or rejection of the workpiece.

Workpiece localization also finds many important applications in robotic assembly[37]. In [37], a localization method was used in robotic arc welding, where the welding torch has to be positioned accurately in the weld groove. In GAS-Metal-Arc-Welding(GMAW), the uncertain error of positioning a cross-seam must be less than the diameter of the electrode. Accuracy of the normal to the seam must be even higher. Therefore, accurately localizing a torch is essential. In mechanical assembly, tight fitting workpieces can be assembled based on knowing the relative positions

and orientations of the workpieces; Successful grasping depends also on knowing the accurate orientation of a workpiece prior to attempting the grasp.

### 1.3 Previous Work

Workpiece localization has been studied extensively in the last decade. Related studies can be found in the works of [3, 5, 11, 12, 18, 20, 22, 29, 30, 34], where both measurement points and corresponding home surface points are given, and that of [2, 15, 19, 21, 23, 25] where only measurement data and surface correspondence are known.

Workpiece localization with applications in manufacturing and robotic assembly was studied in [19]. This problem [2, 19, 25] was formulated as a *least squares* problem: Given a set of measurement points  $y_i \in \mathbb{R}^3, i = 1, \dots, n$ , with the corresponding home surface  $S_i$ , find  $g \in SE(3)$  and  $x_i \in S_i$  so as to minimize

$$\mathcal{E}(g, x_1, \dots, x_n) = \sum_{i=1}^n \|y_i - gx_i\|^2 \quad (1.1)$$

where  $g \in SE(3)$  is the Euclidean transformation transforming the CAD frame of the workpiece to some known world reference frame, and  $x_i \in S_i$  is the corresponding home surface point of  $y_i$ . A distinctive advantage of this formulation is that it allows the same function to be minimized for workpieces of any shape. Workpiece geometry changes only the description of the home surface point  $x_i \in S_i$ . Several geometric algorithms have been proposed for this minimization problem. Most localization algorithms including, in particular, the ICP algorithm [2], and the Hong-Tan algorithm[21] and Menq's algorithm[25], employ an iterative technique where the home surface points and the Euclidean transformation were optimized separately by holding the others fixed.

In [19], a minimization algorithm was used to localize polyhedral workpieces. Using successive polyhedral approximations the algorithm was extended to workpieces with sculptured surfaces. But, the algorithm requires good prior estimates of the workpiece's position and nested loops which slow down computations considerably. In [25], non-linear optimization techniques were used to solve nonlinear equations for locating 3-D objects with complex and sculptured surfaces. Computational effi-

ciency was enhanced by computing generalized inverses. However, due to the use of local parameterizations of the rotation group, accuracy of computed results is found to be unsatisfactory, and small part deviations are required. Also, when applied to a large number of points, the cost of solving these nonlinear equations becomes prohibitive.

Hong-tang[21] developed a method and apparatus for determining the position and orientation of mechanical objects. By making use of a different objective function, a tangent-homing algorithm (or the Hong-Tan algorithm) was developed for workpiece localization with either sparse or dense data. In [23], using the geometric properties of the Euclidean group, variations of the objective function were calculated and an algebraic formula for the optimal Euclidean transformation was derived. Based on these results, an iterative algorithm (or the Variational algorithm) for workpiece localization was developed. Both the Hong-Tan algorithm and the Variational algorithm are geometric in nature and make no use of local parameterizations.

In [29], the problem of optimal model matching for two 3-D point sets was studied and a formula based on singular value decomposition (SVD) for optimal Euclidean transformation was derived. The result was used in [5] to study the general model matching problem in a Lie group. In [1, 20], the SVD formula of Nadas was corrected and re-derived using linear algebra techniques, along with computational considerations. In [2], Horn's formula [22] and a similar iterative approach were used to solve the general localization problem where the model shape can be a set of line segments or a set of parametric surfaces. In [22], unit quaternions were used to formulate solutions of the optimal model matching problem.

Menq [25] developed a system and the corresponding algorithm for automatically measuring the surface profiles of complicated workpieces. Similarly, Pakh and Ahn[36] developed a precision inspection system for aircraft parts with very thin features based on CAD/CAI integration.

## 1.4 Problem Statements

Localization research has attracted much attention because of its importance in robotics and manufacturing. However, there still remains much research work needs

to be done in this area to make the workpiece localization and their algorithms fully practical. In the application of workpiece localization, one of the following three possibilities could occur: (a) points from the finished surfaces of the workpiece fully constrain the rigid motions (position and orientation) of the workpiece; (b) the workpiece is symmetric, e.g., a cylinder or a plane, and rigid motions along the symmetry directions of the workpiece can not be determined; and (c) the workpiece either is a raw stock or has both finished and unfinished surfaces and points from the finished surfaces are inadequate to fully constrain the rigid motions of the workpiece. In case (c), the problem is to align the CAD model with the workpiece such that all points measured on the finished surfaces of the workpiece match closely to corresponding surfaces on the model while all unmachined surfaces lie outside the model to guarantee the presence of material to be machined at a later time. The localization problem associated with each of the three types of workpieces will be respectively referred to as: (a) the *general 3-dimensional localization problem*; (b) the *symmetric localization problem*; and (c) the *hybrid localization/envelopment problem*. A systematic study of all three problems will be very necessary to their practical applications in real manufacturing environments.

Current research on the localization problem is inadequate to the needs of manufacturing in at least three aspects: reliability, performance evaluation, and ability to ensure the presence of enough material on surfaces to be machined when measured points can not uniquely determine the Euclidean transformation of a workpiece. The details are as follows:

- (1) Existing localization algorithms pay little attention to reliability analysis. Better reliability analysis will insulate the procedures from factors such as measurement errors and object distortion, which is an important product quality issue and a key of whether the localization method can be used effectively in manufacturing industry or not.
- (2) Most localization algorithms need a good initial guess of the location of the workpiece and require unacceptably long guessing time. To fully automate the process of workpiece localization and reduce human interference errors, it is desirable, in practice, to have robust localization algorithms. Several algo-

rithms have been presented for workpiece localization during the last decade. It is necessary to evaluate and analyze the performance of these localization algorithms in terms of accuracy, convergence and computational efficiency. The performance analysis will not only help industrial end-users to know the performances as well as the limitations of the localization algorithms, but also allow them to choose proper algorithms for their particular applications.

- (3) Very few existing localization algorithms consider the hybrid workpiece localization/envelopment problem. The aim of the envelopment algorithms is to optimize the tool paths while rigorously ensuring that further machining will reach specified shapes and tolerances. The hybrid localization/envelopment problem has its main applications in machining of partially machined workpieces, e.g., setting up castings or forgings for post machining or reclamping a partially machined workpiece as it proceeds through successive stages of machining.

In order to fully and reliably automate the process of workpiece localization for a real manufacturing environment, the critical issues to be considered include:

- High accuracy and reliable results of localization;
- Less human interference;
- Short process time;
- High flexibility.

Affecting the reliability and accuracy of computed results are probing locations, the number of measurement points and algorithms used. Affecting the process time is the time it takes to probe and sample the workpiece, to obtain initial condition estimate and then to compute the Euclidean transformation. The process time should be substantially less than the time it takes to set up a workpiece. For applications involving laser or vision-based probing, or workpieces with high tolerancing, the number of measurement points can be very large and the process time is likely to be dominated by the computation time of the algorithm which, if not optimized,



can render real-time implementation of the approach impossible. If localization algorithms can compute an accurate solution without any prior knowledge of location of the workpiece, then human interference errors can be reduced, and at the same time the process time can be shortened.

All algorithms[6] developed in the past are local algorithms. They need a sufficiently accurate estimation of the initial transformation. Otherwise, the algorithms diverge or converge to a local minimum which may be in an incorrect position and orientation. In these cases, reliable localization can not be guaranteed. Therefore, it is very important that we study the convergence of the algorithms and provide effective methods to verify the localization results of the algorithms.

By using non-touch sensors such as cameras, dense measurement data from the surfaces of a workpiece can be sampled. With these dense data, globally convergent solutions can be obtained using special algorithms[37]. However, with these dense data and model-based matching method, the results of localization lack the required accuracy needed for direct use in most manufacturing situations[37]. It is only capable of estimating the location of a part within a few percent of its scale in the presence of considerable noise.

## 1.5 Contributions of This Work

The main contributions of this dissertation are as follows:

1. We explored a geometric theory for the unified treatment of localization to three types of workpiece: general 3-dimensional workpieces, partially machined workpieces, and special geometry workpieces. we formulated the general 3-dimensional localization problem as a least squares problem (LSP) on the Euclidean group,  $SE(3)$ . We developed the two algorithms for solving the LSP and showed how different considerations in updating the Euclidean transformations lead to different algorithms. We proved the local convergence of three localization algorithms and presented a method to improve the performance of these algorithms.

2. We developed a reliability analysis method to verify the reliability of localization results using a statistical method. Simulation and experimental results show effectiveness of this method. This allows the localization method to be applied effectively to real manufacturing tasks.
3. We formulated the hybrid localization/envelopment problem (HLEP) as a symmetric localization problem on the homogeneous space  $SE(3)/G_0$  of the Euclidean group and a minimization problem on  $G_0$  subject to inequality constraints, where  $G_0 \subset SE(3)$  is the symmetry subgroup formed by the finished surfaces of the workpiece. Then, we developed the efficient algorithms using the method of solving a sequence of the linear programming for the problem. We also addressed the hybrid localization/inspection/machinability problem and developed a methodology for treating localization, on-line inspection and machinability of workpieces simultaneously using the geometric properties of the homogeneous space. This method provides the transformation of a workpiece, the tolerance values of finished surfaces, and maximum machinable volumes existing on unfinished surfaces. Thus one can decide if further machining is necessary according to the results obtained. It is also possible to adaptively adjust the machining so as to improve the product quality using this method.
4. Making use of these algorithms we developed, we proposed a computer aided setup (CAS) system and implemented the system on an open architecture machining tool environment. Availability of the CAS system eliminates the need of having an operator fixture workpiece accurately, thus simplifying and accelerating greatly the machining cycle.

## 1.6 Organization of the Dissertation

This dissertation is organized into seven chapters. The following is a summary of the contents of each chapter.

In Chapter 2, we first review rigid body motions in  $\mathbf{R}^3$ , providing basic geometric concepts for workpiece localization. Then, we formulate the general 3-dimensional localization problem as a least squares problem (LSP) on the Euclidean group,  $SE(3)$ .

The mathematics of LSP is analyzed in detail where necessary conditions are derived for the optimal Euclidean transformation and the optimal home surface points. We describe in detail an iterative method for solving LSP and show how different considerations in updating the Euclidean transformations lead to different algorithms. We show the local convergence of three localization algorithms and present a method to improve the performance of these algorithms. We give simulation results showing convergence, accuracy and computational efficiency of the various geometric algorithms.

In Chapter 3, we provide an effective method to analyze the reliability of workpiece localization. First, we discuss the factors affecting the accuracy and reliability of localization results. Then, using the F-test method in statistics, we analyze the translational and rotational reliability and present the upper bounds of localization errors. Finally, we show the effectiveness of the analysis method with simulation and experimental results.

In Chapter 4, we deal with localization of partially finished workpieces. First, we study the geometric properties of the homogeneous space  $SE(3)/G_0$ , where  $G_0 \subset SE(3)$  is the symmetry subgroup formed by the finished surfaces of a workpiece. Then, we propose a hybrid localization/envelop problem of localizing the partially finished workpiece. We formulate the hybrid as a symmetric localization problem on the homogeneous space  $SE(3)/G_0$  of the Euclidean group and a minimization problem on  $G_0$  subject to inequality constraints. We solve the envelopment problem by solving a sequence of linear programming problems where the solution from the symmetric localization problem is used as an initial condition. In this chapter, we also address the issue of hybrid localization/inspection/machinability using the minimax method. We develop a methodology for treating localization, on-line inspection and machinability of workpieces simultaneously using the geometric properties of the homogeneous space. We present simulation results for demonstrating the efficiency of our method for the hybrid problem. Finally, we analyze and compare the performance of the localization results obtained using the least squares method and the minimax method, respectively.

In Chapter 5, we deal with localization of workpieces with special geometry

shapes. We first classify 3D workpieces with a planar standard surface in contact with or parallel to the machine table surface as 2.5D workpieces, then, analyze their configuration spaces. We show that this localization problem can be simplified into a two-dimension problem. Thus, corresponding localization algorithms are simpler. Finally, we present three algorithms for the 2D localization problem.

In Chapter 6, we introduce how we implemented the computer-aided workpiece setup system on an open architecture CNC milling machine tool. First, we describe briefly the open architecture CNC system. Next, we introduce how to implement the CAS system on the CNC machine tools. Then, we present the structure and operational principle of the CAS system. Finally, we demonstrate the validation of the localization algorithms on the CAS system with experimental results.

In Chapter 7, we summarize the entire dissertation and present possible future research work.



## Chapter 2

# Geometric Analysis and Algorithms for Workpiece Localization

### 2.1 Introduction

In this chapter, we introduce some fundamental concepts of rigid motion in  $\mathbf{R}^3$ , and define notations to be used in this thesis. Then, we consider localization of a general 3-dimensional workpiece for which the standard or finished surfaces of the workpiece completely define (or constrain) the rigid motions of the workpiece. We analyze the geometric properties of workpiece localization and formulate the localization problem. Then, we develop two algorithms, the Variational and Tangent algorithms for the solution of the problem. We discuss in a unified framework the two algorithms and other several existing geometric algorithms. We show the local convergence of three localization algorithms and present a method to improve the performance of these algorithms. Finally, we evaluate the performance of these algorithms in terms of accuracy, convergence, and computational efficiency.

### 2.2 Rigid Motions

The geometries of the Euclidean group  $SE(3)$  play an important role in the study of workpiece localization. In this section, we review briefly rigid motions in  $\mathbf{R}^3$  and collect some useful concepts and properties of  $SE(3)$ .

The Euclidean group  $SE(3)$  is formally defined as the set of isometries of  $\mathbf{R}^3$ ,

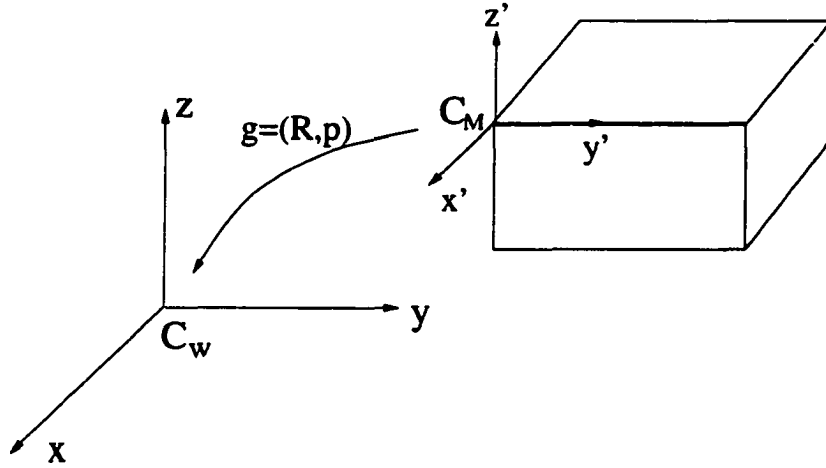


Figure 2.1: A rigid motion of an object in the reference frame

i.e., the set of length and orientation preserving transformations of  $\mathbb{R}^3$ .

**Definition 2.2.1.** A mapping  $g : \mathbb{R}^3 \rightarrow \mathbb{R}^3$  is a rigid body transformation if it satisfies the following properties:

1. Length is preserved:  $\|g(p_1) - g(p_2)\| = \|p_1 - p_2\|, \forall p_1, p_2 \in \mathbb{R}^3$ .
2. The cross product is preserved:  $g(v_1) \times g(v_2) = g(v_1 \times v_2), \forall v_1, v_2 \in \mathbb{R}^3$ .

Consider a rigid object moving in a reference frame as shown in Figure 2.1. Attach a frame  $C_M$  on the object and let the reference frame be  $C_W$ . Then, at each instance, the configuration space of the rigid object can be completely identified with the Euclidean group  $SE(3)$ , which is a well-known example of a Lie group - a topological group with differential structures.

The rotation group of  $\mathbb{R}^3$ , denoted  $SO(3)$ , consists of the set of  $3 \times 3$  special orthogonal matrices, i.e.,

$$SO(3) = \{R \in \mathbb{R}^{3 \times 3} \mid \det R = +1, RR^T = I\}.$$

Denote  $p \in \mathbb{R}^3$  position and  $R \in SO(3)$  orientation of a frame  $C_M$  with respect to the reference frame  $C_W$ , then using homogeneous representation, an element

$g = (R, p)$  of  $SE(3)$  is written as a  $4 \times 4$  matrix of the form

$$g = \begin{bmatrix} R & p \\ 0 & 1 \end{bmatrix}$$

and the group operation corresponds to matrix multiplication.

Rigid body transformations can be combined to form rigid transformations. Let  $g_{bc} \in SE(3)$  be the configuration of a frame  $C$  relative to a frame  $B$ , and  $g_{ab} \in SE(3)$  be the configuration of the frame  $B$  relative to a frame  $A$ . Then, the configuration of  $C$  relative to  $A$  is given by

$$g_{ac} = g_{ab}g_{bc} = \begin{bmatrix} R_{ab}R_{bc} & R_{ab}p_{bc} + p_{ab} \\ 0 & 1 \end{bmatrix}. \quad (2.1)$$

Equation (2.1) defines the composition rule for rigid motions. Clearly,  $SE(3)$  in homogeneous representation is a Lie group. The group operation is naturally the matrix multiplication. It satisfies:

1. If  $g_1, g_2 \in SE(3)$ , then  $g_1g_2 \in SE(3)$ . The group operation is a differentiable mapping.
2. The identity element of  $SE(3)$  is  $I \in \mathbb{R}^{4 \times 4}$ .
3. If  $g = \begin{bmatrix} R & p \\ 0 & 1 \end{bmatrix} \in SE(3)$ , the inverse of  $g$  is given by

$$g^{-1} = \begin{bmatrix} R^T & -R^T p \\ 0 & 1 \end{bmatrix} \in SE(3)$$

so that  $g^{-1} = (-R^T p, R^T)$ . The inverse mapping is differentiable.

4. The composition rule for rigid transformation is associative.

The Lie algebra of  $SO(3)$ , denoted  $so(3)$ , is identified with the set of  $3 \times 3$  skew-symmetric matrices, which can be further identified with  $\mathbb{R}^3$  via the map:

$$\Lambda : \mathbb{R}^3 \longrightarrow so(3) : \omega = (\omega_1, \omega_2, \omega_3) \mapsto \hat{\omega} = \begin{bmatrix} 0 & -\omega_3 & \omega_2 \\ \omega_3 & 0 & -\omega_1 \\ -\omega_2 & \omega_1 & 0 \end{bmatrix}.$$

Note that we have  $\hat{\omega}x = \omega \times x$  for  $\omega, x \in \mathbb{R}^3$ , where  $\times$  is the vector cross product operation in  $\mathbb{R}^3$ .



The exponential map of  $SO(3)$

$$\exp : so(3) \longrightarrow SO(3) : \hat{\omega} \longmapsto e^{\hat{\omega}}$$

where

$$e^{\hat{\omega}} = I + \frac{\hat{\omega}}{\|\omega\|} \sin\|\omega\| + \frac{\hat{\omega}^2}{\|\omega\|^2} (1 - \cos\|\omega\|)$$

defines the canonical coordinates of  $SO(3)$ .

Given  $R \in SO(3)$ , there exists a unit vector  $\omega \in \mathbb{R}^3$  and an angle  $\theta$  such that

$$R = e^{\hat{\omega}\theta}$$

To see this, let

$$R = \begin{bmatrix} r_{11} & r_{12} & r_{13} \\ r_{21} & r_{22} & r_{23} \\ r_{31} & r_{32} & r_{33} \end{bmatrix} \quad (2.2)$$

and define  $v_\theta = 1 - \cos\theta$ ,  $c_\theta = \cos\theta$ , and  $s_\theta = \sin\theta$ , then, we can have

$$\theta = \cos^{-1}\left(\frac{\text{trace}(R) - 1}{2}\right) \quad (2.3)$$

and if  $\theta \neq 0$ , we have

$$\omega = \frac{1}{2s_\theta} \begin{bmatrix} r_{32} - r_{23} \\ r_{13} - r_{31} \\ r_{21} - r_{12} \end{bmatrix}. \quad (2.4)$$

Note that there is an ambiguity in the value of  $\theta$ , in the sense that  $\theta \pm 2\pi n$  or  $-\theta \pm 2\pi n$  could be chosen as well. If the  $2\pi - \theta$  had been chosen in the equation (2.3), the axis of rotation would have been  $-\omega$ . Indeed, the exponential map is many-to-one map from  $\mathbb{R}^3$  onto  $SO(3)$ . If  $R = I$ , then  $\theta = 0$  and  $\omega$  can be chosen arbitrarily. If  $R \neq I$ , the above construction shows that there are two distinct  $\omega$  and  $\theta \in [0, 2\pi)$  such that  $R = \exp(\hat{\omega}\theta)$ .

The components of the vector  $\omega\theta \in \mathbb{R}^3$  given by (2.3) and (2.4) are called the exponential coordinates for  $R$ .

**Theorem 2.2.1. (Euler)** *Any orientation  $R \in SO(3)$  is equivalent to a rotation about a fixed axis  $\omega \in \mathbb{R}^3$  through an angle  $\theta \in [0, 2\pi)$*

This method of representing a rotation is also known as the equivalent axis representation.

The Lie algebra of  $SE(3)$ , denoted  $se(3)$ , is given by the set of  $4 \times 4$  matrices of the form

$$\hat{\xi} = \begin{bmatrix} \hat{\omega} & v \\ 0 & 0 \end{bmatrix}, \quad \omega, v \in \mathbb{R}^3$$

The vector  $\xi = (v, \omega) \in \mathbb{R}^6$  is referred to as the twist coordinates of  $\hat{\xi} \in se(3)$ . Let  $\{\xi_i\}_{i=1}^6$  be the canonical basis of  $\mathbb{R}^6$ , i.e.,  $\xi_i$  has a "1" in the  $i^{\text{th}}$  entry and a "0" otherwise, then a basis of  $se(3)$  is given by  $\{\hat{\xi}_i\}_{i=1}^6$ . Note that  $\hat{\xi}_i, i = 1, \dots, 3$  represents, respectively, infinitesimal translations, and  $\hat{\xi}_i, i = 4, \dots, 6$ , represents infinitesimal rotations about the principal axis directions.

The exponential map of  $SE(3)$ , defined by

$$\begin{aligned} \exp : se(3) &\longrightarrow SE(3) : \hat{\xi} \longmapsto e^{\hat{\xi}} \\ e^{\hat{\xi}} &= \begin{bmatrix} e^{\hat{\omega}} & Av \\ 0 & 1 \end{bmatrix}, \quad \text{for } \omega \neq 0; \end{aligned}$$

or,

$$e^{\hat{\xi}} = \begin{bmatrix} I & v \\ 0 & 1 \end{bmatrix}, \quad \text{for } \omega = 0$$

where

$$A = I + \frac{\hat{\omega}}{\|\omega\|^2} (1 - \cos\|\omega\|) + \frac{\hat{\omega}^2}{\|\omega\|^3} (\|\omega\| - \sin\|\omega\|),$$

gives the canonical coordinates of  $SE(3)$  near the identity.

## 2.3 Least Squares Formulation of Localization

As described in the last chapter, the localization problems associated with the three types of workpieces can be classified as: (a) the *general 3-dimensional localization problem*; (b) the *symmetric localization problem*; and (c) the *hybrid localization/envelopment problem*. In this chapter, we will focus our study on the problem (a), the general 3-dimensional localization. The problems (b) and (c) will be considered in Chapter 4.

Consider a workpiece that is arbitrarily fixtured to a machine table as shown in Figure 2.2. A surface of the workpiece is called a standard surface if it is completely machined according to the specifications of the finished product, and an

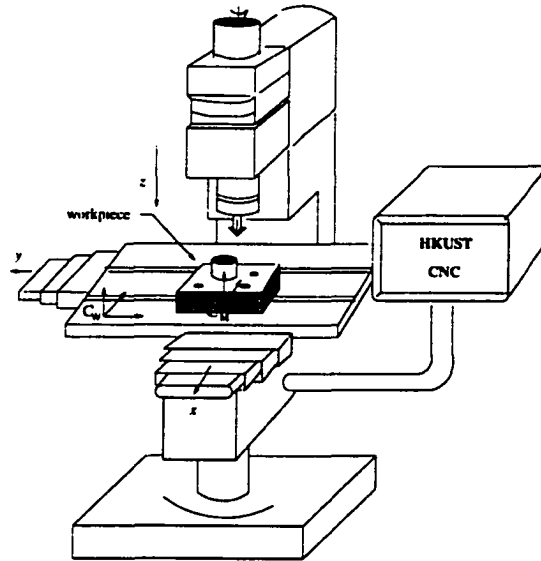


Figure 2.2: Workpiece localization in a manufacturing environment

envelope surface if it is an unfinished surface which encloses the surface of the finished product. An envelope surface is either a surface of the stock or a surface of the workpiece produced at an intermediate stage of manufacturing. We assume that only the standard surfaces are probed to determine the position and orientation of the workpiece.

We further assume that the CAD model of the finished product is available, and thus we have the geometrical data that describes the standard surfaces (design surfaces) of the workpiece. Let  $S_i$  be the  $i^{\text{th}}$  standard surface, we denote the parametric equation by

$$S_i = \{x_i \in \mathbb{R}^3 \mid x_i = \psi_i(u_i, v_i)\} \quad (2.5)$$

where  $(u_i, v_i)$  are independent parametric variables, generally referred to as the surface coordinates, or by an implicit representation of the form

$$S_i = \{x_i \in \mathbb{R}^3 \mid h_i(x_i) = 0\}. \quad (2.6)$$

Depending on the representation of CAD systems,  $\psi_i(u_i, v_i)$  can be either polynomial of  $(u_i, v_i)$  (B-spline) or rational polynomial functions of  $(u_i, v_i)$  (NURBS).

Denote by  $C_M$  the model frame of the workpiece and  $C_W$  the machine reference frame. Let  $p \in \mathbb{R}^3$  and  $R \in SO(3)$  be the (unknown) position and orientation of  $C_M$  relative to  $C_W$ . Then,  $g = (p, R) \in SE(3)$  describes the Euclidean transformation of  $C_M$  relative to  $C_W$ , i.e., if  $y \in \mathbb{R}^3$  is a point expressed in  $C_W$ , then

$$g^{-1}y = R^T y - R^T p$$

is the expression of  $y$  in  $C_M$ . Let the surface  $S_i$  that corresponds to  $y_i$  be called the *home surface* of  $y_i$ . For notational simplicity,  $S_i$  here denotes the home surface of  $y_i$ , which should not be confused with the notation  $S^j, j = 1, \dots, J$  used for the surfaces of the workpiece in its CAD model. In other words, if  $y_i$  and  $y_j$  were sampled from the same surface say  $S^k$ , then  $S_i$  and  $S_j$  are described by the CAD model of the same  $S^k$ . Correspondence between  $y_i$  and  $S_i$  is either assumed to be known or established during the measurement process. If the surface were perfect and there were no measurement errors then for each  $y_i \in \mathbb{R}^3$  there exists an  $x_i \in S_i$  such that

$$R^T y_i - R^T p = x_i, i = 1, \dots, n,$$

In practice, however, machining inaccuracies and measurement errors will destroy the equalities. Therefore a more appropriate approach to workpiece localization can be described as follows:

**Problem 2.3.1. (Least Squares Problem (LSP))**

Given measurement data  $Y = \{y_i \in \mathbb{R}^3, i = 1, \dots, n\}$ , find  $g \in SE(3)$  and corresponding home surface points  $x_i \in S_i, i = 1, \dots, n$  so as to minimize the function

$$\boxed{\mathcal{E}(g, x) = \sum_{i=1}^n \|g^{-1}y_i - x_i\|^2} \quad (2.7)$$

subject to the home surface constraint

$$S_i = \{x_i \in \mathbb{R}^3 | x_i = \psi_i(u_i, v_i)\}, i = 1, \dots, n \quad (2.8)$$

## 2.4 Geometric Analysis of Least Squares Problem

Let  $Q = SE(3) \times \mathbb{R}^{3n}$ . Then,  $\mathcal{E}$  is a function defined on  $Q$  with the home surface constraint given by (2.8). To find the optimal solution(s) of  $\mathcal{E}$ , we define

$$\bar{y} = \frac{1}{n} \sum_{i=1}^n y_i \quad \text{and} \quad \bar{x} = \frac{1}{n} \sum_{i=1}^n x_i$$

which are called the centroid of  $\{y_i\}_{i=1}^n$  and  $\{x_i\}_{i=1}^n$ , respectively. Let

$$\tilde{y}_i = y_i - \bar{y} \quad \text{and} \quad \tilde{x}_i = x_i - \bar{x}.$$

Let

$$W = \sum_{i=1}^n \tilde{y}_i \tilde{x}_i^T \quad (2.9)$$

and denote the singular value decomposition (SVD) of  $W$  by

$$W = U \begin{bmatrix} \sigma_1 & 0 & 0 \\ 0 & \sigma_2 & 0 \\ 0 & 0 & \sigma_3 \end{bmatrix} V^T$$

where  $U, V \in \mathbb{R}^{3 \times 3}$  are unitary, and  $\sigma_1 \geq \sigma_2 \geq \sigma_3 \geq 0$  are the singular values of  $W$ .

**Theorem 2.4.1.** *If  $\text{rank}(W) = 3$ , then the optimal solution of  $\mathcal{E}(\cdot, x)$  is unique and is given by*

$$\boxed{\begin{array}{l} R^* = UV^T \\ p^* = \bar{y} - R^* \bar{x} \end{array}} \quad (2.10)$$

The minimal value of the objective function at  $(R^*, p^*)$  is

$$\mathcal{E}^*(x) = \sum_{i=1}^n (\|\tilde{x}_i\|^2 + \|\tilde{y}_i\|^2) - 2(\sigma_1 + \sigma_2 + \sigma_3).$$

**Proof:**

Rewrite the objective function as

$$\begin{aligned} \mathcal{E} &= \sum_{i=1}^n \|R^T \tilde{y}_i - \tilde{x}_i + R^T \bar{y} - R^T p - \bar{x}\|^2 \\ &= n \|R^T \bar{y} - R^T p - \bar{x}\|^2 + \sum_{i=1}^n \|R^T \tilde{y}_i - \tilde{x}_i\|^2 \end{aligned} \quad (2.11)$$

(2.11) is minimized if

$$p^* = \bar{y} - R^* \bar{x} \quad (2.12)$$

where  $R^*$  minimizes the function

$$\mathcal{E}_1(R) = \sum_{i=1}^n \|R^T \tilde{y}_i - \tilde{x}_i\|^2 \quad (2.13)$$

Expanding (2.13), using the identity  $\|y\|^2 = \text{tr}(yy^T)$ , yields

$$\mathcal{E}_1(R) = a - 2\text{tr}(R^T W)$$

where

$$a = \sum_{i=1}^n \|\tilde{y}_i\|^2 + \|\tilde{x}_i\|^2.$$

It is shown in [23] that if  $n \geq 4$  and the points  $y_i$  and  $x_i$  are generic enough then  $W$  is nonsingular. Using standard minimization techniques in a Lie group [24] we compute directional derivatives of the objective function (2.13). For this we express a tangent vector to  $SO(3)$  at a point  $R^T$  as  $\hat{\omega}R^T \in T_{R^T}SO(3)$ , where for  $\omega \in \mathbb{R}^3$ ,

$$\hat{\omega} = \begin{bmatrix} 0 & -\omega_3 & \omega_2 \\ \omega_3 & 0 & -\omega_1 \\ -\omega_2 & \omega_1 & 0 \end{bmatrix}$$

Thus,  $R \in SO(3)$  is a critical point of the objective function (2.13) if and only if for all  $\omega \in \mathbb{R}^3$

$$\begin{aligned} 0 &= \langle d\mathcal{E}_1(R), \hat{\omega}R^T \rangle \\ &= \left. \frac{d}{dt} \right|_{t=0} \mathcal{E}_1(e^{\hat{\omega}t} R^T) \\ &= -2 \left. \frac{d}{dt} \right|_{t=0} \text{tr}(e^{\hat{\omega}t} R^T W) \\ &= -2\text{tr}(\hat{\omega}R^T W) \end{aligned} \tag{2.14}$$

(2.14) implies that

$$R^T W \text{ is symmetric.}$$

Let

$$R^T W = S \tag{2.15}$$

for some symmetric matrix  $S$ . Because  $R \in SO(3)$ , we have

$$S^2 = S^T S = W^T W \tag{2.16}$$

Solving from (2.16) for  $S$ , using SVD of  $W$ , we have

$$S = (W^T W)^{1/2} = V \begin{bmatrix} \pm\sigma_1 & 0 & 0 \\ 0 & \pm\sigma_2 & 0 \\ 0 & 0 & \pm\sigma_3 \end{bmatrix} V^T \tag{2.17}$$

By permuting the signs of  $\sigma_i$ 's in (2.17) we obtain 8 possible solutions for  $S$ , where one is a maximum, six saddle points and one minimal. The minimal solution is obtained when positive sign in (2.17) is chosen. Thus, when  $\text{rank}(W) = 3$ , the optimal rotation matrix is given by

$$R^* = UV^T \quad (2.18)$$

Substituting the solution of  $S$  into (2.13) gives the minimum value of the objective function at  $(R^*, p^*)$ .  $\square$

*Remark 1.* (a) Eq. (2.10) will be referred to as the Nadas Formula, as a similar but incorrect version of it first appeared without proof in [29]. There, the  $W$  matrix was incorrectly defined to be  $\sum_i y_i x_i^T$ . Nadas Formula was corrected and proved in [20] and later in [1].

(b) The optimal rotation matrix in Nadas Formula can also be computed using gradient flow (or steepest descent algorithm), where the objective function is given by Eq. (2.9), the metric by the killing form and the gradient equation is

$$\dot{R} = WR^T - RW.$$

(c) An equivalent formulation of Nadas Formula in terms of unit quaternions is given by Horn [22], where the optimal solution  $q_R = (q_0, q_1, q_2, q_3)^T$  is the unit eigenvector corresponding to the maximum eigenvalue of the matrix

$$Q(W) = \begin{bmatrix} \text{tr}(W) & b^T \\ b & W + W^T - \text{tr}(W)I_3 \end{bmatrix} \quad (2.19)$$

where

$$\hat{b} = W - W^T$$

is a skew-symmetric matrix, and  $\text{tr}(\cdot)$  stands for the trace operator. (2.19) is used in [2] for the ICP algorithm.

## 2.5 Optimal Home Surface Points

Assume that the *home surface* of  $y_i \in \mathbb{R}^3$  is known and is denoted  $S_i$ .  $y_i$ ,  $i = 1, \dots, n$  is relative to the frame  $C_W$ .  $x_i \in \mathbb{R}^3$  is called the home surface point corresponding

to  $y_i$  and is constrained to lie on the home surface  $S_i$ .  $x_i$  is relative to the CAD model frame. Geometrically, the optimal home surface point  $x_i^*$  of  $y_i$  is the nearest point on the surface  $S_i$  from the transformed point, i.e., the distance  $\|g^{-1}y_i - x_i\|$  is the shortest, as shown in Figure 2.3. Solving for the optimal home surface points is one of the two key procedures in the localization algorithms.

Usually the surfaces used to localize workpieces include planar surfaces, cylindrical surfaces, spherical surfaces, conic surfaces and sculptured surfaces, etc. For most simple surfaces, there are explicit expressions of surface equations and analytic solutions for the optimal home surface points, while for complex surfaces such as sculptured surfaces, they are described by implicit parametric equations. For example, in CAD/CAM practice, free form surfaces are generally described by 3-degree B-spline surfaces. B-spline surfaces are constructed by taking a bidirectional net of control points, two knot vectors, and the products of the univariate B-spline functions,

$$\psi(u, v) = \sum_{i=0}^n \sum_{j=0}^m N_{i,3}(u) N_{j,3}(v) P_{i,j}$$

where  $N_{i,3}(u)$ ,  $N_{j,3}(v)$  are B-spline functions, and  $P_{i,j}$  are control points. B-spline functions vary according to the interval of knots.

Here we mainly introduce how to solve for the home surface points on the complicated surfaces. Assume that a surface is parametrically described by  $x = \psi(u, v)$ , where  $(u, v)$  is the parametric coordinate of the surface. We now use the Lagrange multiplier technique to the optimal solution of home surface points  $x_i \in \mathbb{R}^3$ ,  $i = 1, \dots, n$  to minimize the function  $\mathcal{E}(g, \cdot)$  subject to the constraint

$$h_i(x_i) = 0.$$

where the above equation is the home surface equation. First observe that the constraint is imposed separately on each of the  $x_i$ 's, and thus the directional derivatives can be calculated independently to obtain decoupled results.

**Proposition 2.5.1.** *A necessary condition for  $x_i^* \in \mathbb{R}^3$ ,  $i = 1, \dots, n$ , to minimize the function  $\mathcal{E}(R, p, \cdot)$  is that*

$$\begin{cases} \langle x_i - R^T(y_i - p), \psi_{u,\cdot}^i \rangle = 0 \\ \langle x_i - R^T(y_i - p), \psi_{v,\cdot}^i \rangle = 0 \end{cases} \quad (2.20)$$



where  $x_i = \psi^i(u_i, v_i)$ ,  $\psi^i : \mathbb{R}^2 \rightarrow \mathbb{R}^3$  is the parametric description of  $S_i$  and the minimum of  $\mathcal{E}(R, p, \cdot)$  is given by

$$\mathcal{E}^*(R, p) = \sum_{i=1}^n \langle R^T(y_i - p) - x_i^*, n_i \rangle^2 \quad (2.21)$$

where  $n_i \in \mathbb{R}^3$  is the surface normal of  $S_i$  at  $x_i^*$ .

**Proof.** Using the Lagrange multiplier technique we define

$$\mathcal{E}_L(R, p, x_1, \dots, x_n) = \mathcal{E}(R, p, x_1, \dots, x_n) + \sum_{i=1}^n \lambda_i h_i(x_i)$$

where  $\lambda_i \in \mathbb{R}$  is the Lagrangian multiplier corresponding to the  $i^{\text{th}}$  constraint  $h_i(x_i) = 0$ . Computing the directional derivative of  $\mathcal{E}_L$  with respect to  $x_i$  in the direction  $z_i \in \mathbb{R}^3$  yields

$$\begin{aligned} 0 &= \langle D\mathcal{E}_L, z_i \rangle = \left. \frac{d}{dt} \right|_{t=0} \mathcal{E}(R, p, \dots, x_i + tz_i, \dots) \\ &= \text{tr}(-2R^T y_i z_i^T + 2R^T p z_i^T) + \langle \lambda_i \nabla h_i, z_i \rangle, \quad \forall z_i \in \mathbb{R}^3 \end{aligned}$$

where  $\nabla h_i \in \mathbb{R}^3$  is the gradient of  $h_i$ . This implies that

$$\frac{1}{2} \lambda_i \nabla h_i(x_i^*) + x_i^* - R^T(y_i - p) = 0, \quad i = 1, \dots, n. \quad (2.22)$$

Differentiating  $\mathcal{E}_L$  with respect to  $\lambda_i$  yields the constraint  $h_i(x_i) = 0$ . Solving for the constraint gives the parametric equation of  $S_i$ :

$$\psi^i : \mathbb{R}^2 \rightarrow \mathbb{R}^3 : (u_i, v_i) \mapsto \psi^i(u_i, v_i)$$

The tangent plane to  $S_i$  at  $x_i = \psi^i(u_i, v_i)$  is spanned by the two vectors

$$\psi_{u_i}^i = \frac{\partial \psi^i}{\partial u_i}, \quad \psi_{v_i}^i = \frac{\partial \psi^i}{\partial v_i}$$

Thus, projecting (2.22) to the tangent plane of  $S_i$  and using

$$\langle \nabla h_i, \psi_{u_i}^i \rangle = \langle \nabla h_i, \psi_{v_i}^i \rangle = 0$$

give (2.20). To obtain (2.21), define

$$n_i = \frac{\nabla h_i}{\|\nabla h_i\|}$$

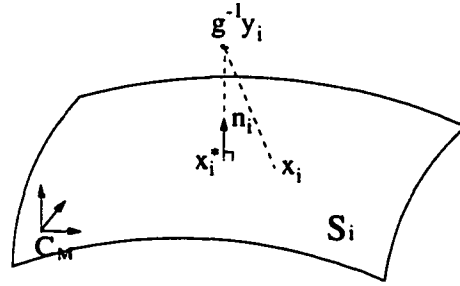


Figure 2.3: Relationship between a transformed measurement point and a corresponding home surface point

Solving from (2.22) for  $\lambda_i$  yields

$$\lambda_i = \frac{2}{\|\nabla h_i\|} \langle R^T(y_i - p) - x_i^*, n_i \rangle.$$

Therefore,

$$\begin{aligned} \mathcal{E} &= \sum_i \langle R^T(y_i - p) - x_i^*, R^T(y_i - p) - x_i^* \rangle \\ &= \sum_i \langle R^T(y_i - p) - x_i^*, \frac{\lambda_i}{2} \nabla h_i \rangle \\ &= \sum_i \frac{1}{\|\nabla h_i\|} \langle R^T(y_i - p) - x_i^*, n_i \rangle \langle R^T(y_i - p) - x_i^*, \nabla h_i \rangle \\ &= \sum_i \langle R^T(y_i - p) - x_i^*, n_i \rangle^2 \end{aligned}$$

The system of two nonlinear equations in (2.20) defines implicitly the home surface point  $x_i^*$  nearest to the transformed point  $\tilde{y}_i = R^T(y_i - p)$ . Given  $\tilde{y}_i$  and the home surface equation  $x_i = \psi^i(u_i, v_i)$  we can use numerical methods (e.g., Newton's Method) to solve for  $x_i^*$ . Eq. (2.22) shows that the optimal  $x_i^*$  must satisfy the condition

$$x_i^* + \tilde{\lambda}_i n_i = \tilde{y}_i, \quad i = 1, \dots, n$$

In other words,  $\tilde{y}_i - x_i^*$  must be perpendicular to the home surface at  $x_i^*$  as shown in Figure 2.3.

Depending on the geometry of  $S_i$ , Newton's method may give different solutions, i.e. there may be multiple solutions for  $x_i^*$  with different initial conditions  $(u_i, v_i)$ . As shown in Figure 2.4, two points  $x_i$  and  $x_i'$  satisfy Eq. (2.20). Obviously, point  $x_i$  is the nearest home surface point. Point  $x_i'$  is just a perpendicular point. The problem

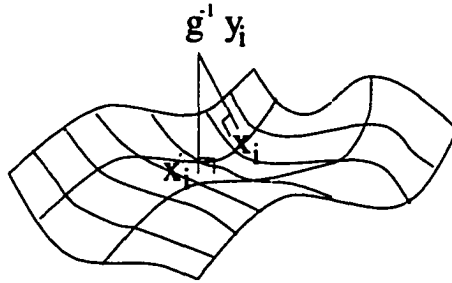


Figure 2.4: Different perpendicular points of a given transformed measurement point  $\tilde{y}_i$  at the same surface  $S_i$

of having multiple solutions can result in a local minimal if initial conditions were not properly chosen. To alleviate this problem, we suggest the following method: First, choose a set of reference points on the sculptured surface, see Figure 2.5. Then, compare the transformed measurement point with each of the reference points and retain the point with the shortest distance. Finally, use the parametric values of the shortest reference point as initial conditions for  $(u_i, v_i)$ . If a sufficient set of reference points are used then global minima can be guaranteed. Another advantage for adopting this method is that we can relax the requirement on  $g_0$ , for otherwise a good prior estimate of  $g_0$  is needed.

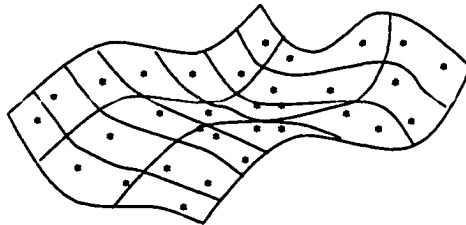


Figure 2.5: Reference points used to improve the convergence of localization algorithms

## 2.6 The Geometric Algorithms for Workpiece Localization

The objective function given in (2.7) depends on the Euclidean transformation  $g \in SE(3)$  and the home surface point  $x_i \in S_i, i = 1, \dots, n$ . If one set of the variables is fixed, the objective function becomes a simple function of the remaining

variables. The Alternating Variable Method [13, 31], in which a function is minimized by changing one variable at a time and the process continues iteratively until convergence occurs, is particularly suited for this problem. One may note that the method has not been a popular method in numerical analysis, partly because of the lack of a theory which supports the method and partly because of the construction by Powell [31] of a problem for which the method fails to converge to a critical point. However, we will show here that for this class of problems the method works very well and is also convergent with properly chosen initial conditions.

**Algorithm 1. (Alternating Variable Method )**

**Input:** (a) Measurement data  $Y = \{y_i \in \mathbb{R}^3, i = 1, \dots, n\}$  and home surface  $S_i$  of  $y_i$ .

**output:** (a) The optimal transformation  $g^*$ .

**Step 0:** (a) Set  $k = 0$ ;

(b) Initialize  $g^0$ ;

(c) Compute  $y_i^0 = (g^0)^{-1}y_i$ ;

(d) Compute  $x_i^0$ ;

(e) Compute  $\mathcal{E}^0 = \mathcal{E}(g^0, x^0)$ ;

(f)  $k = k + 1$ .

**Step 1:** (a) Apply Newton's algorithm to (2.20) to solve for  $x_i^k$ ;

(b) Compute  $g^k$  using  $(x_i^k, g^{k-1})$ ;

(c) Compute  $y_i^k = (g^k)^{-1}y_i$ ;

(d) Compute  $\mathcal{E}^k = \mathcal{E}(g^k, x^k)$ ;

(e) If  $(1 - \mathcal{E}^k/\mathcal{E}^{k-1}) < \delta_1$ , exit. Else

(f) Set  $k = k + 1$  and return to Step 1(a).

**Remark 2.** (i) For Step 0(b), set  $p^0 = \bar{y}$  and  $R^0 = I$ .

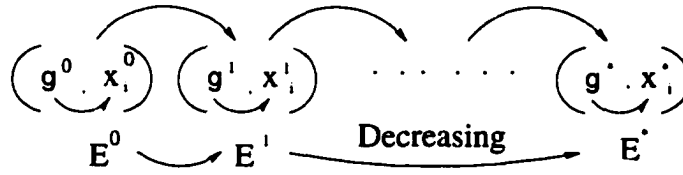


Figure 2.6: Iterative sequence showing construction of a localization solution

- (ii) For workpieces having complex geometries, e.g., with sculptured surfaces, initial condition in Step 0(d) can be generated by using the method described in the last section.
- (iii)  $\delta_1 > 0$  in Step 1(e) is a preset threshold specifying the desired precision of the calculated results. In actual implementation, we combine it with another termination condition  $\mathcal{E}^k < \delta_2$  for some  $\delta_2 > 0$  to achieve global optimal solution. The iteration terminates when  $k$  exceeds a certain large number. By repeating the iterative method with different initial conditions in  $R^0$ , we enhance the chances of obtaining the global optimal solutions.

Figure 2.6 shows the construction of the iterative sequence  $(g_k, x_i^k)$  of the above algorithm.

Given  $g^{k-1}$  and  $x_i^k, i = 1, \dots, n$ , the Euclidean transformation update  $g^k$  in Step 1(b) can be computed in a number of ways. How  $g^k$  is computed affects not only convergence but also accuracy and reliability of the computed results. Here we show the Variational and Tangent algorithms we developed, and present three existing methods for computing  $g^k$ , which are known as the ICP (Iterative Closest Point) algorithm [2], Menq’s algorithm [25] and the Hong-Tan algorithm [21].

**Algorithm 2. (The Variational Algorithm )**

Use  $y_i$  and  $x_i^k, i = 1, \dots, n$  to compute the  $W$  matrix of (2.9) and its singular value decomposition and denote the results by

$$W = U\Sigma V^T.$$

Set

$\begin{aligned} R^k &= UV^T \\ p^k &= \bar{y} - R^k \bar{x}^k \end{aligned}$	(2.23)
-------------------------------------------------------------------------------	--------

**Algorithm 3. (The Tangent Algorithm)**

Express  $g^k$  in terms of  $g^{k-1}$  as [28]

$$g^k = g^{k-1} e^{\hat{\xi}} \quad (2.24)$$

where

$$\hat{\xi} = \begin{bmatrix} \hat{\omega} & v \\ 0 & 0 \end{bmatrix} \in \mathbb{R}^{4 \times 4}, \quad \text{for } \omega, v \in \mathbb{R}^3$$

is called a twist with twist coordinates  $\xi = (v, \omega) \in \mathbb{R}^6$ . For small values of  $\xi$ , (2.24) can be approximated by

$$g^k \cong g^{k-1} (I + \hat{\xi})$$

Substituting the above expression into (2.7) and minimizing the result with respect to  $\xi \in \mathbb{R}^6$  yield

$$\boxed{A\xi = b} \quad (2.25)$$

where

$$A = \begin{bmatrix} \sum_{i=1}^n \hat{y}_i^{k-1} & -\sum_{i=1}^n \hat{y}_i^{k-1} \cdot \hat{y}_i^{k-1} \\ nI & -\sum_{i=1}^n \hat{y}_i^{k-1} \end{bmatrix} \in \mathbb{R}^{6 \times 6}$$

and

$$b = \begin{bmatrix} -\sum_{i=1}^n y_i^{k-1} \times x_i^k \\ -\sum_{i=1}^n (x_i^k - y_i^{k-1}) \end{bmatrix}$$

Applying Gauss elimination to (2.25) we solve for  $\xi$  and the result is then substituted back into (2.24) to update the Euclidean transformation.

**Algorithm 4. (The ICP Algorithm [2])**

Compute the unit eigenvector  $q_R \in \mathbb{R}^4$  corresponding to the largest eigenvalue of the matrix  $Q(W)$  defined in (2.19), and set

$$R^k = \begin{bmatrix} q_0^2 + q_1^2 - q_2^2 - q_3^2 & 2(q_1 q_2 + q_0 q_3) & 2(q_1 q_3 - q_0 q_2) \\ 2(q_1 q_2 - q_0 q_3) & q_0^2 + q_2^2 - q_1^2 - q_3^2 & 2(q_2 q_3 + q_0 q_1) \\ 2(q_1 q_3 + q_0 q_2) & 2(q_2 q_3 - q_0 q_1) & q_0^2 + q_3^2 - q_1^2 - q_2^2 \end{bmatrix}$$

and

$$p^k = \bar{y} - R^k \bar{x}^k$$

**Algorithm 5. (Menq's Algorithm [25])**

Menq's algorithm computes the transformation update  $g^k = (p^k, R^k)$  based on Gauss-Newton method. First, generalized inverse is computed to give

$$R = \begin{bmatrix} r_{11} & r_{12} & r_{13} \\ r_{21} & r_{22} & r_{23} \\ r_{31} & r_{32} & r_{33} \end{bmatrix} = (YY^T)^{-1}(YX^T) \quad (2.26)$$

where

$$Y = [\hat{y}_1, \hat{y}_2, \dots, \hat{y}_n]$$

$$X = [\hat{x}_1^k, \hat{x}_2^k, \dots, \hat{x}_n^k]$$

However, the matrix in (2.26) is not necessary in  $SO(3)$ , so Euler angle approximation is obtained,

$$\beta = \text{atan2}(-r_{31}, \sqrt{r_{11}^2 + r_{21}^2})$$

$$\alpha = \text{atan2}(r_{21}/\cos\beta, r_{11}/\cos\beta)$$

$$\gamma = \text{atan2}(r_{32}/\cos\beta, r_{33}/\cos\beta)$$

and the results are then substituted to compute the rotation matrix update  $R^k$  and

$$p^k = \bar{y} - R^k \bar{x}^k$$

**Algorithm 6. (The Hong-Tan Algorithm [21])**

The Hong-Tan algorithm represents a substantial departure from the other algorithms in which the Euclidean transformation update is computed by minimizing the sum of squared distances to the home surface points. Here, let

$$g^k = g^{k-1} e^{\hat{\xi}} \quad (2.27)$$

and  $\xi \in \mathbb{R}^6$  is computed by minimizing the sum of squared distances to the tangent plane to  $S_i$  at  $x_i^k$ , i.e., the function

$$\mathcal{E}(\xi) = \sum_{i=1}^n \langle (g^k)^{-1} y_i - x_i^k, n_i^k \rangle^2. \quad (2.28)$$

The system of linear equations from which  $\xi \in \mathbb{R}^6$  is solved is given by

$$\boxed{A\xi = b} \quad (2.29)$$

where

$$A = \begin{bmatrix} \sum_{i=1}^n (y_i^{k-1} \times n_i^k)(n_i^k)^T & \sum_{i=1}^n (y_i^{k-1} \times n_i^k)(y_i^{k-1} \times n_i^k)^T \\ \sum_{i=1}^n n_i^k(n_i^k)^T & \sum_{i=1}^n n_i^k(y_i^{k-1} \times n_i^k)^T \end{bmatrix}$$

and

$$b = \begin{bmatrix} \sum_{i=1}^n (y_i^{k-1} \times n_i^k) \langle y_i^{k-1} - x_i^k, n_i^k \rangle \\ \sum_{i=1}^n \langle y_i^{k-1} - x_i^k, n_i^k \rangle n_i^k \end{bmatrix}$$

Using Gauss elimination in the above equation to solve for  $\xi$  yields the desired transformation update  $g^k$ .

All but the Hong-Tan algorithm will be collectively referred to as the least squares algorithms. Local convergence of the least squares algorithms is given by the following theorem.

**Theorem 2.6.1.** *Assume that  $(g^0, x^0)$  is chosen so that the function  $\mathcal{E}$  has only one critical point  $(g^*, x^*)$  which is a local minimum in the region*

$$U : \{(g, x) \in SE(3) \times S : \mathcal{E}(g, x) \leq \mathcal{E}(g^0, x^0)\},$$

where  $S = S_1 \times \cdots \times S_n$  and  $x = (x_1, \cdots, x_n)$ . Then the sequence of points  $(g^k, x^k)$  generated by the least squares algorithms converges to  $(g^*, x^*)$ .

**Proof:** By using any of the least squares algorithms for computing  $g^k$  from  $x^k$  for  $k \geq 1$ , we can assume that  $g^k = \phi(x^k)$ , where  $\phi : S \rightarrow SE(3)$  is a continuous map. By the construction of the algorithm, we have

$$\mathcal{E}(g^{k-1}, x^{k-1}) \geq \mathcal{E}(g^{k-1}, x^k) \geq \mathcal{E}(g^k, x^k), \quad k \geq 1. \quad (2.30)$$

Set  $\mathcal{E}^k = \mathcal{E}(g^k, x^k)$ . Then  $\{\mathcal{E}^k\}$  is monotonically decreasing and bounded from below. Thus,  $\mathcal{E}^k \rightarrow \mathcal{E}^\infty$  as  $k \rightarrow +\infty$  for some  $\mathcal{E}^\infty \geq 0$ .

Consider now the sequence  $\{(g^{k-1}, x^k)\}$  in  $U$ . It is easy to see that  $U$  is compact. Thus the sequence  $\{(g^{k-1}, x^k)\}$  has a convergent subsequence  $\{(g^{k_j-1}, x^{k_j})\}$  converging to a point  $(\bar{g}, x^\infty) \in U$ . Set  $g^\infty = \phi(x^\infty)$ . Then  $g^{k_j} \rightarrow g^\infty$  as  $j \rightarrow +\infty$  because  $\phi$  is continuous, and consequently  $\mathcal{E}(g^\infty, x^\infty) = \mathcal{E}^\infty$ . We claim that  $\bar{g} = g^\infty$ . Indeed, we know from (2.30) that  $\mathcal{E}(g^{k_j-1}, x^{k_j}) \rightarrow \mathcal{E}^\infty$  as  $j \rightarrow +\infty$ . Thus

$$\mathcal{E}(\bar{g}, x^\infty) = \mathcal{E}^\infty = \mathcal{E}(g^\infty, x^\infty).$$



On the other hand, we know from the proof of Theorem 2.4.1 that the function  $\mathcal{E}(\cdot, x^\infty)$  has only one (global) minimum point which is  $g^\infty$ . Thus  $\bar{g} = g^\infty$ .

We now show that  $(g^\infty, x^\infty) = (g^*, x^*)$ . By the way  $x^{k+1}$  is constructed from  $g^k$  and  $x^k$ , we have  $\frac{\partial}{\partial x} \mathcal{E}(g^{k+1}, x^{k+1}) = 0$  for each  $j$ . By letting  $j$  go to  $+\infty$ , we get  $\frac{\partial}{\partial x} \mathcal{E}(g^\infty, x^\infty) = 0$ . But we also have  $\frac{\partial}{\partial g} \mathcal{E}(g^\infty, x^\infty) = 0$  by the definition of  $g^\infty$ . Thus  $(g^\infty, x^\infty)$  is a critical point of  $\mathcal{E}$  in  $U$ , and so it must be  $(g^*, x^*)$ .

We now show that the whole sequence  $\{(g^k, x^k)\}$  converges to the local minimum point  $(g^*, x^*)$ . If not, then there exists an open neighborhood  $U_0$  of  $(g^*, x^*)$ ,  $U_0 \subset U$ , such that an infinite subsequence of  $\{(g^k, x^k)\}$  lies in  $U \setminus U_0$ . Again since  $U$  is compact, this infinite subsequence of  $\{(g^k, x^k)\}$  must have a convergent subsequence  $\{(g^{m_j}, x^{m_j})\}$ . The limit point of  $\{(g^{m_j}, x^{m_j})\}$  lies outside  $U_0$ , so it can not be  $(g^*, x^*)$ . On the other hand, the sequence  $\{(g^{m_j-1}, x^{m_j-1})\}$  has a convergent subsequence. By applying our earlier arguments to this convergent subsequence, we see that the limit point of  $\{(g^{m_j}, x^{m_j})\}$  must be  $(g^*, x^*)$ . This is a contradiction. Hence the whole sequence  $\{(g^k, x^k)\}$  converges to  $(g^*, x^*)$ .  $\square$

## 2.7 The Localization Algorithms with Global Convergence

Theorem (2.6.1) indicates that with improper initial conditions, both the Variational and the Tangent Algorithms can lead to local minima or incorrect solutions. Simulation studies performed on workpieces with sculptured surfaces showed [6] that the two algorithms can recover true solutions for initial orientation errors as large as 45 degrees. For large orientation errors, however, the Hong-Tan algorithm can be violently divergent. To fully automate the process of workpiece localization and reduce human interference errors, it is desirable in practice to have globally convergent algorithms. For this we make the following observations:

- The value of the objective function near the true solution, modular measurement and machining errors, should be small. Also, the change of the Euclidean transformation,  $\xi \in \mathbb{R}^6$ , defined by

$$e^{\hat{\xi}} = g_{k+1}^{-1} g_k$$

should be small near the true solution;

- Small perturbations can be used to bring an algorithm out of local minima;
- Instead of a single initial condition, a set of initial conditions uniformly covering the entire rotation space can be used until the global minimum is achieved.

Incorporating the above observations in Algorithm 1 in the last section, we obtain a globally convergent algorithm for workpiece localization. A flow chart illustrating the procedure of the algorithm is given in Figure 2.7. Initial conditions in translation are generated by simply setting  $p_0 = \bar{y}$ . For orientations we let  $(\alpha, \beta, \gamma)$  be the yaw-pitch-roll angles. Since each of the original algorithms can handle at least 45 degrees of orientation error, we assume that  $\beta$  is estimated with an error of 45 degrees. A set of initial conditions in orientation are then generated as in Table 2.1.

Initial conditions for  $(u_i, v_i)$  in solving for the home surface points  $x_i^k$  also have important implications on the algorithms. We use the method described in the last section to choose them so as to guarantee the nearest points to be found.

**Algorithm 7. (Global Localization Algorithm)**

**Input:** Measurement points  $y_i, i = 1, \dots, n$ ;

CAD model of the workpiece;

**Output:** Euclidean transformation  $g^* = (R^*, p^*)$ .

**Step 0:** (a) Set  $k = 0$ ;

(b) Take initial values  $\alpha_0, \beta_0, \gamma_0$  from Table 2.1 to obtain  $g_0 = (R^0, p^0)$ ;

(c) Compute  $x_i^0, i = 1, \dots, n$ ;

(d) Compute  $\mathcal{E}_0$ ;

**Step 1:** (a) Compute updated transformation  $g_{k+1}$ ;

(b) Compute  $x_i^{k+1}, i = 1, \dots, n$ ;

(c) Calculate  $\mathcal{E}_{k+1}$ ;

(d) If the results satisfy the globally convergence criteria, then exit;

Else if  $\mathcal{E}_{k+1}$  is a local minimum, then add perturbation and return to Step

Angles	Initial orientation values							
$\alpha_0(^{\circ})$	45	45	45	45	135	135	135	135
$\beta_0(^{\circ})$	45	45	45	45	45	45	45	45
$\gamma_0(^{\circ})$	45	135	-45	-135	45	135	-45	-135
$\alpha_0(^{\circ})$	-45	-45	-45	-45	-135	-135	-135	-135
$\beta_0(^{\circ})$	45	45	45	45	45	45	45	45
$\gamma_0(^{\circ})$	45	135	-45	-135	45	135	-45	-135

Table 2.1: Initial orientation states

1(a).

Else set  $k=k+1$  and return to Step 1(a).

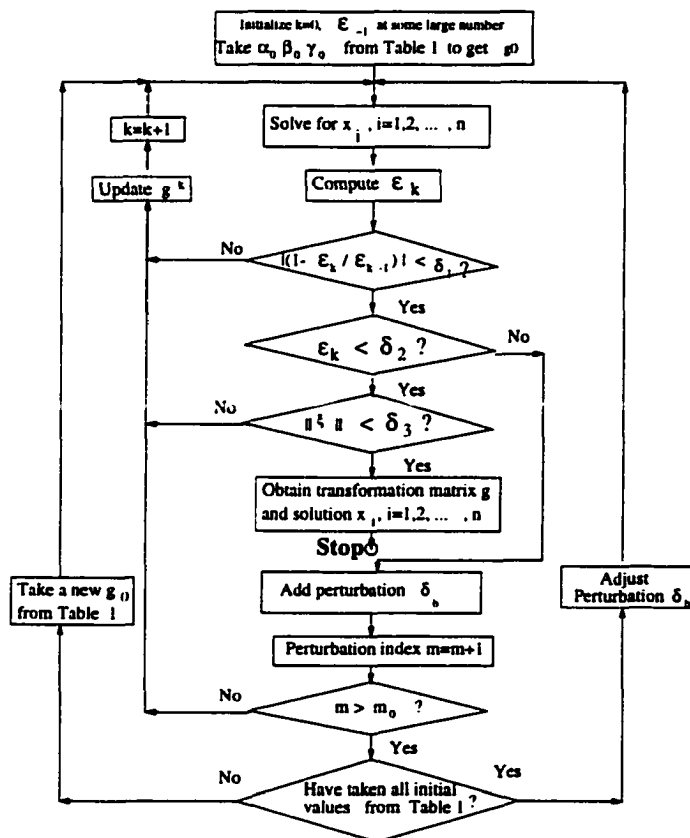


Figure 2.7: Flow chart of the global localization algorithms

## 2.8 Performance Analysis of Localization Algorithms

Critical issues to consider when adopting the above approach in a real manufacturing environment are: (1) reliability and accuracy of workpiece localization and (2) process time, which should be substantially less than the time taken to set up a workpiece. Affecting the reliability and the accuracy of workpiece localization are probing accuracy, locations of measured points, the number of measurement points, and localization algorithms used. While localization algorithms is a key factor affecting the performance of a localization system. In this section, we study and analyze, along with extensive simulation results, the performance of the localization algorithms in terms of robustness with respect to variations of initial conditions, accuracy and computational efficiency of localization results.

Figure 2.8 and 2.9 show the workpieces used in the simulation study. Workpiece A is a 2.5D object having a total of 3 conic faces. Workpiece B is a turbine blade from a Royce-Royce engine. The CAD model of the workpiece was designed using Pro/Engineer software and the IGES files were sent to a Pentium PC for simulation experiments. The IGES database of the part consists of 10 sculptured surfaces in NURBS representation.

Measurement data were simulated as follows: (i) A total of 70 points relative to  $C_M$  were chosen uniformly from the surfaces of each of the workpieces; (ii) A known transformation was applied to these points to get the measurement points relative to  $C_W$ ; and (iii) random noise with a normal distribution  $N(\mu, \sigma^2)$  was added to the data to simulate measurement and dimensional errors. The mean value  $\mu$  of the distribution depends on the particular measurement process whereas a nonzero  $\mu$  indicates measurement bias. The variance  $\sigma^2$  depends on the particular machining process such as milling or grinding [33]. How the statistical parameters as well as the sampling process affect reliability and accuracy of the localization solutions is studied in [7, 25, 32]. In our simulation experiments, we choose different amounts of errors in measurement data to verify the influence of the errors on the performance of localization results. In addition, we also analyze whether the algorithms amplify the errors or not.

Let  $g_a = (p_a, R_a) \in SE(3)$  and  $g_e = (p_e, R_e) \in SE(3)$  be, respectively, the actual

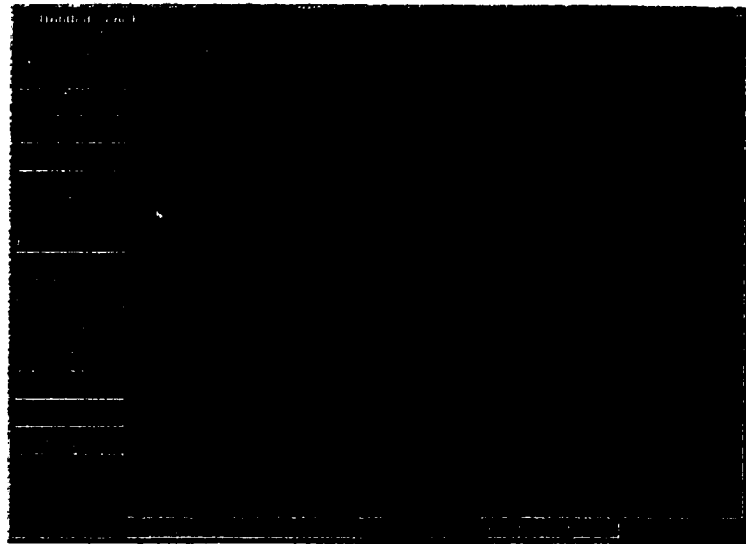


Figure 2.8: Shading model of a 2.5D Workpiece (A)

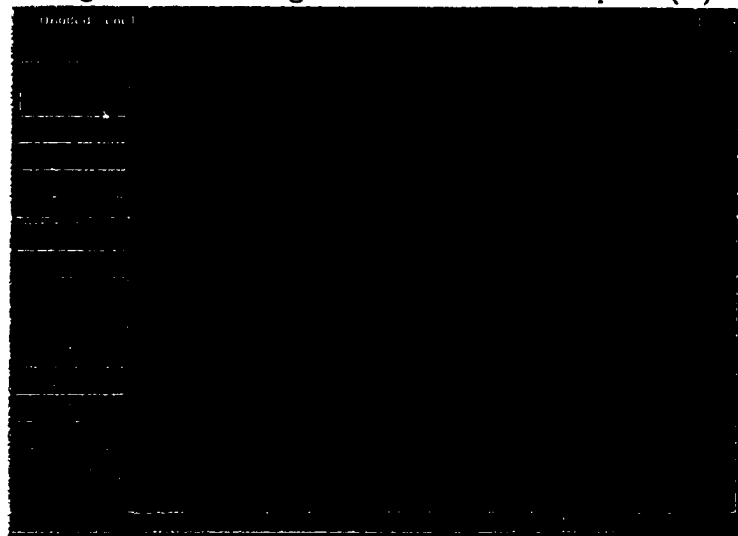


Figure 2.9: Shading model of a turbine blade(Workpiece B)

and estimated Euclidean transformations. We define the rotational and translational errors to be

$$\mathcal{E}_R = |\theta|, \quad \text{where } e^{\hat{\omega}\theta} = R_e^T R_a, \quad \|\omega\| = 1$$

and

$$\mathcal{E}_p = \|p_e - p_a\|$$

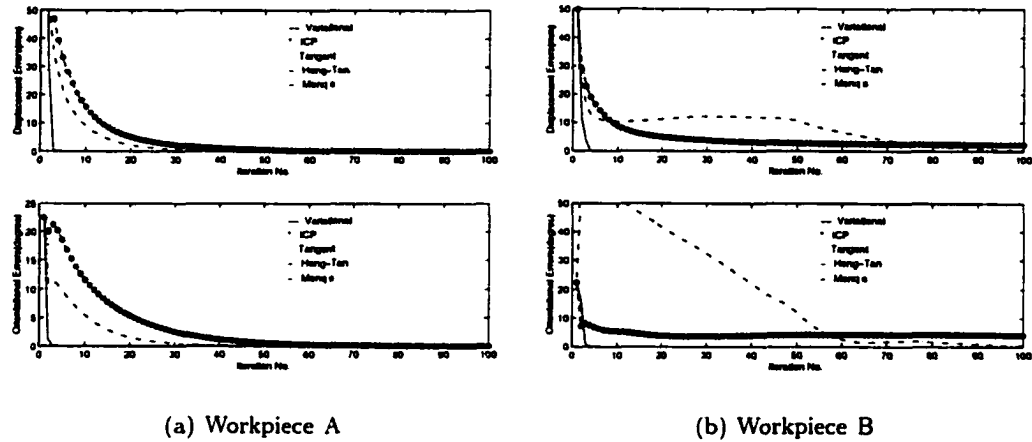
### 2.8.1 Robustness

In the first set of simulation experiments, we study the *robustness* property of the localization algorithms with respect to variations in initial condition. For this we choose a set of 30 measurement points from the data set of 70 and apply it to all algorithms. The initial conditions are set such that  $p^0 = \bar{y}$  and  $R^0$  is varied stepwise from zero degree to an angle about the equivalent axis  $\omega_a$  of the actual orientation  $R_a$  at which the algorithm fails to converge or converges to a local minimum.

Figure 2.10 plots orientational and translational errors computed with each of the algorithms as a function of the number of iterations. It was observed that all algorithms converged successfully for orientation errors as large as 60 degrees for workpiece A and 30 degrees for workpiece B. When the orientational error exceeds this range, however, the algorithms could converge to a local minima or diverge. The ICP and the Tangent algorithms have slightly better robustness property for these workpieces than the other algorithms. Figure 2.11 shows the convergence region for each of the algorithms.

### 2.8.2 Global Convergence

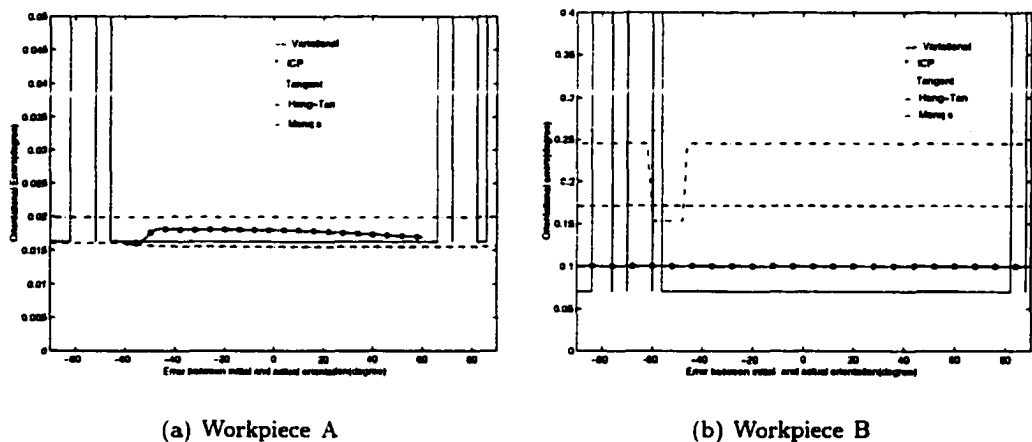
We tested the global convergence of the algorithms with globally convergent algorithm, where the updated Euclidean transformation is computed by either the Variational, the Tangent or the Hong-Tan methods. For this we choose a set of 35 measurement points from the data set of 70 and apply it to all algorithms. We varied the actual transformation over a wide range for both workpieces. By properly choosing the termination conditions and perturbations, and using the initial conditions in Table 2.1, each of the algorithms becomes globally convergent, i.e., they are all successful in recovering the actual transformations. We repeated the experiments



(a) Workpiece A

(b) Workpiece B

Figure 2.10: A profile of convergence by each of the algorithms, where the Hong-Tan algorithm converges in a few iterations.



(a) Workpiece A

(b) Workpiece B

Figure 2.11: Regions of convergence in terms of the maximal orientation errors for each of the algorithms

Actual transformation						HTA		VA		TA	
$\alpha$	$\beta$	$\gamma$	$p_x$	$p_y$	$p_z$	$\mathcal{E}_R$	$\mathcal{E}_p$	$\mathcal{E}_R$	$\mathcal{E}_p$	$\mathcal{E}_R$	$\mathcal{E}_p$
50	-45	-150	100	-100	100	0.020	0.038	0.134	0.204	0.358	0.371
150	0	150	100	-100	100	0.051	0.043	0.292	0.323	0.219	0.276
70	-45	70	100	-100	100	0.043	0.083	0.120	0.110	0.304	0.324
-70	40	-70	100	-100	100	0.036	0.091	0.167	0.207	0.346	0.417
-30	-30	-30	100	-100	100	0.069	0.033	0.085	0.145	0.277	0.370
-150	0	150	100	-100	100	0.046	0.017	0.115	0.171	0.300	0.386
170	20	-170	100	-100	100	0.025	0.049	0.190	0.242	0.362	0.403
120	40	120	100	-100	100	0.018	0.011	0.142	0.188	0.362	0.403

Table 2.2: Transformation errors of the three algorithms at various actual transformations for Workpiece B. Unit of orientation error: degree; unit of translation error: mm. HTA: Hong-Tan algorithm, VA: Variational algorithm, TA: Tangent algorithm.

with different number of measurement points, the results were similar.

Table 2.2 shows some typical simulation results for Workpiece B. In this simulation experiment, we choose  $\mu = 0.002$  and  $\sigma = 0.01$ .

### 2.8.3 Accuracy

We first compare the accuracy of several localization algorithms, then analyze the influence of errors on the accuracy of the algorithms.

The accuracy of an algorithm is defined by the orientational errors  $\mathcal{E}_R$  and translational errors  $\mathcal{E}_p$  after the algorithm has been applied to a workpiece. We consider that under the same termination conditions and with the same measurement data, which of the localization algorithms will yield the most accurate results? Figure 2.12 plots the estimation errors for each of the algorithms as a function of the number of measurement points.

From the figure we see that the Hong-Tan algorithm has a better accuracy property than the other algorithms when using the measurement points sampled from the sculptured surfaces of the turbine blade to do the localization. The five algorithms have similar localization accuracy when the measurement points are sampled from the planar or cylinder surfaces. Thus under the same conditions, workpieces with simple geometries can be localized more reliably and with better accuracy than workpieces with complicated geometries. Figure 2.13 displays the estimation errors for the Hong-Tan algorithm in terms of the number of measurement points with



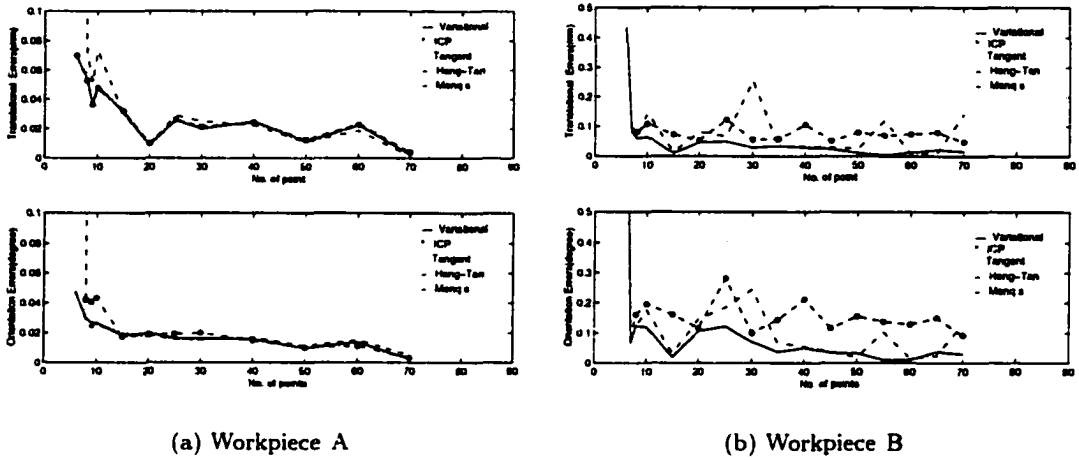


Figure 2.12: Accuracy of estimation achieved by each of the algorithms as a function of the numbers of measurement points

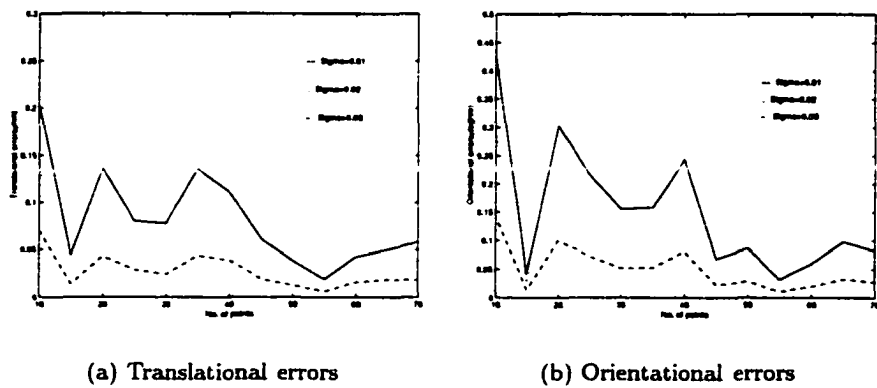


Figure 2.13: Transformation errors versus the number of measurement points, where the mean of the measurement noises is 0.002 and the variances of the measurement noises are  $\sigma = 0.01, 0.02$  and  $0.03$ , respectively

three different errors in measurement points  $\mu = 0.002$  and  $\sigma_1 = 0.01$ ,  $\sigma_2 = 0.02$  and  $\sigma_3 = 0.03$ , respectively. From this figure we see that transformation errors increase as the errors in the measurement data increases. However, the Hong-Tan algorithm does not amplify the errors in the measurement data. Simulation results show that the other algorithms also have the similar property.

### 2.8.4 Computational efficiency

Table 2.3 and 2.4 show the computational time versus the number of measurement points for Workpiece A and B obtained using the five algorithms. In the simulation  $(\alpha_0, \beta_0, \gamma_0) = (-20, -20, -20)$  (degree) and  $p_0 = \bar{y}$ . For workpieces having conic faces such as Workpiece A computational efficiency of each of the localization algorithms was quite satisfactory. The corresponding computational efficiency test result for workpiece A and Workpiece B are displayed in Figure 2.14, where the vertical axes correspond to computation time in second and the horizontal axes correspond to the number of measurement points. Based on the simulation results we have the following observations:

- Computational time in general increases with the number of measurement points. However, with less than 10 points longer computation time is required as more iterations are necessary to achieve the same accuracy.
- *Hong-Tan algorithm is substantially faster than the other algorithms, by at least an order of magnitude.* This is due to the fact that Hong-Tan algorithm minimizes the minimal value of the objective function in (2.28). The other algorithms have comparable computational efficiency.
- For workpieces with sculptured surfaces computational efficiency can be improved by probing one or more planar faces, if possible.

## 2.9 Conclusion

In this chapter, we presented a geometric theory for a unified treatment of localization of general 3-dimensional workpieces where points from their finished surfaces

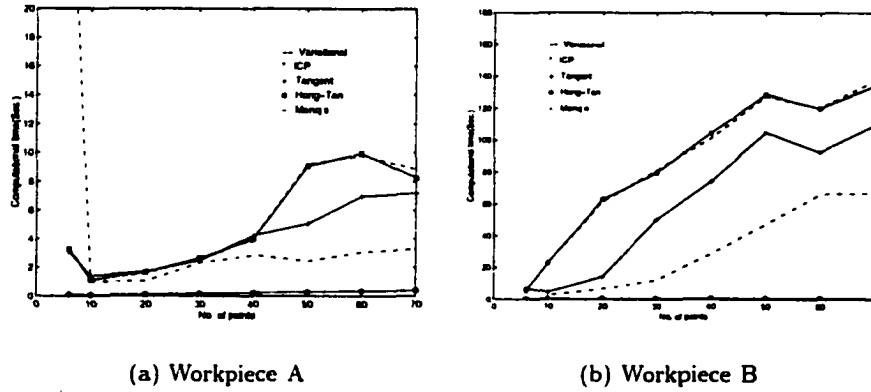


Figure 2.14: Computational time versus the number of measurement points.

No. of Points	Computational time of algorithms(s)				
	Variational	ICP	Tangent	Hong-tan	Menq's
6	3.35	3.24	3.08	0.10	90.4
10	1.1	1.1	1.37	0.05	0.98
20	1.59	1.65	1.70	0.11	1.04
30	2.53	2.64	2.47	0.17	2.31
40	4.01	3.96	4.23	0.22	2.86
50	9.18	9.06	5.05	0.27	2.42
60	9.78	9.94	6.97	0.33	3.07
70	8.35	8.24	7.2	0.39	3.30

Table 2.3: Computational time of the five algorithms for Workpiece A

No. of Points	Computational time of algorithms(s)				
	Variational	ICP	Tangent	Hong-tan	Menq's
6	5.33	5.44	6.92	0.22	**
10	23.0	22.9	4.56	0.11	2.58
20	61.6	62.9	14.1	0.22	6.70
30	81.1	79.5	50.2	0.39	11.9
40	101.2	104.5	74.3	0.50	28.7
50	127.8	128.7	104.9	0.55	**
60	120.3	120.1	92.6	0.66	66.4
70	137.3	134.1	109.7	0.39	3.30

Table 2.4: Computational time of the five algorithms for Workpiece B

fully constrain the rigid motions of the workpieces. First we presented the basic concepts and the properties of the Euclidean group  $SE(3)$ . Then we formulated the localization problem for a general 3-dimensional workpiece as a minimization problem on the Euclidean group  $SE(3)$ . The objective function minimized here is the sum of squared errors from transformed measurement points to their corresponding home surface points. The mathematics of the least squares problem was analyzed in detail where necessary conditions are derived for the optimal Euclidean transformation and the optimal home surface points. We described in detail an iterative method for solving the LSP and showed how different considerations in updating the Euclidean transformation lead to different algorithms.

Using the proposed global convergence techniques, the local algorithms become more robust relative to variation of initial conditions. The performance analysis of the localization algorithms showed that the Hong-Tan algorithm has better accuracy property and is substantially faster than the other four algorithms by at least an order of magnitude. The five algorithms do not amplify the errors in measurement data.



## Chapter 3

# Reliability Analysis for Workpiece Localization

### 3.1 Introduction

The localization algorithms described in Chapter 2 provide a way of determining the transformation that defines position and orientation of a workpiece. However, since there is a finite error associated with each measurement point, the result of localization might be inaccurate or unreliable. The reliability of localization results also depends on probing locations of measurement points, the number of measurement points, measurement errors and surface quality of measured surfaces of a workpiece. Therefore verifying whether the localization results are reliable or not is an important problem that needs to be considered in practical applications. If we can determine whether the localization results satisfy the specified requirements in an automated process or not, then the reliability of the localization system can be guaranteed. In this chapter, we will first analyze factors affecting the reliability of the localization results, then present a method to verify the reliability of the localization results using statistical analysis. Using these methods, for example, we first measure less points (must be greater than 6) from surfaces of a workpiece, then compute the transformation of the workpiece by the localization algorithms, and analyze the reliability of the results. If the results are not reliable, then we measure more points and repeat the above process until the results satisfy the specified requirements. Finally, we can obtain the satisfactory and reliable results with least localization time.

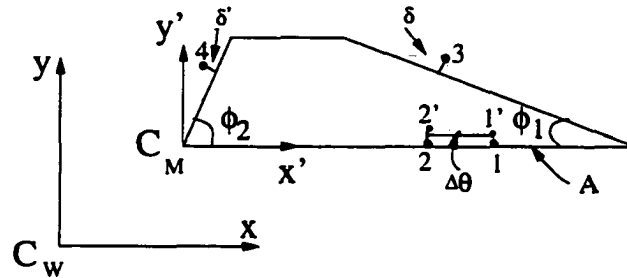


Figure 3.1: A trapezoid to be localized

### 3.2 Choice of Measurement Points

First of all, we use the following example to intuitively describe the reliability of localization with respect to the location of the measurement points and the associated errors.

To determine the orientation of the trapezoid as shown in Figure 3.1, we measure two points, say points 1 and 2, on edge A of the trapezoid. Due to measurement errors, which are usually a function of the accuracy of the probe and the quality of the workpiece surfaces, points 1 and 2 may deviate from the edge, say to points 1' and 2'. Obviously, if the two points are very close to each other, the orientation of the trapezoid computed on the basis of the two points is not orientationally reliable, because the orientational error  $\Delta\theta$  is proportional to the measurement errors divided by the distance between the measurement points 1' and 2'. Thus, the orientational reliability of the computed orientation will be better if the distance between the two measurement points is larger.

Assume now that a point on another edge of the trapezoid is probed to determine the translation of the trapezoid. If point 3, which does not lie on the edge due to measurement errors, is probed, a small measurement error along the normal direction of that edge might cause a large computed translational error along the  $x'$  direction because the translational error is proportional to  $\delta$ , where  $\delta$ , as shown in Figure 3.1, is the measurement error at point 3 divided by  $\sin(\phi_1)$ . In other words, translational reliability of the computed translation along the  $x'$  direction is not sufficiently reliable because  $\phi_1$  is small. If point 4 on another edge is probed and the point has the same magnitude of measurement error as point 3, then translational

reliability along the  $x'$  direction would be increased because  $\phi_2$  is larger than  $\phi_1$ , i.e,  $\delta'$  is less than  $\delta$ .

Similarly, for workpiece localization in 3-dimensions, the measurement errors and locations of measurement points affect the accuracy of the solutions of the localization algorithms as well. That is, the reliability of the solutions of the localization algorithms critically depends on the location of the measurement points and associated the measurement errors. If the computed transformation of a workpiece is not translationally or orientationally reliable, then there is the possibility that the computed transformation does not satisfy a specified accuracy requirement. Thus, it is necessary to verify the reliability of localization.

For dimensional inspection, an important issue is to determine the number and locations of points which represent quality characteristics of a measured feature. One hopes to obtain the maximal information using a minimum of cost and time in an inspection process. Kim[39] introduced a sampling scheme using the concept of surface faceting. The principle of the scheme is to find a set of triangular facets which represent a surface within the accuracy of approximation and to employ their vertices as inspection points. This method concentrates on the complex region and the sample size is controlled simply by the approximation accuracy, which is physically related to the inspection conditions such as tolerance specification, manufacturing and measuring machine performance. The authors claimed that this sampling strategy is more effective than the uniform sampling for the same sample size.

For a given accuracy of a manufacturing process and a tolerance specification, Menq[25] determined the minimal number of inspection points on a surface through hypothesis test and then distributed these points uniformly over the surface in a latticed manner. Woo[51] derived mathematically the sample size from number theory and obtained their locations using Hammersley points in a parametric domain. His simulation results showed that much more points should be used for more complex surfaces to achieve the same level of inspection accuracy. Pahk[53] suggested a hybrid distribution method for a given sample size. The distribution depends on the curvatures of a surface. Cross sections were used to inspect hypoid gears and turbine blades by Litvin[52] and Bojanic[54].



If workpiece localization is used in automatic workpiece setup and the inspection information is not required in the process of setting up a workpiece, the strategy of determining the number and locations of measurement points may be different from one in the dimension inspection. As described in the example of the trapezoid, the measurement points may be uniformly distributed. And they should be separated as far away as possible on surfaces.

In this thesis, we focus on the study of workpiece localization algorithms which are applied in automatic workpiece setup. Thus the points we used are uniformly distributed. The number of measurement points was chosen in different sets in order to compare the influence of the points number on the accuracy of the localization results under the same measurement errors.

### 3.3 Reliability Analysis with F-test Method

In this section, we develop a reliability analysis algorithm with the F-test method in statistics.

#### 3.3.1 Analysis of error bounds

Denote by  $\mathcal{E}_*$  the global minimum of the objective function with optimized  $g^* = (R^*, p^*)$  and  $x_i^*, n_i^*$ ,  $i = 1, \dots, n$ .

$$\mathcal{E}_* = \sum_{i=1}^n \langle (R^*)^T (y_i - p^*) - x_i^*, n_i^* \rangle^2. \quad (3.1)$$

Due to the errors in measurement data, the computed optimal solution  $g^*$  differs from the actual transformation  $g_a = (R_a, p_a)$ . Since  $\mathcal{E}_*$  is the minimum at  $g^*$ , we have

$$\mathcal{E}_a = \sum_{i=1}^n \langle R_a^T (y_i - p_a) - x_i^*, n_i^* \rangle^2 \geq \mathcal{E}_*.$$

Assume that  $\mathcal{E}_*$  is increased by  $\mathcal{E}_1$  such that  $\mathcal{E}_a = \mathcal{E}_* + \mathcal{E}_1$ , where  $\mathcal{E}_1$  is due to translational error and/or orientational error. Again, we assume that the deviations of transformed measurement points  $(g^*)^{-1}y_i$  and  $g_a^{-1}y_i$  from the home surface,  $\langle (R^*)^T (y_i - p^*) - x_i^*, n_i^* \rangle$  and  $\langle R_a^T (y_i - p_a) - x_i^*, n_i^* \rangle$  for  $i = 1, 2, \dots, n$ , are both normally distributed. Then,  $\mathcal{E}_*$  and  $\mathcal{E}_a$  are the sample variances of the samples  $\langle (R^*)^T (y_i - p^*) - x_i^*, n_i^* \rangle$  and  $\langle R_a^T (y_i - p_a) - x_i^*, n_i^* \rangle$  for  $i = 1, 2, \dots, n$ , respectively.

Thus, we can use the F-test in statistical analysis to compare the variances of the two samples. Let

$$F = \frac{\mathcal{E}_a}{\mathcal{E}_*}$$

be the F-distribution. The two samples have the same size  $n$  and both of them have six unknown parameters. Thus, they have the same degree of freedom,  $l = n - 6$ .

Since we know that  $\mathcal{E}_a \geq \mathcal{E}_*$ , the null and alternative hypotheses can be formulated:

$$\begin{aligned} H_0 &: \sigma_1^2 = \sigma_2^2 \\ H_1 &: \sigma_1^2 > \sigma_2^2 \end{aligned}$$

this is a one-tailed test. From the critical values table of the F-distribution, we can find the critical value  $F_{\epsilon(l,l)}$  at the  $\epsilon$ -level corresponding to the degrees of freedom  $(l, l)$ , where  $\epsilon$  is a confidence limit[63]. Then, when  $F > F_{\epsilon(l,l)}$ , there is an evidence in favor of  $H_1$ . By the definition of the critical value of the F-distribution[63], we have

$$P(F > F_{\epsilon(l,l)}) = \epsilon.$$

This also means that

$$P(F < F_{\epsilon(l,l)}) = 1 - \epsilon. \quad (3.2)$$

In other words, the probability that  $F = (\mathcal{E}_* + \mathcal{E}_1)/\mathcal{E}_* < F_{\epsilon(l,l)}$  is equal to  $(1 - \epsilon)$ . Using this result, we can compute the upper bound of the translational error and the orientational error. These error bounds can be used to verify whether the solutions of the localization algorithms satisfy a specified accuracy requirement or not; i.e., whether the solutions can be used reliably to localize the workpiece or not.

### 3.3.2 Translational reliability

Let  $\delta p = (\delta p_x, \delta p_y, \delta p_z)^T$  be the translational errors in  $x, y$  and  $z$ -axis directions, respectively, and

$$d = \sqrt{\delta p_x^2 + \delta p_y^2 + \delta p_z^2}$$

the translational error. Then, the deviation of the measurement points from their home surfaces along the normal directions is given by

$$\begin{aligned} \varepsilon_p &= \begin{bmatrix} \varepsilon_p^1 \\ \varepsilon_p^2 \\ \vdots \\ \varepsilon_p^n \end{bmatrix} = \begin{bmatrix} n_1^T \\ n_2^T \\ \vdots \\ n_n^T \end{bmatrix} \delta p \\ &:= N_p \cdot \delta p, \end{aligned}$$

where  $n_i$  is the surface normal of  $S_i$  at  $x_i^*$ . Let  $\mathcal{E}_p = \varepsilon_p^T \varepsilon_p$ , then

$$\begin{aligned} \mathcal{E}_p &= \delta p^T N_p^T N_p \delta p \\ &:= \delta p^T J_p \delta p. \end{aligned}$$

Therefore, the value of the objective function at  $x_i^*$  and  $g_a$  due to the translational errors is given by  $\mathcal{E}_a = \mathcal{E}_* + \mathcal{E}_p$ . From (3.2), we have

$$P(\mathcal{E}_a/\mathcal{E}_p < F_{\epsilon(t,l)}) = 1 - \epsilon.$$

That is, the probability of

$$\mathcal{E}_p/\mathcal{E}_* < (F_{\epsilon(t,l)} - 1) \quad (3.3)$$

is equal to  $(1 - \epsilon)$ .

**Proposition 3.3.1.** *Translational error  $d$  along any direction is bounded by*

$$d \leq ((F_{\epsilon(t,l)} - 1)\mathcal{E}_*/\lambda_p)^{\frac{1}{2}}, \quad (3.4)$$

where  $\lambda_p$  is the smallest eigenvalue of  $J_p$ . The worst case direction, in which the translational error is the largest, is the direction of the eigenvector corresponding to  $\lambda_p$ .

**Proof.** Assume that the eigenvalues of  $J_p$  are arranged in the order:  $\lambda_1 \geq \lambda_2 \geq \lambda_3$ . Since  $J_p$  is symmetric and positive definite, the  $\lambda_i$ 's are positive, and the corresponding unit eigenvectors  $v_1, v_2, v_3$  are orthogonal with each other. Then

$$J_p v_i = \lambda_i v_i \quad \text{for } i = 1, 2, 3.$$

Since the eigenvectors span  $\mathbb{R}^3$ ,  $\delta p \in \mathbb{R}^3$  can be written as a linear combination of the  $v_i$ 's:

$$\delta p = a_1 v_1 + a_2 v_2 + a_3 v_3$$

Using  $d^2 = \delta p^T \delta p = a_1^2 + a_2^2 + a_3^2$ , yields

$$\mathcal{E}_p = \delta p^T J_p \delta p \geq d^2 \lambda_3.$$

Let  $\lambda_p = \lambda_3$ , we have

$$d < ((F_{\epsilon(l,l)} - 1) \mathcal{E}_* / \lambda_p)^{\frac{1}{2}}.$$

□

### 3.3.3 Rotational reliability

Let  $R_a \in SO(3)$  be the actual orientation matrix, then the computed orientation matrix is

$$R_* (\hat{w}, \theta) = e^{\hat{w}\theta} R_a,$$

where  $\theta$  is the orientational error about an axis  $w \in \mathbb{R}^3$ . If  $\theta$  is small, then

$$R_* \cong (I + \hat{w}\theta) R_a.$$

The deviation of the measurement points from their home surfaces along their normal directions as a result of the orientational error is given by

$$\begin{aligned} \varepsilon_r &= \begin{bmatrix} \varepsilon_r^1 \\ \varepsilon_r^2 \\ \vdots \\ \varepsilon_r^n \end{bmatrix} = - \begin{bmatrix} (n_1 \times q_1)^T \\ (n_2 \times q_2)^T \\ \vdots \\ (n_n \times q_n)^T \end{bmatrix} w\theta \\ &:= N_r \cdot w\theta, \end{aligned}$$

where  $q_i = R_a^T y_i$ . Let  $\mathcal{E}_r = \varepsilon_r^T \varepsilon_r$ , then

$$\begin{aligned} \mathcal{E}_r &= w^T N_r^T N_r w\theta^2 \\ &:= w^T J_r w\theta^2. \end{aligned} \tag{3.5}$$

Therefore, due to the orientational error  $\theta$ ,  $\mathcal{E}_a = \mathcal{E}_* + \mathcal{E}_r$ . From the F-test, we have

$$\mathcal{E}_r / \mathcal{E}_* < (F_{\epsilon(l,l)} - 1). \tag{3.6}$$

**Proposition 3.3.2.** *Rotational error  $\theta$  along any direction is bounded by*

$$\theta < ((F_{\epsilon(t,l)} - 1)\mathcal{E}_s/\lambda_r)^{\frac{1}{2}}, \quad (3.7)$$

where  $\lambda_r$  is the smallest eigenvalue of  $J_r$ . The most unreliable direction in orientation is the eigenvector direction corresponding to  $\lambda_r$ .

**Proof.** It follows from that of Prop. 3.3.1.

Using the results of Prop. 3.3.1 and Prop. 3.3.2, we can estimate the upper bound of the translational error  $d$  and the orientational error  $\theta$ , and verify whether the upper bounds are less than the specified accuracy. If not, those solutions can not be used reliably to localize the workpiece. We need to either increase measurement points or choose other proper measurement locations until the reliability test is satisfied.

### 3.3.4 Simulations

Fourteen sets of measurement data with different measurement noise ( $\mu_1 = 0.02, \sigma_1 = 0.03$ ) and ( $\mu_2 = 0.02, \sigma_2 = 0.01$ ) were used to test the reliability of localization for Workpiece B. Setting the confidence limit defined in last section to  $\epsilon = 0.01$ , we computed the upper bounds of the translational errors and the orientational errors by the Hong-Tan algorithm. This means that the confidence of the upper bound errors is 99%.

The results are shown in Figure 3.2. From the figure we see that the upper bound errors increase when the measurement noise increases, while they decrease as the number of measurement points increases. When measurement points are spread out uniformly, the corresponding upper bound of the errors becomes smaller than that of the measurement points which are not spread out uniformly.

## 3.4 Conclusion

This chapter provided an effective method to analyze the reliability of workpiece localization. we discussed the factors affecting the accuracy and reliability of localization results. Using the F-test method in statistics, we analyzed the translational and rotational reliability of localization results. We provided the error upper bounds

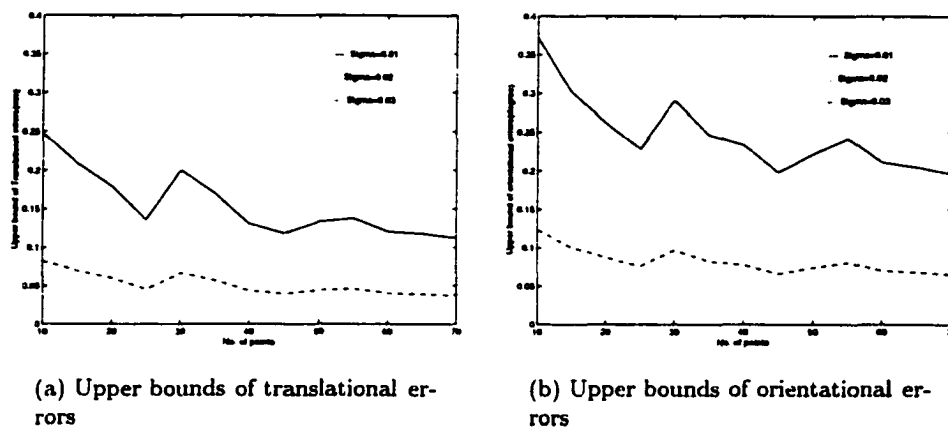


Figure 3.2: Upper bounds of transformation errors versus the number of measurement points.

of localization results, with which we can verify whether the upper bounds are less than the specified accuracy or not. Finally, we showed simulation results to demonstrate the effectiveness of the analysis methods.



## Chapter 4

# Localization of Partially Finished Workpieces

### 4.1 Introduction

A partially finished workpiece has both finished and unfinished surfaces and points from the finished surfaces are inadequate to fully constrain the rigid motions of the workpiece. In this case, the localization problem is to align the CAD model with the workpiece such that all points measured on the finished surfaces of the workpiece match closely to corresponding surfaces on the model while all unmachined surfaces lie outside the model to guarantee the presence of material to be machined at a later time. Applications of the study include workpiece setup, refixturing and dimensional inspections in a flexible manufacturing environment.

In this chapter, we first introduce some basic concepts on the homogeneous space of the Euclidean group and its geometric properties, which will be used to formulate and solve the hybrid problem. Then, we discuss the hybrid problem using two kinds of methods, the least squares method and the minimax method. In addition, we formulate the envelopment problem under different considerations. In the least squares method, the machine volumes on unfinished surfaces should satisfy specified requirements. While in the minimax method, the problem is formulated to find maximal machine volumes existing on unfinished surfaces. Finally, we compare the performance of the two methods in terms of accuracy and tolerance values.



## 4.2 Configuration Spaces of Symmetric Features

Observe first that when the finished surfaces of a workpiece are inadequate to fully constrain the rigid motions of the workpiece, the set of free motions remaining while aligning the finished surfaces with the corresponding surfaces on the model must form a subgroup  $G_0$  of the Euclidean group,  $SE(3)$ . The subgroup  $G_0$  is referred to as the symmetry subgroup of the finished surface(s). For instance, if the finished surface is a plane, then  $G_0$  consists of translations on the plane and rotations about the normal of the plane. On the other hand, if the finished surfaces are two intersecting planes, then  $G_0$  consists of translations along the line of intersection. Since rigid motions in  $G_0$  do not change the location and orientation of the finished surfaces, the configuration space in which the finished surfaces are aligned with the corresponding surfaces of the model may be identified with the homogeneous space  $SE(3)/G_0$ .

In Chapter 2, we introduced that  $SE(3)$  is identified with the configuration space of a feature, where an element  $g = (p, R) \in SE(3)$  represents the position and orientation of the feature.

If the feature is symmetric, however, then it has a symmetry subgroup  $G_0 \subset SE(3)$ , and two Euclidean transformations  $g_1$  and  $g_2$  such that  $g_1^{-1} \cdot g_2 \in G_0$  would leave the feature unchanged. If  $g_1^{-1} \cdot g_2 \in G_0$ , then  $g_1$  is said to be equivalent to  $g_2$ , i.e.,  $g_1 \sim g_2$ . For example, if the feature is the  $xy$ -plane, then the set of transformations of the form

$$G_0 = \{e^{(\lambda_1 \hat{\epsilon}_1 + \lambda_2 \hat{\epsilon}_2 + \lambda_3 \hat{\epsilon}_3)} \mid \lambda_1, \lambda_2, \lambda_3 \in \mathbf{R}\} \quad (4.1)$$

leave the  $xy$ -plane unchanged. In other words, the set of transformations of the form  $gG_0$ , for some  $g \in SE(3)$ , represents the same location of the feature and the configuration space of the symmetric feature is more properly identified with the set

$$SE(3)/G_0 = \{gG_0 \mid g \in SE(3)\}. \quad (4.2)$$

$SE(3)/G_0$  is called the (left) coset space. It can be equipped with a topology and a differentiable structure to make it a differentiable manifold of dimension (6 –

$\dim(G_0)$  [4]. In fact,  $SE(3)/G_0$  admits a transitive action of  $SE(3)$  given by

$$\psi : SE(3) \times SE(3)/G_0 \longrightarrow SE(3)/G_0 : (h, gG_0) \longmapsto h \cdot gG_0. \quad (4.3)$$

Physically,  $h \cdot gG_0$  is the plane obtained by applying the rigid motion  $h \in SE(3)$  to the plane  $gG_0$ . In other words,  $gG_0$  can itself be thought of as the plane obtained by applying the rigid motion  $g = (p, R) \in SE(3)$  to the  $xy$ -plane. It is the plane which passes through the point  $p \in \mathbb{R}^3$  with the normal vector  $v_3 \in \mathbb{R}^3$ , where  $R = (v_1, v_2, v_3) \in SO(3)$ . An action is said to be transitive if any two planes are related by a rigid transformation and a differentiable manifold with a transitive action of a Lie group is called a homogeneous space[4] of the Lie group.

We give three additional examples to illustrate the generality of the approach.

**Example 4.2.1. (Two intersecting planes)**

Consider two planes for which the line of intersection is given by the  $z$ -axis. The group of rigid motions which leave the two intersecting planes unchanged is the set of translations along the  $z$ -axis,

$$G_0 = \{e^{\lambda \hat{\xi}_3} | \lambda \in \mathbb{R}\}. \quad (4.4)$$

Thus, the configuration space of the two intersecting planes is given by  $SE(3)/G_0$ , which is a homogeneous space of dimension 5.

**Example 4.2.2. (A cylinder)**

Consider the case when the finished surface is a cylindrical surface. A cylindrical feature is represented by its axis, that is, a line in  $\mathbb{R}^3$ . Let the reference configuration of the cylinder be the  $z$ -axis, then, the set of rigid motions leaving the cylinder unchanged consists of rotations about and translations along the axis,

$$G_0 = \{e^{(\lambda_1 \hat{\xi}_3 + \lambda_2 \hat{\xi}_6)} | \lambda_1, \lambda_2 \in \mathbb{R}\} \quad (4.5)$$

and the configuration space of the cylinder is given by the 4-dimensional homogeneous space  $SE(3)/G_0$ . Given a point  $gG_0 \in SE(3)/G_0$  with  $g = (p, R)$ , we have all information on the location of the cylinder, where  $p \in \mathbb{R}^3$  is a point on the axis and  $v_3 \in \mathbb{R}^3$  is the direction vector of the cylinder.

**Example 4.2.3. (A helicoid surface)**

Consider the case when the finished surface is a helicoid surface as shown in Figure 4.1. A helicoid feature is represented by its axis and pitch. Let the reference configuration of the helicoid be the  $z$ -axis, then, the symmetry subgroup  $G_0^*$  of the helicoid surface is a one-parameter subgroup of  $SE(3)$  generated by a twist  $\hat{\xi}_6 \in se(3)$  with a pitch  $p_\xi \in (0, \infty)$  along the  $z$ -axis, i.e.,

$$G_0^* = \{e^{\hat{\xi}_6 \theta} \mid \theta \in [0, 2\pi]\}$$

and the configuration space of the helicoid surface is given by the 5-dimensional homogeneous space  $SE(3)/G_0$ .

In addition to the above examples, there exist other types of symmetric features, e.g., spheres, cones and tabulated surfaces, and we refer to Figure 4.1 for the symmetry subgroups of these features. In machining practices, however, usually a plane or a pair of parallel planes, a pair of intersecting planes or a cylindrical surface is used as reference (or finished) surfaces. Three planes in general position would uniquely determine the Euclidean transformation of the workpiece and make the problem a (regular) localization problem. Thus, the three cases considered above would account for all possibilities of finished surfaces in general machining practices.

The exponential coordinates on  $SE(3)$  can be extended to give a coordinate system on its homogeneous space  $SE(3)/G_0$ . Let  $\mathcal{G}_0$  be the Lie algebra (i.e., the tangent space to  $G_0$  at the identity) of  $G_0$ , and choose a complementary space  $\mathcal{M}_0$  so that

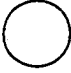
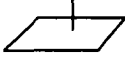






$$\mathcal{M}_0 \oplus \mathcal{G}_0 = se(3). \quad (4.6)$$

For example, let  $G_0$  be the symmetry group of the  $xy$ -plane given by (4.1) and  $\{\xi_i\}_{i=1}^6$  the canonical basis of  $\mathbb{R}^6$ , then

$$\mathcal{G}_0 = \text{span}\{\hat{\xi}_1, \hat{\xi}_2, \hat{\xi}_6\} \quad (4.7)$$

and

$$\mathcal{M}_0 = \text{span}\{\hat{\xi}_3, \hat{\xi}_4, \hat{\xi}_5\}.$$

Features	Symbols	Symmetry Group $G_1$	Configuration Space $Q$	Description of symmetry group	Dimension
Sphere		$SO(3)$	$SE(3)/G_0^0 = T(3)$	Rotation about the center of sphere	3
Plane		$SE(2)$	$SE(3)/G_0^0$	Rotation about the normal of the plane & translation in the plane	3
Cylinder		$SO(2) \times T(1)$	$SE(3)/G_0^1$	Rotation about and translation along the axis	4
Intersecting planes		$T(1)$	$SE(3)/G_0^1$	Translation along the direction of the intersecting line of two planes	5
Cone (resolved surface)		$SO(2)$	$SE(3)/G_0^1$	Rotation about the axis of cone	5
Tabular Surface		$T(1)$	$SE(3)/G_0^1$	Translation along the sweeping direction	5
Sculptured Surface without symmetry		$I$	$SE(3)$	Identity element	6
Helicoid Surface		$G_0^1$	$SE(3)/G_0^1$	Screw motion along the helicoid axis	5

Note:  $G_0^1$  is a one-parameter subgroup of  $SE(3)$  generated by a twist  $\xi \in se(3)$  with a pitch  $p \in (0, \infty)$  along the helicoid axis

Figure 4.1: Symmetric features and their configuration spaces

It is not difficult to see that the map

$$\begin{aligned} \Psi : \mathcal{M}_0 \oplus \mathcal{G}_0 &\longrightarrow SE(3) \\ (\hat{m}, \hat{\lambda}) &\longmapsto \exp(\hat{m}) \exp(\hat{\lambda}) \end{aligned} \quad (4.8)$$

is a local diffeomorphism. Let  $g \in SE(3)$  be a representative of  $gG_0$ , and decompose  $g$  into

$$g = \exp(\hat{m}) \exp(\hat{\lambda}), \quad \hat{m} \in \mathcal{M}_0, \hat{\lambda} \in \mathcal{G}_0.$$

Let  $r = \dim(\mathcal{G}_0)$ ,  $\bar{r} = 6 - r$ ,  $(\hat{\eta}_1, \dots, \hat{\eta}_r)$  a basis of  $\mathcal{G}_0$  and  $(\hat{\eta}_{r+1}, \dots, \hat{\eta}_6)$  a basis of  $\mathcal{M}_0$ . Express

$$\hat{m} = m_1 \hat{\eta}_{r+1} + \dots + m_r \hat{\eta}_6$$

for some  $m = (m_1, \dots, m_r) \in \mathbb{R}^r$ . Then, the map

$$\begin{aligned} \tilde{\Psi} : SE(3)/G_0 &\longrightarrow \mathbb{R}^r \\ gG_0 &\longmapsto (m_1, \dots, m_r) \end{aligned} \quad (4.9)$$

is well defined, i.e., independent of the choice of representative elements, and gives the desired coordinate system for  $SE(3)/G_0$ . Note that restricting the exponential map of  $SE(3)$  to  $G_0$  defines the exponential coordinates on  $G_0$ .

Note that if  $P$  and  $P'$  are two elements in  $\mathcal{P}$  such that  $P' = g_0P$ , where  $\mathcal{P}$  denote the space of all planes in  $\mathbb{R}^3$  and  $g_0$  is a Euclidean transformation, then, their symmetry subgroups are related by

$$G_{P'} = g_0G_Pg_0^{-1}.$$

Furthermore, their Lie algebras are related by the Adjoint transformation

$$\mathcal{G}_{P'} = Ad_{g_0}(\mathcal{G}_P),$$

and

$$\hat{\lambda}' = Ad_{g_0}\hat{\lambda} = \lambda_1 Ad_{g_0}\hat{\xi}_1 + \lambda_2 Ad_{g_0}\hat{\xi}_2 + \dots + \lambda_r Ad_{g_0}\hat{\xi}_r.$$

where

$$Ad_{g_0} = \begin{bmatrix} R_0 & \hat{p}_0 R_0 \\ 0 & R_0 \end{bmatrix}.$$

Correspondingly their complementary spaces at the point  $g_0 \in SE(3)$  are simply related by

$$\mathcal{M}_{P'} = Ad_{g_0}(\mathcal{M}_0).$$

In other words, the symmetry subgroups of two different planes in  $\mathcal{P}$  are simply conjugate of each other, and all have the same dimension. This allows us to simply choose any plane in  $\mathcal{P}$  for our study and the rest can be obtained by the adjoint transformation.

## 4.3 Hybrid Localization/Envelopment Problem

### 4.3.1 Problem Formulation

The hybrid workpiece localization/envelopment problem is to align the CAD model with the workpiece such that all points measured on the finished surfaces of the

workpiece match closely to corresponding surfaces on the model while all unmachined surfaces lie outside the model to guarantee the presence of material to be machined at a later time. We now give a geometric formulation of the problem.

Denote by  $C_M$  the model frame of the workpiece and  $C_W$  the machine reference frame. Let  $\{y_i \in \mathbb{R}^3, i = 1, \dots, n\}$  be a set of points measured from the finished surfaces of the workpiece, and  $\{z_i \in \mathbb{R}^3, i = 1, \dots, m\}$  be a set of points measured from the unfinished surfaces.  $y_i$  and  $z_i$  are expressed in  $C_W$ . Let  $G_0(\lambda)$  be the symmetry subgroup of the finished surfaces, parameterized by  $\lambda \in \mathbb{R}^r$  (i.e.,  $\lambda \in \mathbb{R}^r$  is the exponential coordinates of  $G_0$ ), and  $g \in SE(3)$  the Euclidean transformation taking  $C_M$  to  $C_W$ . We assume that the correspondence between a measured point with its home surface is known (e.g., register the home surface when performing the measurement), and the CAD model of the workpiece is available.

**Problem 4.3.1. (The hybrid localization/envelopment problem)**

Find  $g_0 \in SE(3)/G_0$  so that the following objective function is minimized

$$\mathcal{E}_l(g) = \sum_{i=1}^n \langle g^{-1}y_i - x_i, n_i \rangle^2, \quad (4.10)$$

where  $x_i \in \mathbb{R}^3$  is the corresponding point of  $y_i$  on its home surface  $S_i$ , i.e., a point on  $S_i$  which is nearest to  $g^{-1}y_i$ , and  $n_i \in \mathbb{R}^3$  the unit normal vector to the home surface at  $x_i$ . Let

$$g(\lambda) := g_0 G_0(\lambda) \quad (4.11)$$

and find  $g(\lambda) \in SE(3)$  to minimize the objective function

$$\mathcal{E}_e(g(\lambda)) = \sum_{i=1}^m \langle g^{-1}(\lambda)z_i - w_i, n_i \rangle^2, \quad (4.12)$$

subject to the inequality constraints

$$\langle g^{-1}(\lambda)z_i - w_i, n_i \rangle \geq \delta_i \quad i = 1, \dots, m, \quad (4.13)$$

where  $w_i \in \mathbb{R}^3$  is the corresponding point of  $z_i$  on its home surface  $\bar{S}_i$ ,  $n_i$  the outward unit normal vector of  $\bar{S}_i$  at  $w_i$ , and  $\delta_i$  the machine volume of the unfinished surface  $\bar{S}_i$ .

Note that in (4.10) and (4.12), the residual error we choose to minimize is the signed distance from the measurement point  $g^{-1}y_i$  (or  $g^{-1}z_i$ ) to the corresponding home surface, i.e., the projection of  $g^{-1}y_i - x_i$  along the outward unit normal vector  $n_i$ . In contrast to the usual approach which minimizes the sum of squared errors of  $\|g^{-1}y_i - x_i\|^2$  [19, 25], this formulation leads to faster and more accurate algorithms as concluded in Chapter 2. Furthermore, the hybrid problem under this formulation is decomposed into a symmetric localization problem on  $SE(3)/G_0$ , i.e., to match closely the measured points on the finished surfaces of the workpiece to the corresponding surfaces on the model, and an envelopment problem on  $G_0$ , i.e., to align the workpiece with the model along the directions of  $G_0$  so that all unmachined surfaces lie outside the model. This decomposition is made possible by the decomposition formula (4.11). The inequality constraints in (4.13) ensure that the distance from the measured points on each unfinished surface to the corresponding surface of the model is greater than the volume of the material to be removed (see Figure 4.2). If the finished surfaces of the workpiece fully constrain the rigid motion of the workpiece then  $G_0 = I$ , the identity transformation, and the problem becomes simply the regular localization problem as discussed in Chapter 2. On the other hand, if there are no finished surfaces, then the problem becomes an envelopment problem on  $SE(3)$ .

Since the two problems are decoupled we can first solve the symmetric localization problem and then use the solution  $g_0$  in (4.10) as an initial condition to solve the envelopment problem. The solution of the later problem will then automatically ensure simultaneous satisfaction of the requirement imposed by the hybrid problem.

### 4.3.2 The Symmetric Localization Algorithm

When finished surfaces of a workpiece can not fully constrain the rigid motions of the workpiece and the finished features have symmetric properties, then the general localization problem becomes a symmetric Localization problem. The paper[16] discusses the symmetry localization problem and develops a Fast Symmetric Localization(FSL) algorithm for the problem (4.10). Here we review the Fast Symmetric Localization (FSL) algorithm.

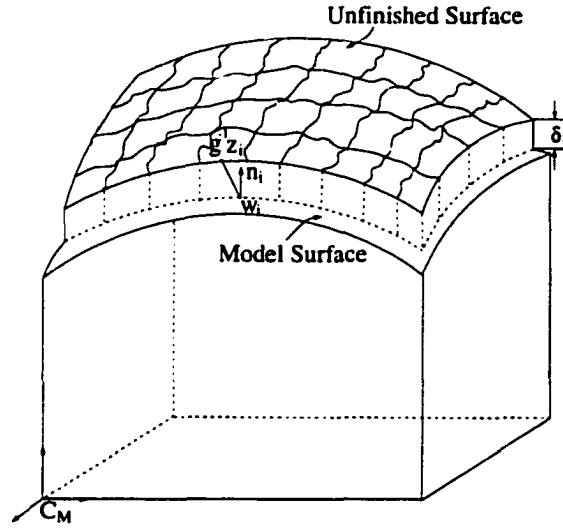


Figure 4.2: Signed distance from a transformed measurement point to the corresponding home surface

The FSL algorithm starts with an initial condition  $g^0 \in SE(3)/G_0$  to compute the corresponding point  $x_i^0$  and  $n_i^0$  of  $(g^0)^{-1}y_i$ ,  $i = 1, \dots, n$ , by minimizing the function

$$\langle (g^0)^{-1}y_i - x_i, n_i \rangle^2$$

subject to the home surface constraints. For most symmetric surfaces, an explicit solution of the above problem can be obtained [16]. With  $(g^k, x_i^k)$  computed, the Euclidean transformation update  $g^{k+1} \in SE(3)/G_0$  is then computed as follows: First, let  $\{\hat{\eta}_1, \dots, \hat{\eta}_r\}$  be a basis of  $\mathcal{G}_0$ , the Lie algebra of  $G_0$ , and choose a basis  $\{\hat{\eta}_{r+1}, \dots, \hat{\eta}_6\}$  for the complementary subspace  $\mathcal{M}_0$  of  $\mathcal{G}_0$ , i.e.,

$$\mathcal{M}_0 \oplus \mathcal{G}_0 = se(3).$$

Express  $g^{k+1}$  in terms of  $g^k$  as

$$g^{k+1} = g^k e^{(m_1 \hat{\eta}_{r+1} + \dots + m_r \hat{\eta}_6)}, \quad (4.14)$$

and find  $m = (m_1, \dots, m_r) \in \mathbb{R}^r$  by minimizing the function

$$\mathcal{E}(m) = \sum_{i=1}^n \langle (g^{k+1})^{-1}y_i - x_i^k, n_i^k \rangle^2. \quad (4.15)$$



From the minimization process, a system of linear equations is obtained for  $m \in \mathbb{R}^r$

$$Am = b, \quad (4.16)$$

where  $A = (a_{ij}) \in \mathbb{R}^{r \times r}$  and  $b = (b_i) \in \mathbb{R}^r$  are given by

$$\begin{aligned} a_{ij} &= \sum_{l=1}^n s_{il}s_{jl}, & s_{ij} &= (n_j^k)^T \hat{\eta}_i x_j^k, \\ b_i &= \sum_{l=1}^n t_l s_{il}, & t_j &= (n_j^k)^T ((g^k)^{-1} y_j - x_j^k). \end{aligned}$$

Applying the solution of equation (4.16) to (4.14) gives the desired transformation update and the iteration continues until the objective function (4.10) ceases to decrease. Then, the optimal solution  $g_0$  for problem (4.10), called a representative transformation in later sections, is obtained. Note that a key point of the FSL algorithm is that the Euclidean transformation update in (4.14) is computed only along the directions of  $\mathcal{M}_0$ , as perturbations along  $\mathcal{G}_0$  would yield no useful information with the given symmetry of the problem.

**Algorithm 8. (The Fast Symmetric Localization (FSL) algorithm[16])**

**Input:** (a) Measurement data  $\{y_i\}_{i=1}^n$ ;

(b) CAD description of the finished surfaces with symmetry subgroup  $G_0$ , and a basis  $\{\hat{\eta}_{r+1}, \dots, \hat{\eta}_6\}$  for  $\mathcal{M}_0$ ;

**Output:** Optimal solution  $g_0 \in SE(3)/G_0$ ;

**Step 0:** (a) Set  $k = 0$ ;

(b) Initialize  $g^0$ ;

(c) Solve for  $x_i^0$  and  $n_i^0$ ,  $i = 1, \dots, n$ ;

(d) Calculate  $\mathcal{E}_i^0 = \sum_i \langle (g^0)^{-1} y_i - x_i^0, n_i^0 \rangle^2$ ;

**Step 1:** (a) Let  $g^{k+1} = g^k e^{(m_1 \hat{\eta}_{r+1} + \dots + m_r \hat{\eta}_6)}$  and solve from (4.16) for  $m \in \mathbb{R}^r$ ;

(b) Solve for  $x_i^{k+1}$  and  $n_i^{k+1}$ ;

(c) Calculate  $\mathcal{E}_i^{k+1}$ ;

(d) If  $(1 - \mathcal{E}_i^{k+1}/\mathcal{E}_i^k) > \epsilon$ , set  $k = k + 1$  and go to Step 1(a); Else exit and report results.

### 4.3.3 The Envelopment Algorithms

With the solution  $g_0$  of the symmetric localization algorithm as the initial condition of the envelopment problem, we solve the envelopment problem. The corresponding home surface point  $w_i^0$  and  $n_i^0$  of  $(g^0)^{-1}z_i, i = 1, \dots, m$  is computed by minimizing the function

$$\langle (g^0)^{-1}z_i - w_i, n_i \rangle^2$$

subject to the home surface constraint. Similar with the method described in Chapter 2, Newton's algorithm together with a parametric description of the home surface can be used to solve this problem.

The envelopment problem is a nonlinear constraint optimization problem. To solve it easily, we use the following method to convert the nonlinear optimization problem into a sequence of linear programming(LP) problems.

In general, the solution of a constrained minimization problem of the form

$$\min_{q \in \mathbb{R}^n} \{ \psi(q) | \phi(q) \leq 0 \} \quad (4.17)$$

where  $\psi : \mathbb{R}^n \rightarrow \mathbb{R}$  is a  $C^1$ -function and  $\phi : \mathbb{R}^n \rightarrow \mathbb{R}^m$  a set of nonlinear constraints, can be obtained by solving a sequence of linear programming (LP) problems with properly chosen initial conditions. To derive the corresponding LP problem, let  $q^k \in \mathbb{R}^n$  be an initial condition satisfying the constraints and consider

$$q^{k+1} = q^k + \bar{q} \quad (4.18)$$

where  $\bar{q} \in \mathbb{R}^n$  is a perturbation term. Computing the Taylor series expansion of  $\psi(\cdot)$  and  $\phi(\cdot)$  at  $q^k$  and retaining the first-order terms yield

$$\psi(q^{k+1}) \approx \psi(q^k) + \langle d\psi(q^k), \bar{q} \rangle$$

and

$$\phi(q^{k+1}) \approx \phi(q^k) + D\phi(q^k) \cdot \bar{q}$$

where  $d\psi(q^k) \in \mathbb{R}^{1 \times n}$  and  $D\phi(q^k) \in \mathbb{R}^{m \times n}$  are, respectively, the differential of  $\psi$  and the Jacobian of  $\phi$  at  $q^k$ . Then the solution of the LP problem

$$\min_{\bar{q} \in \mathbb{R}^n} \{ \langle d\psi(q^k), \bar{q} \rangle | \phi(q^k) + D\phi(q^k) \cdot \bar{q} \leq 0 \} \quad (4.19)$$

ensures that the constraints are satisfied while the function is minimized.

Now we apply the above method to the envelopment problem. Consider that the Euclidean transformation update is of the form

$$g^{k+1} = g^k e^{\hat{\lambda}}, \quad (4.20)$$

where

$$\hat{\lambda} = \lambda_1 \hat{\eta}_1 + \cdots + \lambda_r \hat{\eta}_r$$

and  $(\hat{\eta}_1, \dots, \hat{\eta}_r)$  is a basis of  $\mathcal{G}_0$ . Then,  $\lambda = (\lambda_1, \dots, \lambda_r) \in \mathbb{R}^r$  is computed by solving the following linear programming problem

$$\min_{\lambda \in \mathbb{R}^r} \{ \langle d\mathcal{E}_e(g^k), \lambda \rangle \mid f(g^k) + Df(g^k) \cdot \lambda \leq 0 \}, \quad (4.21)$$

where  $d\mathcal{E}_e \in \mathbb{R}^r$  is the differential of  $\mathcal{E}_e$  at  $g^k$ ,

$$f : \mathbb{R}^r \longrightarrow \mathbb{R}^m, \lambda \longmapsto \begin{bmatrix} \langle g^{-1}(\lambda)z_1 - w_1, n_1 \rangle - \delta_1 \\ \vdots \\ \langle g^{-1}(\lambda)z_m - w_m, n_m \rangle - \delta_m \end{bmatrix} \quad (4.22)$$

is the vector of constraints and  $Df \in \mathbb{R}^{m \times r}$  the Jacobian of  $f(\cdot)$ . Let  $d\mathcal{E}_e := (a_1, \dots, a_r) \in \mathbb{R}^r$ , and  $Df := (b_{ij}) \in \mathbb{R}^{m \times r}$ , then

$$\begin{aligned} a_j &= -\sum_{i=1}^m 2\beta_i \langle \hat{\eta}_j(g^k)^{-1} z_i, n_i \rangle, \\ b_{ij} &= -\langle \hat{\eta}_j(g^k)^{-1} z_i, n_i \rangle, \\ \beta_i &= \langle (g^k)^{-1} z_i - w_i^k, n_i \rangle. \end{aligned}$$

We summarize the preceding discussions into the following envelopment algorithm:

**Algorithm 9. (The Envelopment algorithm)**

**Input:** (a) Measurement data  $\{z_i\}_{i=1}^m$ ;

(b) CAD model of the workpiece and a basis  $(\hat{\eta}_1, \dots, \hat{\eta}_r)$  for  $\mathcal{G}_0$ ;

(c) A representative transformation  $g_0 \in SE(3)/G_0$  from the FSL algorithm.

**Output:** Optimal solution  $g^* \in SE(3)$  of the hybrid problem.

**Step 0:** (a) Set  $k = 0$  and  $g^0 = g_0$ ;

(b) Compute  $w_i^0$  and  $n_i^0$ ,  $i = 1, \dots, m$ ;

(c) Calculate  $\mathcal{E}_e^0 = \sum_i \langle (g_0)^{-1} z_i - w_i^0, n_i^0 \rangle^2$ ;

**Step 1:** (a) Let  $g^{k+1} = g^k e^{\hat{\lambda}}$ ,  $\hat{\lambda} \in \mathcal{G}_0$ , and solve for  $\lambda \in \mathbb{R}^r$ ;

(b) Solve for  $w_i^{k+1}$  and  $n_i^{k+1}$ ,  $i = 1, \dots, m$ ;

(c) Calculate  $\mathcal{E}_e^{k+1}$ ;

(d) If  $(1 - \mathcal{E}_e^{k+1}/\mathcal{E}_e^k) < \epsilon$  and  $\langle (g^{k+1})^{-1} z_i - w_i^{k+1}, n_i^{k+1} \rangle \geq \delta_i$ , then report the satisfactory solution  $g^* = g^{k+1}$ ; Else, set  $k = k + 1$

(e) If  $k \leq K_0$ , then go to Step 1(a); Else, report that a satisfactory solution does not exist and exit.

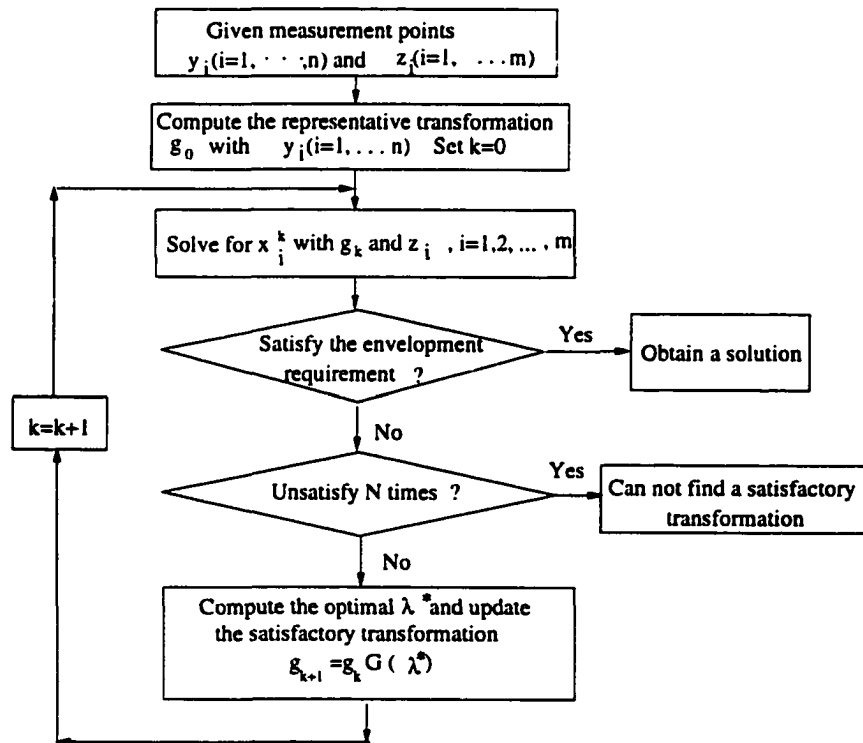


Figure 4.3: Flowchart of the hybrid localization/envelopment algorithm

#### 4.3.4 The Hybrid Algorithms

Combining the FSL algorithm and the Envelopment algorithm, and using the solution  $g_0$  of the FSL algorithm as the initial condition of the Envelopment algorithm yield the Hybrid algorithm. Figure 4.3 shows the procedure of the Hybrid algorithm.

#### 4.3.5 Simulation Results

In this section, we perform simulation studies of the proposed hybrid algorithm using two typical examples from manufacturing practices. In the simulation study, measurement data were generated by first choosing a set of points distributed uniformly on the CAD surfaces of the workpiece, next adding machine volumes to the unfinished surfaces, then applying a known Euclidean transformation to these points and adding random noise to the results. The noise data, which simulates measurement and machining errors, is assumed to be normally distributed with a mean  $\mu$  and a variance  $\sigma^2$ . Based on a particular machining process, we choose ( $\mu = 0.02, \sigma = 0.01$ ).

##### Example 4.3.1. (A workpiece with one finished surface)

We consider first the case of a workpiece having a (planar) finished surface  $S_1$  and several unfinished planar surfaces ( $\bar{S}_1, \bar{S}_2, \bar{S}_3$ ) as shown in Figure 4.4, where the dashed lines show the CAD model of the workpiece and the solid lines show the actual workpiece. The finished surface coincides with the  $xy$ -plane of the CAD frame and thus the symmetry subgroup and its complementary subspace are given by

$$G_0 = \{e^{(\lambda_1 \hat{\xi}_1 + \lambda_2 \hat{\xi}_2 + \lambda_3 \hat{\xi}_3)} \mid \lambda_1, \lambda_2, \lambda_3 \in \mathbf{R}\}$$

and

$$\mathcal{M}_0 = \text{span}\{\hat{\xi}_3, \hat{\xi}_4, \hat{\xi}_5\}.$$

Thirty points were measured from the finished surface of the workpiece and the fast symmetric localization algorithm is used to align the surface with the corresponding surface of the CAD model. Figure 4.4(a) shows the workpiece before the symmetric localization and Figure 4.4(b) shows the workpiece after the solution from the FSL algorithm has been applied to the workpiece. Note that in Figure 4.4(b) the finished

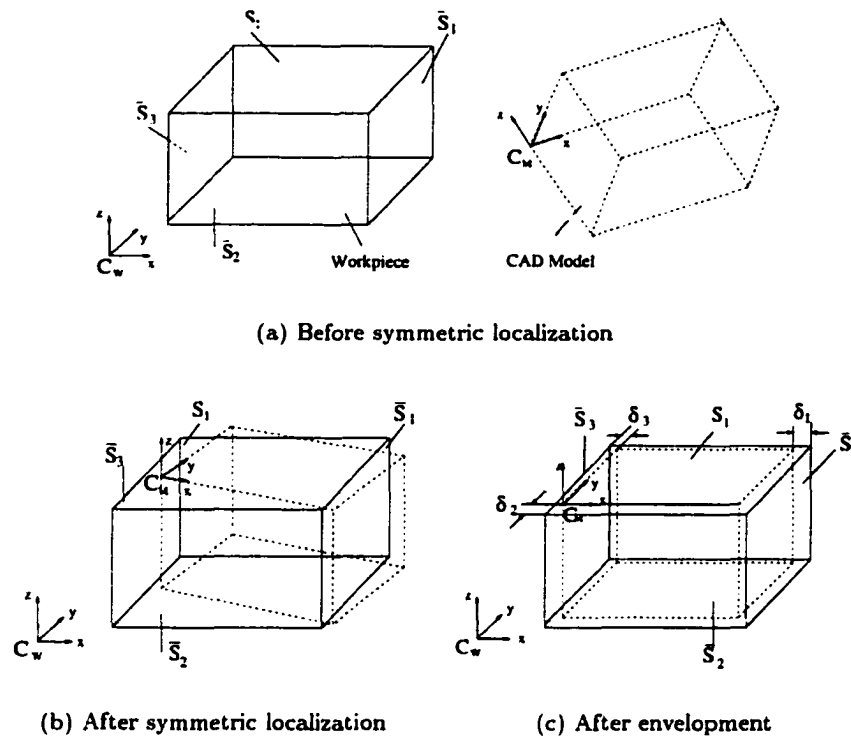


Figure 4.4: A workpiece having one finished surface

surface of the workpiece matches closely with the corresponding surface of the CAD model but the workpiece does not fully envelop the CAD model. Seventy measurement points were then measured from the unfinished surfaces of the workpiece and the Envelopment algorithm was applied to the workpiece with the solution from the FSL algorithm as the initial condition. The CAD model was finally aligned with the workpiece along the symmetry subgroup of  $S_1$  so that all measurement points from the unfinished surfaces are now outside the CAD model to guarantee the presence of materials to be machined at a later time, and the result is shown in Figure 4.4(c).

Table 4.1 gives the numeric values of the Euclidean transformation computed at different stages. The total computation time under a Pentium/166MHz is 0.04 seconds (8 iterations) for the symmetric localization algorithm and 0.06 seconds for the Envelopment algorithm.

Figure 4.5 shows that after applying the hybrid localization/envelopment algo-

Exact transformation	Initial condition
$R = \begin{bmatrix} 0.866025 & -0.500000 & 0.000000 \\ 0.500000 & 0.866025 & 0.000000 \\ 0.000000 & 0.000000 & 1.000000 \end{bmatrix}$ $p = [ 20.00 \quad 10.00 \quad 20.00 ]^T$	$R_0 = \begin{bmatrix} 0.749825 & 0.124110 & 0.649892 \\ 0.433698 & 0.649600 & -0.624441 \\ -0.499669 & 0.750078 & 0.433260 \end{bmatrix}$ $p_0 = [ -40.00 \quad 50.00 \quad 80.00 ]^T$
Solution of FSL algorithm	Solution of the Envelopment algorithm
$R_* = \begin{bmatrix} 0.173684 & -0.984808 & 0.000156 \\ 0.984808 & 0.173648 & 0.000122 \\ -0.000147 & 0.000133 & 1.000000 \end{bmatrix}$ $p_* = [ -40.251901 \quad 50.040353 \quad 20.00971 ]^T$	$R^* = \begin{bmatrix} 0.863946 & -0.503585 & 0.000156 \\ 0.503585 & 0.863946 & 0.000122 \\ -0.000147 & 0.000133 & 1.000000 \end{bmatrix}$ $p^* = [ 20.152927 \quad 10.040321 \quad 20.00971 ]^T$ $\delta_1 = 1.8, \delta_2 = 1.9, \delta_3 = 1.6$

Table 4.1: Solutions computed at different stages for Example 4.3.1

rithm to the workpiece, all measured points from all unfinished surfaces have enough machining volumes for later stages of machining.

**Example 4.3.2. (A workpiece with two finished intersecting surfaces)**

Consider next the case of a workpiece having two planar finished surfaces  $S_1$  and  $S_2$  which intersect along a line, see Figure 4.6. The symmetry subgroup of the finished surfaces is given by

$$G_0 = \{e^{\lambda \hat{\xi}_3} | \lambda \in \mathbb{R}\}$$

and the complementary space  $\mathcal{M}_0$  of  $\mathcal{G}_0$  is spanned by

$$\mathcal{M}_0 = \text{span}\{\hat{\xi}_1, \hat{\xi}_2, \hat{\xi}_4, \hat{\xi}_5, \hat{\xi}_6\}.$$

The configuration space of the symmetric localization problem is five-dimensional. Forty measurement points were taken from the finished surfaces of the workpiece to align the workpiece with the corresponding surfaces of the CAD model, and the result is shown in Figure 4.6(b). Fifty measurement points from the unfinished sculptured surface of the workpiece were used to envelop the CAD model along the symmetry subgroup of the finished surfaces, and the result is shown in Figure 4.6(c). Table 4.2 shows the transformations computed at different stages. The computational time is 0.04 seconds (9 iterations) for the symmetric localization algorithm and 0.2 seconds (3 iterations) for the Envelopment algorithm.

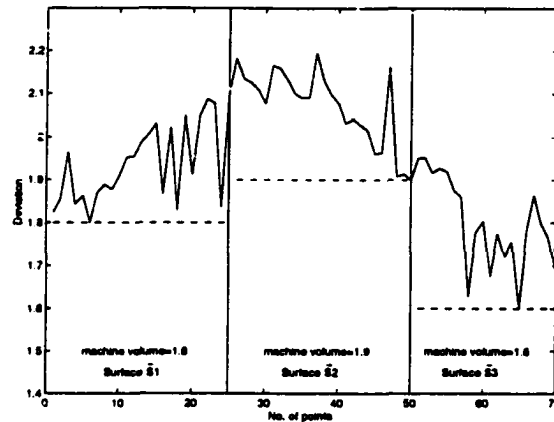


Figure 4.5: Deviations of transformed measurement points from their CAD model surfaces

In the simulation study, we also analyzed the robustness of the hybrid algorithm with respect to variations in the initial conditions. We set the initial translation to be the centroid of the measurement data and vary the orientation from  $-100$  degrees to  $+100$  degrees. The simulation results showed that the algorithm converges for all these initial conditions and is indeed robust. This reconfirmed part of our observations made in [16].

#### Example 4.3.3. (A satisfactory transformation)

A complicated workpiece, like the turbine blade shown in Figure.2.9 has three finished surfaces and two unfinished blade surfaces. We find a satisfactory transformation such that the three finished surfaces lie within their profile tolerance zones  $t = 0.03mm$  and one blade surface has at least  $0.5mm$  machine volume to be precisely machined.

In this example, the three finished surfaces can uniquely determine the representative transformation  $g_0$ . The symmetry group of the finished surfaces is identified as a unit matrix, i.e.,  $G_0 = I$ . We measure 50 points uniformly on each one of the four surfaces respectively.

Table 4.3 displays the exact and computed Euclidean transformations at the different stages. The simulation results also show that if the specified tolerance is  $t = 0.02mm$ , then a satisfactory transformation can not be obtained. This means



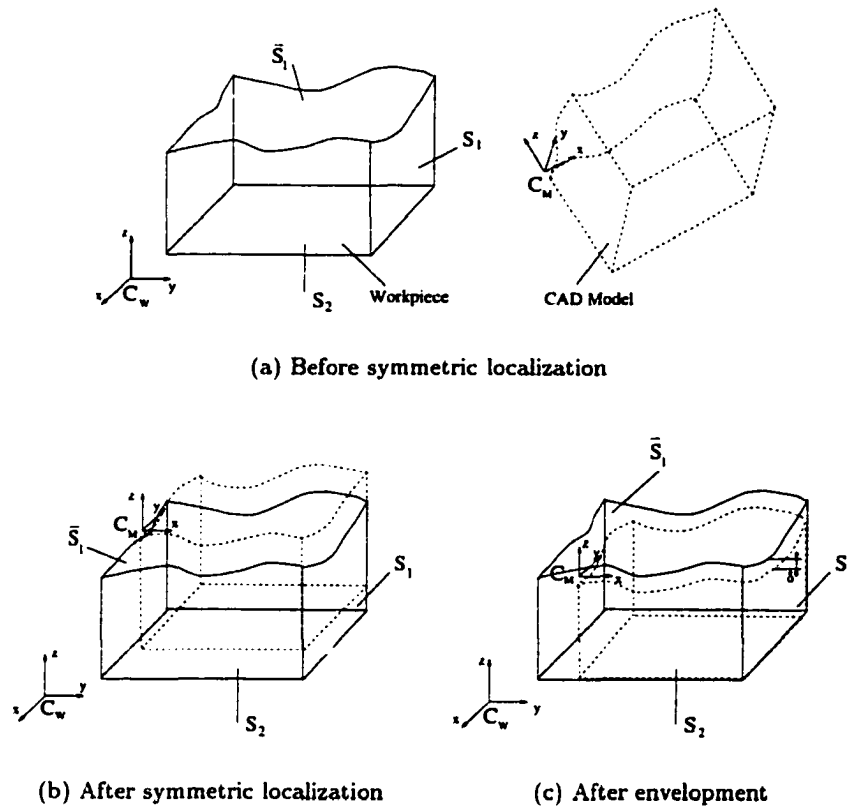


Figure 4.6: A workpiece having two intersecting finished surfaces and one sculptured unfinished surface

that the finished surfaces do not satisfy the requirements of the specified tolerance zones, a further machining is not necessary.

#### 4.4 Hybrid Localization/Inspection/Machinability Problem

In this section, we will consider the workpiece localization, the on-line inspection and the machinability problem simultaneously. The idea here is as follows: First, arbitrarily fixture a partially machined workpiece on the machine table using general purpose fixtures. Next, program a sensor to sample a number of points on the finished surfaces and unfinished surfaces of the workpiece, respectively. Then, compute the actual position and orientation of the workpiece, the tolerance zones of the fin-

Exact transformation	Initial condition
$R = \begin{bmatrix} 0.866025 & -0.500000 & 0.000000 \\ 0.500000 & 0.866025 & 0.000000 \\ 0.000000 & 0.000000 & 1.000000 \end{bmatrix}$ $p = [ 20.00 \quad 10.00 \quad 20.00 ]^T$	$R_0 = \begin{bmatrix} 0.749825 & 0.124110 & 0.649892 \\ 0.433698 & 0.649600 & -0.624441 \\ -0.499669 & 0.750078 & 0.433260 \end{bmatrix}$ $p_0 = [ -40.00 \quad 50.00 \quad 80.00 ]^T$
Solution of the FSL algorithm	Solution of the Envelopment algorithm
$R_* = \begin{bmatrix} 0.866133 & -0.499813 & 0.000657 \\ 0.499813 & 0.866133 & 0.000594 \\ -0.000866 & -0.000186 & 1.000000 \end{bmatrix}$ $p_* = [ 20.1529 \quad 9.96403 \quad 80.00 ]^T$	$R^* = \begin{bmatrix} 0.866133 & -0.499813 & 0.000657 \\ 0.499813 & 0.866133 & 0.000594 \\ -0.000866 & -0.000186 & 1.000000 \end{bmatrix}$ $p^* = [ 20.1529 \quad 9.96403 \quad 19.9604 ]^T$ $\delta_1 = 1.9$

Table 4.2: Solutions computed at different stages for Example 4.3.2

Exact transformation	$R = \begin{bmatrix} 0.866025 & -0.500000 & 0.000000 \\ 0.500000 & 0.866025 & 0.000000 \\ 0.000000 & 0.000000 & 1.000000 \end{bmatrix}$ $p = [ 20.00 \quad 10.00 \quad 20.00 ]^T$
Representative transformation	$R_0 = \begin{bmatrix} 0.866133 & -0.499813 & 0.000657 \\ 0.499813 & 0.866133 & 0.000594 \\ -0.000866 & -0.000186 & 1.000000 \end{bmatrix}$ $p_0 = [ 20.051226 \quad 9.966207 \quad 19.975242 ]^T$
Satisfactory transformation	$R^* = \begin{bmatrix} 0.865898 & -0.500221 & -0.000004 \\ 0.500221 & 0.865897 & -0.000489 \\ 0.000248 & 0.000422 & 1.000000 \end{bmatrix}$ $p^* = [ 20.005722 \quad -10.009142 \quad 19.989716 ]^T$ $t = 0.03, \delta_1 = 0.5$

Table 4.3: Solutions computed at different stages for Example 4.3.3

ished surfaces and the machinable volumes existing on the unfinished surfaces with the measurement data supplied by the sensor and the CAD model of the workpiece. If the tolerance values of the finished surfaces are satisfied the specified requirements and the unfinished surfaces have enough machinable volumes to be machined, we have obtained a satisfactory transformation which will be used to modify originally generated tool paths. Otherwise, it is unnecessary to proceed to further machining. This process makes use of general purpose fixtures and integrates the workpiece localization and on-line inspection, thus greatly accelerating machining cycles and improving product quality. In this section, we use the minimax method to formu-

late the problem. Thus, the problem becomes to match all points measured on the finished surfaces of the workpiece to corresponding CAD model surfaces with minimum zone tolerances while all unmachined surfaces lie outside the CAD model of the workpiece with maximal machinable volumes. Then, we develop a simple algorithm to solve the problem using a similar technique, the LP programming method with one used in the last section.

#### 4.4.1 Minimax Formulation of the Hybrid Problem

In this section, we use the minimax method and the differential geometric tools described in Section 4.1 to formulate the hybrid localization/inspection/machinability problem.

Denote by  $C_M$  the model frame of a workpiece and  $C_W$  a machine reference frame. Let  $\{y_{ji} \in \mathbb{R}^3, i = 1, \dots, n_j\}$  be a set of points measured from the  $j^{\text{th}}$  finished surface of the workpiece, and  $\{z_{ji} \in \mathbb{R}^3, i = 1, \dots, n_j\}$  be a set of points measured from the  $j^{\text{th}}$  unfinished surface.  $n_j$  is the number of the measurement points from the  $j^{\text{th}}$  surface.  $y_{ji}$  and  $z_{ji}$  are expressed in  $C_W$ . Let  $SE(3)/G_0$  be the configuration space of the finished surfaces  $S_j (j = 1, \dots, l_1)$ , and  $G_0(\lambda)$  the symmetry subgroup of the finished surfaces, parameterized by  $\lambda \in \mathbb{R}^r$  (i.e.  $\lambda \in \mathbb{R}^r$  is the exponential coordinates of  $G_0$ ), and  $g \in SE(3)$  the Euclidean transformation taking  $C_M$  to  $C_W$ . We assume that the correspondence between a measured point and its home surface is known (e.g., register the home surface when performing the measurement), and the CAD model of the workpiece is available.

Let  $t_j, j = 1, \dots, l_1$  be the tolerance zone of each finished surface of a workpiece and  $d(g, y)$  be a signed distance of a transformed point  $g^{-1}y$  to the surface  $S$ . Then the tolerance zone of each finished surface is defined by

$$t_j = \min_{g \in SE(3)/G_0} (\max_{y_j \in S_j} d(y_{ji}, g) - \min_{y_j \in S_j} d(y_{ji}, g)) \quad (4.23)$$

where  $j = 1, \dots, l_1$  is the number of the finished surfaces. If  $g^{-1}y$  lies outside the workpiece, then  $d(y, g) \geq 0$ , otherwise  $d(y, g) \leq 0$ .

Apparently, to find an optimal  $g$  which satisfies  $t_j$  in (4.23), we need to solve a minimax function which is a discontinuous and computationally undesirable. Let

$Q = SE(3)/G_0 \times \underbrace{\mathbb{R} \times \cdots \times \mathbb{R}}_{l_1} = SE(3)/G_0 \times \mathbb{R}^{l_1}$ . Then, by extending the configuration space to  $Q$ , the above minimax function can be transformed into a nonlinear inequality constraint optimization problem. Using this way, the hybrid localization/inspection/machinability problem can be described as follows.

**Problem 4.4.1. (The localization/inspection/machinability problem)**

Find  $(g, t_1, \cdots, t_{l_1}) \in Q$  so as to minimize the function

$$\mathcal{E}_s(g, t_1, \cdots, t_{l_1}) = \sum_{j=1}^{l_1} w_j t_j \quad (4.24)$$

subject to the constraints

$$\begin{aligned} 0 &\leq t_j \\ -t_j &\leq d_j(y_{ji}, g) \leq t_j, \quad j = 1, \cdots, l_1 \end{aligned} \quad (4.25)$$

where

$$d_j(y_{ji}, g) = \langle g^{-1}y_{ji} - x_{ji}, n_{ji} \rangle, \quad i = 1, \cdots, n_j$$

$w_j$  is the weight determined according to the specified tolerance value of each finished surface,  $x_{ji} \in \mathbb{R}^3$  is the corresponding optimal home surface point of  $y_{ji}$ , i.e., a point on its home surface of  $y_{ji}$  which is nearest to  $g^{-1}y_{ji}$ ,  $l_1$  is the number of the finished surfaces and  $n_j$  is the number of measurement points on the  $j^{\text{th}}$  finished surface. Then, the solutions  $t_j (j = 1, \cdots, l_1)$  of the above problem are the minimum zone tolerances of the finished surfaces, and  $g_0$  is the optimal transformation. Let

$$g(\lambda) := g_0 G_0(\lambda) \quad (4.26)$$

and find  $g(\lambda) \in SE(3)$  to maximize the objective function

$$\mathcal{E}_c(g(\lambda), \delta) = \delta \quad (4.27)$$

subject to the constraints

$$\begin{aligned} 0 &\leq \delta \\ \delta &\leq d_j(z_{ji}, g(\lambda)) \quad i = 1, \cdots, n_j \quad j = 1, \cdots, l_2 \end{aligned} \quad (4.28)$$

where

$$d_j(z_{ji}, g(\lambda)) = \langle g(\lambda)^{-1}z_{ji} - h_{ji}, n_{ji} \rangle,$$

$h_{ji} \in \mathbb{R}^3$  is the corresponding optimal home surface point of  $z_{ji}$  on the home surface of the unfinished surface  $\bar{S}_j$ ,  $n_{ji}$  the (outward) unit normal vector of  $\bar{S}_j$  at  $h_{ji}$ , and  $\delta$  the maximal machinable volume of the unfinished surface  $\bar{S}_j$ .

By Equation (4.26) the coupled problem can be decomposed into a symmetric minimum zone localization and inspection problem on  $SE(3)/G_0$ , and a machinability problem on  $G_0$ . The first problem finds a representative transformation  $g_0$  and the minimum zone tolerance  $t_j (j = 1, \dots, l_1)$  of each finished surface. If one of the tolerances does not satisfy the specified requirement, we report that the workpiece is out of tolerance and further machining is unnecessary. Otherwise, with the representative transformation  $g_0$  as the initial condition of the machinability problem, we can proceed to solve the second problem to obtain the existing maximal machinable volume of each unfinished surface. If the machinable volume does not satisfy the specified requirement, then we have to reject the workpiece, i.e., it is unnecessary to perform the further machining. Otherwise, we obtain a satisfactory transformation, which makes not only the finished surfaces satisfy the tolerance requirement but also the unfinished surface have enough material to be machined in later machining.

**Problem 4.4.2. (A unique transformation)**

In the case that the finished surfaces of a workpiece fully constrain the rigid motion of the workpiece, the symmetry subgroup becomes identity, i.e.,  $G_0 = I$ . Then the problem degenerates as to find  $g \in SE(3)$  and  $t = (t_1, \dots, t_{l_1}) \in \mathbb{R}^{l_1}$  to minimize the objective function

$$\mathcal{E}(g, d) = \sum_{i=1}^{l_1} w_j t_j \quad (4.29)$$

subject to

$$0 \leq t_j \quad (4.30)$$

$$-t_j \leq d_j(y_{ji}, g) \leq t_j, \quad j = 1, \dots, l_1, \quad (4.31)$$

where

$$d_j(y_{ji}, g) = \langle g^{-1}y_{ji} - x_{ji}, n_{ji} \rangle \quad i = 1, \dots, n_j,$$

where  $t_j (j = 1 \cdots l_1)$  are the profile tolerance values of the finished surfaces, respectively;  $l_1$  is the number of the finished surfaces.

In this problem, if the computed  $t_j$  is less than the specified tolerance of the  $j^{\text{th}}$  finished surface, then the finished surface is satisfactory. Otherwise, the finished surface is out of tolerance. However, even though the finished surfaces have satisfied the specified tolerance values, we still need to check whether all unfinished surfaces have enough machine volumes remaining. If all tolerance values and the machine volume conditions are satisfied, then we say that the Euclidean transformation solved is satisfactory and we can use it to localize the workpiece and proceed to the further machining stages.

#### 4.4.2 The Localization/Inspection/Machinability Algorithm

Since the hybrid problem can be decoupled into two problems using the geometric properties of the homogeneous space, we can solve the two problems independently by using the solution of the first problem as the initial condition of the later problem. The solution of the later problem will then automatically ensure simultaneous satisfaction of the requirement imposed by the hybrid problem. We use an iteration method to solve the problem. The corresponding home surface points are solved by the same method described previously.

When updating the transformation  $g$ , the two decoupled problems are nonlinear constraint optimization problems. Using a similar technique as in the last section, the solution of the both problems can be computed by solving a sequence of linear programming problems.

Let the symmetry group of the finished surfaces be  $G_0$  and  $\mathcal{M}_0$  be a complementary subspace to the Lie algebra  $\mathcal{G}_0$  of  $G_0$ . Choose a basis  $(\hat{\eta}_1, \cdots, \hat{\eta}_r)$  of  $\mathcal{M}_0$  and write

$$\hat{m} = \sum_{i=1}^r \hat{\eta}_i m_i$$

for some  $m = (m_1, \cdots, m_r) \in \mathbf{R}^r$ . We consider that the variable perturbations in the problem (4.24) and (4.25) can be expressed as:

$$(g^{k+1}, t_1^{k+1}, \cdots, t_{l_1}^{k+1}) = (g^k e^{\hat{m}}, t_1^k + \tilde{t}_1, \cdots, t_{l_1}^k + \tilde{t}_{l_1}), \quad (4.32)$$

where  $\hat{m} \in \mathcal{M}_0$ .

Then, with (4.19) and (4.32), we can linearize the nonlinear problem into the following LP problem. The linearized objective function is:

$$\mathcal{E}_s(m, \tilde{t}_1, \dots, \tilde{t}_{l_1}) = \sum_{j=1}^{l_1} w_j \tilde{t}_j \quad (4.33)$$

subject to the linearized constraints

$$\begin{aligned} 0 &\leq t_j^k + \tilde{t}_j & (4.34) \\ -m^+ &\leq m \leq m^+ \\ -(t_j^k + \tilde{t}_j) &\leq d_j^k - \langle \hat{m} y_{ji}^k, n_{ji} \rangle \leq t_j^k + \tilde{t}_j \\ &i = 1, \dots, n_j, \quad j = 1, \dots, l_1 \end{aligned}$$

where  $y_{ji}^k = (g^k)^{-1} y_{ji}$ ,  $d_j^k = \langle y_{ji}^k - x_{ji}, n_{ji} \rangle$  and  $m^+ \in \mathbb{R}^r$  are positive and appropriately chosen limits.

Given an initial condition  $g^0$  of the transformation, we use the iteration method to solve for the optimal solution  $(g_0^*, t_j^*)$ . The algorithm can be summarized as follows.

**Algorithm 10. (Symmetric minimum zone localization(SMZL) algorithm)**

**Input:** (a) Measurement data set  $Y = \{y_{ji} \in \mathbb{R}^3, i = 1, \dots, n_j, j = 1, \dots, l_1\}$ ;

(b) CAD description of the finished surfaces with the symmetry subgroup  $G_0$ , and a basis  $\{\hat{\eta}_{r+1}, \dots, \hat{\eta}_6\}$  for  $\mathcal{M}_0$ ;

(c) The weight of each finished surface  $w_j, j = 1, \dots, l_1$ .

**Output:** (a) Optimal representative transformation  $g_0^* \in SE(3)/G_0$  of the finished surfaces;

(b) Minimum zone tolerances  $t_j^*, j = 1, \dots, l_1$ .

**Step 0:** (a) Set  $k = 0$  and initialize  $g^0$ ;

(b) Solve for  $x_{ji}^0, i = 1, \dots, n_j, j = 1, \dots, l_1$ ;

(c) Set  $t_j^0 = \max_i |\langle y_{ji}^k - x_{ji}, n_{ji} \rangle|$ ;

(d) Compute  $\mathcal{E}_s^0 = \sum_{j=1}^{l_1} w_j t_j^0$ ;

**Step 1:** (a) Solve the LP problem (4.33) to obtain  $(m, \tilde{t}_j, j = 1, \dots, l_1)$ ;

(b) Update  $(g^{k+1}, t_j^{k+1})$  according to (4.32);

(c) Solve for  $x_{ji}^{k+1}$  and  $n_{ji}^{k+1}$ ,  $i = 1, \dots, n_j, j = 1, \dots, l_1$ ;

(d) Compute  $\mathcal{E}_s^{k+1}$ ;

(e) If  $(1 - \mathcal{E}_s^{k+1}/\mathcal{E}_s^k) > \epsilon$ , then set  $k = k + 1$  and return to Step 1(a); Else exit and report results.

Similarly, the machinability problem can also be converted into the following LP problem. Choose a basis  $(\hat{\eta}_1, \dots, \hat{\eta}_r)$  of  $\mathcal{G}_0$  and write

$$\hat{\lambda} = \sum_{i=1}^r \hat{\eta}_i \lambda_i$$

Using the update equation

$$(g^{k+1}, \delta^{k+1}) = (g^k e^{\hat{\lambda}}, \delta^k + \bar{\delta}), \quad (4.35)$$

the machinability problem is transformed into the LP problem with the linearized objective function

$$\mathcal{E}_c(\lambda, \bar{\delta}) = -\bar{\delta} \quad (4.36)$$

subject to the linearized constraints

$$\begin{aligned} 0 &\leq \delta^k + \bar{\delta} \\ -\lambda^+ &\leq \lambda \leq \lambda^+ \\ \delta^k + \bar{\delta} &\leq d_j^k - \langle \hat{\lambda} z_{ji}^k, n_{ji}^k \rangle \\ &i = 1, \dots, n_j, \quad j = 1, \dots, l_2 \end{aligned} \quad (4.37)$$

where  $z_{ji}^k = (g^k)^{-1} z_{ji}$ ,  $d_j^k = \langle z_{ji}^k - h_{ji}^k, n_{ji}^k \rangle$ , and  $\lambda^+ \in \mathbb{R}^r$  are positive and appropriately chosen limits.

With the iteration method, the machinability algorithm can be summarized as follows:



**Algorithm 11. (The machinability algorithm)**

- Input:** (a) Measurement data set  $Z = \{z_{ji} \in \mathbb{R}^3, i = 1, \dots, n_j, j = 1, \dots, l_2\}$ ;
- (b) The index of unfinished surfaces of the workpiece; The CAD model of the workpiece and a basis  $(\hat{\eta}_1, \dots, \hat{\eta}_r)$  for  $\mathcal{G}_0$ ;
- (c) A representative transformation  $g_0 \in SE(3)/G_0$  from the SMZL algorithm.

- Output:** (a) Satisfactory transformation  $g^* \in SE(3)$ ;
- (b) The maximal machinable volume  $\delta^*$  of each unfinished surface;

- Step 0:** (a) Set  $k = 0$  and  $g^0 = g_0$ ;
- (b) Solve for  $h_{ji}^0$  and  $n_{ji}^0, i = 1, \dots, n_j, j = 1, \dots, l_2$ ;
- (c) Set  $\delta^0 = \max_{i,j} |\langle z_{ji}^0 - h_{ji}^0, n_{ji}^0 \rangle|$ ;
- (d) Compute  $\mathcal{E}_e^0 = -\delta^0$ ;

- Step 1:** (a) Solve the LP problem in (4.36) and (4.37) to obtain  $(\lambda, \bar{\delta})$ ;
- (b) Update  $(g^{k+1}, \delta^{k+1})$  according to (4.35);
- (c) Solve for  $h_{ji}^{k+1}$  and  $n_{ji}^{k+1}, i = 1, \dots, n_j, j = 1, \dots, l_2$ ;
- (d) Compute  $\mathcal{E}_e^{k+1}$ ;
- (e) If  $(1 - \mathcal{E}_e^{k+1}/\mathcal{E}_e^k) > \epsilon$ , then set  $k = k + 1$  and return to Step 1(a); Else exit and report results.

Combining the SMZL algorithm and the Machinability algorithm, we can obtain the hybrid algorithm as follows:

**Algorithm 12. (The Hybrid algorithm)**

- (a) Use the SMZL algorithm to solve for  $g_0$  and the tolerances  $t_j, j = 1, \dots, l_1$ ;
- (b) If the tolerance values of the finished surfaces satisfy the specified requirements, then proceed to Step (c).  
Else, exit and report that the workpiece is out of tolerance.

- (c) With the solution  $g_0$  of the SMZL algorithm as the initial condition of the Machinability algorithm, solve for the optimal transformation  $g^*$  and the maximal machinable volume  $\delta$ ;
- (d) If the Machinability algorithm has no feasible solution or the machinable volume  $\delta$  is less than the specified volume, then exit and report that there is not enough remaining machinable volume to be machined.  
Else, report the satisfactory transformation.

#### 4.4.3 Simulation Results

In the simulations, we use the same example and measurement data used in Section 5.3.5 to compare the two kind of localization methods.

##### Example 4.4.1. (A workpiece with one finished surface)

In this example, we consider the case of a workpiece having a (planar) finished surface  $S_1$  and several unfinished planar surfaces ( $\bar{S}_1, \bar{S}_2, \bar{S}_3$  and  $\bar{S}_4$ ) as shown in Figure 4.4. In the simulations, we assume the weight of the finished surfaces to be equal to one. Then, with the points from the finished and the unfinished surfaces and the CAD model of the workpiece, we apply the hybrid algorithm to obtain the set of solutions which are shown in Table 4.4. If the computed tolerance  $t_1$  and the machinable volume  $\delta$  are satisfied the specified requirements, we report the optimal transformation  $g^* = (R^*, p^*)$ .

##### Example 4.4.2. (A workpiece with two finished intersecting surfaces)

Consider next the case of a workpiece having two planar finished surfaces  $S_1$  and  $S_2$  which intersect along a line, see Figure 4.6. The configuration space of the symmetric localization problem is five-dimensional. Forty measurement points were taken from the finished surfaces of the workpiece to evaluate the minimum zone tolerance of the finished surfaces  $S_1$  and  $S_2$  and obtain a representative transformation  $g_0$ , thus aligning the workpiece with the corresponding surfaces of the CAD model. Seventy measurement points from the unfinished surface  $\bar{S}_1, \bar{S}_2$  and  $\bar{S}_3$  of the workpiece were used to envelop the CAD model along the symmetry subgroup of the finished surfaces. Using the representative transformation  $g_* = (R_*, p_*)$  from the

Exact transformation	Initial condition
$R = \begin{bmatrix} 0.866025 & -0.500000 & 0.000000 \\ 0.500000 & 0.866025 & 0.000000 \\ 0.000000 & 0.000000 & 1.000000 \end{bmatrix}$ $p = [ 20.00 \quad 10.00 \quad 20.00 ]^T$	$R^0 = \begin{bmatrix} 0.749825 & 0.124110 & 0.649892 \\ 0.433698 & 0.649600 & -0.624441 \\ -0.499669 & 0.750078 & 0.433260 \end{bmatrix}$ $p^0 = [ -40.00 \quad 50.00 \quad 80.00 ]^T$
Solution of SMZL algorithm	Solution of the Machinability algorithm
$R_* = \begin{bmatrix} 0.984807 & -0.173648 & 0.000107 \\ 0.173648 & 0.984807 & -0.000164 \\ -0.000010 & 0.000195 & 1.000000 \end{bmatrix}$ $p_* = [ -40.00 \quad 50.0403 \quad 20.0034 ]^T$ $t_1 = 0.016684$	$R^* = \begin{bmatrix} 0.866195 & -0.499707 & 0.000107 \\ 0.499707 & 0.866195 & -0.000164 \\ -0.000010 & 0.000195 & 1.000000 \end{bmatrix}$ $p^* = [ 20.0069 \quad 10.0048 \quad 20.0034 ]^T$ $\delta = 1.8312$

Table 4.4: Solutions computed at different stages for Example 4.4.1

SMZL algorithm as the initial condition and applying the machinability algorithm, the maximal machinable volume of each unfinished surface and the corresponding optimal transformation  $g^*$  are obtained. Table 4.5 shows the results.

## 4.5 Comparison of the LS and Minimax Method

In this section, we compare the localization results of workpieces obtained by using the least squares method and the minimax method, respectively.

In most literature, the workpiece localization problem is formulated by the least squares problem. The least squares formulation is mathematically well defined and widely accepted in industry. The criterion requires that the sum of the squared errors be minimized, hence all the measurement points contribute to the best match result. Moreover, the fitted features are stable and less sensitive to the effects of asperities. The minimum zone method has received much attention for form tolerance estimation in recent years. It is attractive because it best conforms to the ANSI and ISO standards for form tolerances. In [16], all form tolerances are formulated in the Minimax method and are transformed into linear programming problems by making use of tools from differential geometry and Lie group theory.

For partly finished workpiece localization, the hybrid problem can be separated

Exact transformation	Initial condition
$R = \begin{bmatrix} 0.866025 & -0.500000 & 0.000000 \\ 0.500000 & 0.866025 & 0.000000 \\ 0.000000 & 0.000000 & 1.000000 \end{bmatrix}$ $p = [ 20.00 \quad 10.00 \quad 20.00 ]^T$	$R^0 = \begin{bmatrix} 0.749825 & 0.124110 & 0.649892 \\ 0.433698 & 0.649600 & -0.624441 \\ -0.499669 & 0.750078 & 0.433260 \end{bmatrix}$ $p^0 = [ -40.00 \quad 50.00 \quad 80.00 ]^T$
Solution of SMZL algorithm	Solution of the Envelopment algorithm
$R_* = \begin{bmatrix} 0.866164 & -0.499625 & 0.000098 \\ 0.499627 & 0.866163 & 0.000260 \\ -0.000215 & -0.000176 & 1.000000 \end{bmatrix}$ $p_* = [ 19.9915 \quad 50.0403 \quad 20.01784 ]^T$ $t_1 = 0.01525, t_2 = 0.01508$	$R^* = \begin{bmatrix} 0.866164 & -0.499625 & 0.000098 \\ 0.499627 & 0.866163 & 0.000260 \\ -0.000215 & -0.000176 & 1.000000 \end{bmatrix}$ $p^* = [ 19.9915 \quad 9.9848 \quad 20.01784 ]^T$ $\delta = 1.8433$

Table 4.5: Solutions computed at different stages for Example 4.4.2

into two parts, the symmetric localization and the envelopment problem. In this section, we consider mainly the localization part in the comparison of the two methods. With the same measurement data, we compute and compare the localization errors and form tolerance zones obtained using the LS method and the Minimax method, respectively. First of all, we give three examples and simulation results.

**Example 4.5.1.** Consider the case that only one planar surface is finished. With 4 sets of measurement points distributed uniformly on the surface, the computed and exact localization results of the least squares and minimax methods are shown in Table 4.6. Let the orientation matrix be  $R = [ v_1 \quad v_2 \quad v_3 ] \in \mathbf{R}^{3 \times 3}$  and the translation  $p = [ p_1 \quad p_2 \quad p_3 ]$ . Then,  $v_3 \in \mathbf{R}^3$  in the table is the normal of the plane, which represents the orientation of the plane. The  $p$  is an on-plane point, in which  $p_1, p_2$  are undetermined components due to the symmetry of the planar surface and  $p_3$  is a component determined by the localization algorithms. *toler.* is the computed tolerance zone of the plane.

**Example 4.5.2.** Consider that two intersecting planes of a workpiece are finished. With 4 sets of measurement points, the computed and exact localization results and orientation errors of the two methods are shown in Table 4.7. In the table,  $\mathcal{E}_R$  is the orientational error,  $p \in \mathbf{R}^3$  is the translation of the workpiece. Due to the

Number of Points	Localization Results	
	Least squares	Minimax
15	$v_3 = \begin{bmatrix} 0.4749 \\ -0.1574 \\ 0.8658 \end{bmatrix}, p = \begin{bmatrix} -45.672 \\ -20.567 \\ 20.0054 \end{bmatrix}$ Toler.=0.1783	$v_3 = \begin{bmatrix} 0.4773 \\ -0.1469 \\ 0.8663 \end{bmatrix}, p = \begin{bmatrix} 100.334 \\ -70.334 \\ 20.0972 \end{bmatrix}$ Toler. = 0.1692
20	$v_3 = \begin{bmatrix} 0.4772 \\ -0.1495 \\ 0.8659 \end{bmatrix}, p = \begin{bmatrix} -37.188 \\ -28.074 \\ 20.0134 \end{bmatrix}$ Toler.= 0.2010	$v_3 = \begin{bmatrix} 0.4775 \\ -0.1466 \\ 0.8662 \end{bmatrix}, p = \begin{bmatrix} 100.05 \\ -70.313 \\ 20.1128 \end{bmatrix}$ Toler. = 0.1755
30	$v_3 = \begin{bmatrix} 0.4777 \\ -0.1493 \\ 0.8657 \end{bmatrix}, p = \begin{bmatrix} -40.3625 \\ -28.4813 \\ 19.9801 \end{bmatrix}$ Toler.= 0.2034	$v_3 = \begin{bmatrix} 0.4776 \\ -0.1487 \\ 0.8658 \end{bmatrix}, p = \begin{bmatrix} 100.037 \\ -70.43 \\ 19.9834 \end{bmatrix}$ Toler. = 0.1861
40	$v_3 = \begin{bmatrix} 0.4767 \\ -0.1496 \\ 0.8662 \end{bmatrix}, p = \begin{bmatrix} -39.170 \\ -32.278 \\ 20.0381 \end{bmatrix}$ Toler.= 0.2125	$v_3 = \begin{bmatrix} 0.4668 \\ -0.1742 \\ 0.8670 \end{bmatrix}, p = \begin{bmatrix} 100.905 \\ -73.625 \\ 20.0239 \end{bmatrix}$ Toler. = 0.2032
Exact results	$v_3 = \begin{bmatrix} 0.4755 \\ -0.1545 \\ 0.8660 \end{bmatrix}, p = \begin{bmatrix} 20.00 \\ -10.00 \\ 20.00 \end{bmatrix}$	$v_3 = \begin{bmatrix} 0.4755 \\ -0.1545 \\ 0.8660 \end{bmatrix}, p = \begin{bmatrix} 20.00 \\ -10.00 \\ 20.00 \end{bmatrix}$

Table 4.6: Localization results of a planar surface with 4 sets of points using the least squares and minimax methods, where  $v_3$  is the normal of the plane,  $p$  is the translation and *toler.* is the tolerance zone of the plane

Number of Points	Orientation error $\mathcal{E}_R$		Translation [ $p_1$ $p_2$ $p_3$ ]					
	LS	Minimax	LS			Minimax		
30	0.0052	0.0784	19.9786	-30.17	20.0074	19.9826	-16.13	20.0343
40	0.0356	0.0984	19.9468	-30.17	19.9815	19.9931	-16.13	20.0697
60	0.0410	0.0573	19.9897	-30.17	19.9589	19.9927	-16.13	19.9692
80	0.0260	0.0471	19.9946	-30.17	20.0195	19.9906	-16.13	20.0596
Exact results	0.0	0.0	20.0	-10.0	20.0	20.0	-10.0	20.0

Table 4.7: Localization results of the workpiece with two intersecting planar surfaces and with 4 sets of points using the least squares and minimax methods, where  $p_2$  is a free component

symmetry of the two intersecting planar surfaces,  $p_2$  is a free component and  $p_1, p_3$  are determined by the localization algorithms.

**Example 4.5.3.** When a workpiece has three finished non-parallel planar surfaces, the workpiece's transformation can be determined uniquely by the localization algorithms. With three sets of measurement points consisting of different noise and number, the orientational error  $\mathcal{E}_R$ , the translational error  $\mathcal{E}_p$  and the tolerance values of the workpiece computed by using the least squares and minimax methods are shown in Table 4.8 and 4.9, respectively. In the two tables,  $\mu$  and  $\sigma$  are the mean and variance of the measurement noise in the measurement data. Three values  $Toler.1, 2, 3$  are the form tolerances of three surfaces, respectively. After localizing the workpiece, the deviation of transformed measurement points from the CAD surfaces with different number and noise of measurement points are shown in Figure 4.7 and 4.8.

The simulation results show that in all cases, the form tolerance values of the three surfaces computed by the Minimax method are smaller than those computed

Measurement points Number and Noise			Least Squares Localiz. errors		Minimax Localiz. errors	
No.	$\mu$	$\sigma$	$\mathcal{E}_R$	$\mathcal{E}_p$	$\mathcal{E}_R$	$\mathcal{E}_\mu$
40	0.002	0.01	0.00439	0.00492	0.00880	0.03313
40	0.0	0.1	0.15323	0.15227	0.14535	0.33952
40	0.02	0.1	0.15323	0.21980	0.14535	0.31758
60	0.0	0.01	0.00947	0.01244	0.01078	0.01990
60	0.0	0.05	0.04731	0.06215	0.05851	0.09845
60	0.0	0.1	0.09451	0.12419	0.11691	0.19700
90	0.0	0.01	0.00394	0.00419	0.00287	0.00428
90	0.02	0.01	0.00394	0.03863	0.00977	0.04766
90	0.0	0.05	0.01969	0.02090	0.01437	0.02146
90	0.02	0.05	0.01969	0.05483	0.01437	0.04301

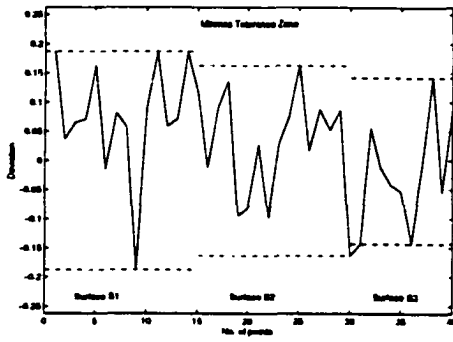
Table 4.8: Comparison of transformation errors between the Least squares and Minimax methods

Measurement points Number and Noise			Least Squares Tolerance zones			Minimax Tolerance zones		
No.	$\mu$	$\sigma$	Toler.1	Toler.2	Toler.3	Toler.1	Toler.2	Toler.3
40	0.002	0.01	0.02595	0.04069	0.03022	0.02101	0.03700	0.03016
40	0.0	0.1	0.38447	0.33401	0.27722	0.37460	0.32561	0.28501
40	0.04	0.1	0.38447	0.33401	0.27722	0.37460	0.32561	0.28501
60	0.0	0.01	0.04118	0.03896	0.00176	0.04108	0.03896	0.00128
60	0.0	0.05	0.20593	0.19487	0.00893	0.20510	0.19585	0.00784
60	0.0	0.1	0.41194	0.38989	0.01814	0.41022	0.39178	0.01420
90	0.0	0.01	0.04562	0.03395	0.01424	0.04564	0.03531	0.00990
90	0.02	0.01	0.04562	0.03395	0.01424	0.04564	0.03531	0.00990
90	0.0	0.05	0.22336	0.19927	0.01820	0.21504	0.19213	0.01430
90	0.02	0.05	0.23453	0.24858	0.00103	0.21504	0.19213	0.01430

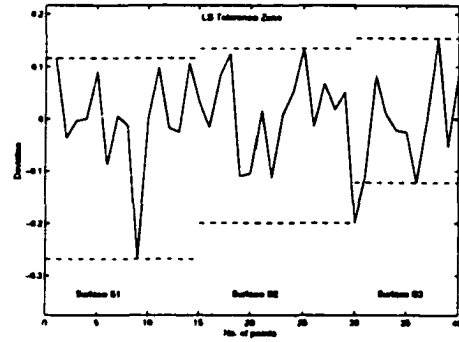
Table 4.9: Comparison of tolerance zones of three surfaces between the Least squares and Minimax methods

by the least squares, however, the conclusion is opposite for localization errors. Although the localization errors are comparable, the errors obtained using the least square method are slightly smaller than those computed by the minimax method. Mean values of measurement noise have influence not on the form tolerance of each surface and orientational errors, but on the translational errors.

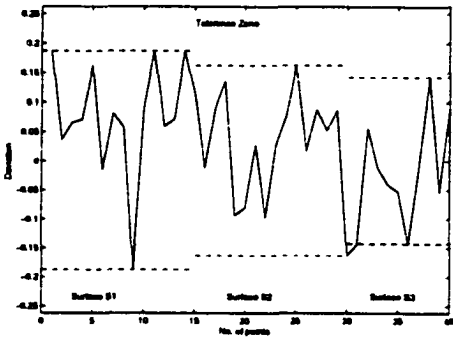
Based on all the above extensive simulation results, we can find that the least squares method has better localization accuracy than the minimax method. Both methods have high computational efficiency. The iteration number of both methods is less than 10 times. Correspondingly, the computational time is less than 0.5 second on a PC Pentium 166MHz. The least square method is robust with respect



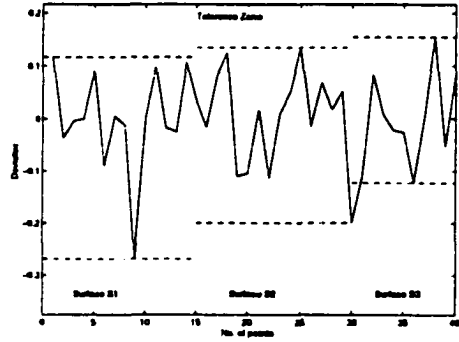
(a) Minimax method,  $\mu = 0.04, \sigma = 0.1$



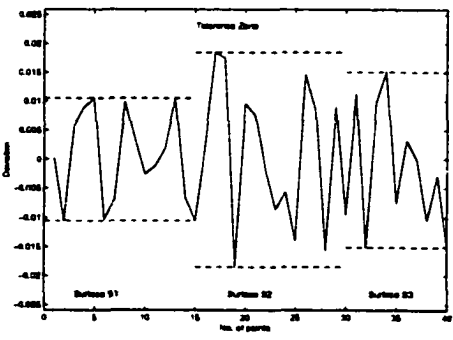
(b) LS method,  $\mu = 0.04, \sigma = 0.1$



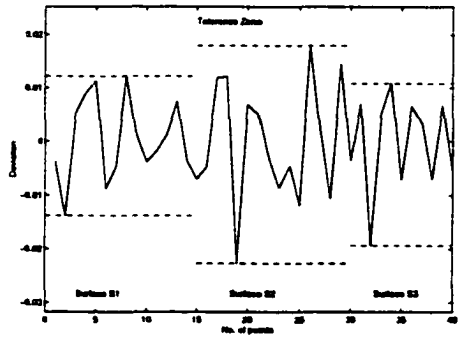
(c) MinMax method,  $\mu = 0.0, \sigma = 0.1$



(d) LS method,  $\mu = 0.0, \sigma = 0.1$



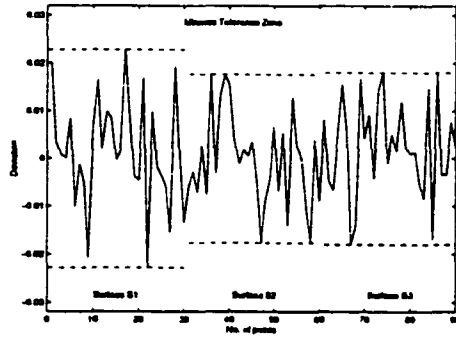
(e) Minimax method,  $\mu = 0.02, \sigma = 0.01$



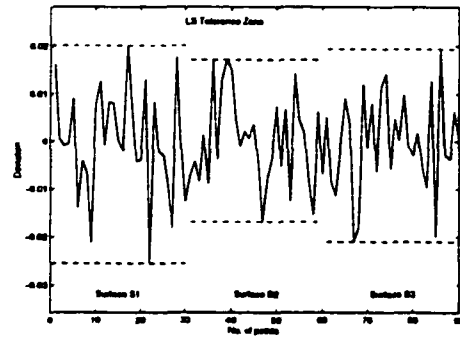
(f) LS method,  $\mu = 0.02, \sigma = 0.01$

Figure 4.7: Deviation of transformed measurement points from their CAD mode surfaces with 40 points and different levels of measurement noise

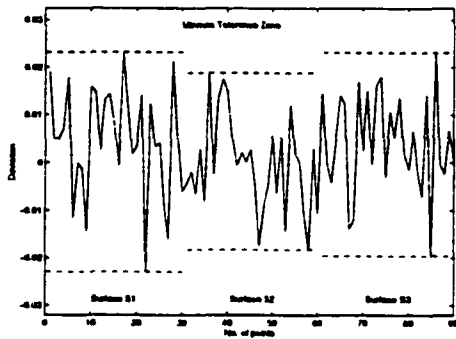




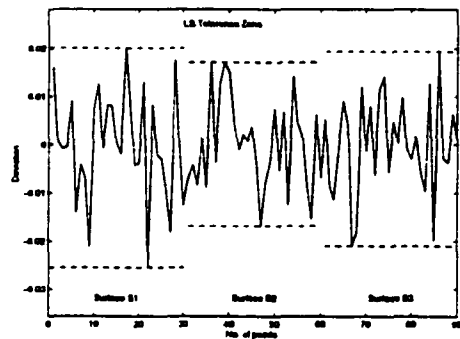
(a) Minimax method,  $\mu = 0.0, \sigma = 0.01$



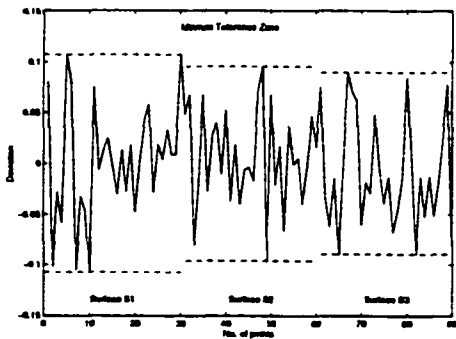
(b) LS method,  $\mu = 0.0, \sigma = 0.01$



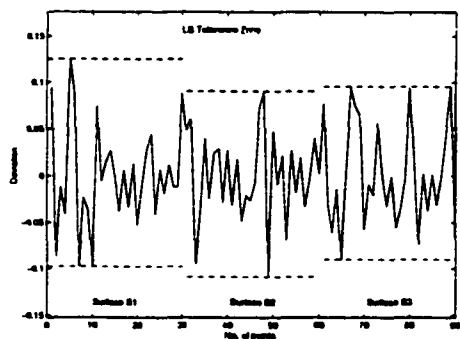
(c) Minimax method,  $\mu = 0.02, \sigma = 0.01$



(d) LS method,  $\mu = 0.02, \sigma = 0.01$



(e) Minimax method,  $\mu = 0.0, \sigma = 0.05$



(f) LS method,  $\mu = 0.0, \sigma = 0.05$

Figure 4.8: Deviation of transformed measurement points from their CAD mode surfaces with 90 points and different levels of measurement noise

to the variation of the initial conditions  $g_0$ , which further confirms the conclusion described in Section 2.8 and [17]. However, the minimax method requires small deviation of the initial guess  $g_0$  away from the true transformation. Especially, the convergence of the minimax method in the three examples is different. The algorithm localizing one finished planar surface in Example 1 has better convergence; The algorithm when localizing two finished surfaces requires a more accurate guess for the initial conditions than that in Example 1; The algorithm when localizing the three surfaces in Example 3 requires small deviation of the initial condition  $g_0$  from the true transformation.

The above analysis results show that the least squares method has better performance in terms of localization accuracy and convergence. The minimax method can obtain the form tolerances which are conformed with ANSY 14.5 standard when using it to localize workpieces.

## 4.6 Conclusion

In this section, we proposed the hybrid localization/envelopment problem and formulated the hybrid problem as a symmetric localization problem on the homogeneous space  $SE(3)/G_0$  of the Euclidean group and a minimization problem on  $G_0$  subject to inequality constraints, where  $G_0 \subset SE(3)$  is the symmetry subgroup formed by the finished surfaces of the workpiece. We solve the envelopment problem by solving a sequence of linear programming problems where the solution from the symmetric localization problem is used as an initial condition. Simulation results demonstrate effectiveness of our method for the hybrid problem. We also addressed the problem of hybrid localization/inspection/machinability. We formulated the problem using the minimax method and transformed them into two nonlinear constraint optimization problems: the symmetric localization/inspection problem and the machinability problem using the geometric properties of the homogeneous space. We developed a simple but efficient algorithm for this problem. The comparison results of the LS method and the Minimax method showed the least squares method has better performance, especially for localization accuracy.

Therefore, for an arbitrarily fixtured workpiece, we can determine the tolerance

values of the finished surfaces, maximal machinable volume existing on the unfinished surfaces and position and orientation of the workpiece using the proposed hybrid algorithms to ensure that further machining will reach specified shapes and tolerances. The proposed method integrates the workpiece localization and on-line inspection, thus greatly accelerating machining cycles and improving product quality.

## Chapter 5

# Localization of Workpieces with Special Geometries

### 5.1 Introduction

A large class of workpieces we encounter can be classified as 2.5-dimensional or "essentially" 2.5-dimensional. We define an "essentially" 2.5-dimensional workpiece to be a workpiece with a planar standard surface in contact with or parallel to the machine table surface. In other words, an ordinary 3-dimensional workpiece may be considered "essentially" 2.5D if in contact with the machine table surface is a planar standard face of the workpiece. When a 2.5D workpiece is fixtured to a machine table, the set of configurations describing relative displacements of the workpiece is given by  $SE(2)$ , the group of rigid motions in  $\mathbb{R}^2$ , and the associated localization problem can be substantially simplified. In this chapter, we introduce a proper procedure for reducing the localization problem from  $SE(3) \times \mathbb{R}^{3n}$  to  $SE(2) \times \mathbb{R}^{2n}$  for 2.5D workpieces.

### 5.2 Problem Formulation

Consider the workpiece shown in Figure 5.1. Assume that in contact with the machine table is a planar surface  $S_0$  and a surface  $S_i$  is to be probed. Let  $h_0$  be the (known) height of the probe. When we measure points on the surface  $S_i$  with the

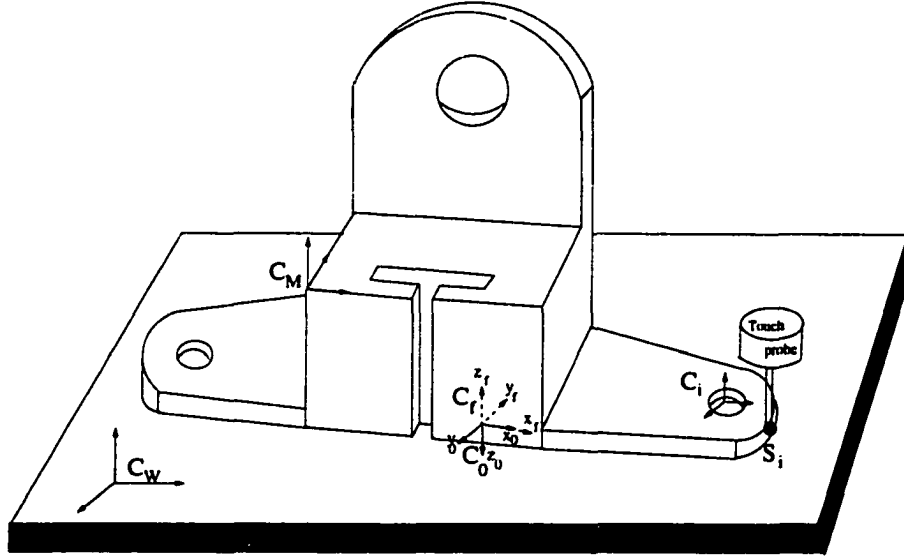


Figure 5.1: Localization of an "essentially" 2.5D workpiece

same height  $h_0$ , then a measurement point  $y_i$  has the form

$$y_i = \begin{bmatrix} \bar{y}_i \\ h_0 \end{bmatrix}, \quad \bar{y}_i \in \mathbb{R}^2 \quad (5.1)$$

In the CAD model of the workpiece, every face has a local coordinate frame relative to which the surface is most conveniently described. Let  $C_i$  be the local coordinate frame of  $S_i$ ,  $C_M$  the CAD model frame,  $C_0$  the contact surface frame,  $C_f$  the contact frame and  $C_W$  the machine reference frame. Let  $g_{M_i} \in SE(3)$  be the transformation from  $C_i$  to  $C_M$ . If  $\psi_i^l(u_i, v_i) \in \mathbb{R}^3$  is the description of  $S_i$  in local frame  $C_i$ , then  $g_{M_i}\psi_i^l(u_i, v_i)$  is the description of  $S_i$  relative to the model frame  $C_M$ . For a planar face  $S_0$  the  $z$ -axis of its local frame  $C_0$  coincides with the outward pointing normal of  $S_0$ . Thus, the position and orientation of  $C_0$  relative to  $C_f$  are given by

$$p_{f0} = 0, \quad \text{and} \quad R_{f0} = \text{diag}(1, -1, -1).$$

We transform the representation of  $S_i$  from its local frame  $C_i$  to the contact frame  $C_f$  by

$$g_{f0} \cdot g_{M0}^{-1} \cdot g_{M_i}\psi_i^l(u_i, v_i) := \psi_i^f(u_i, v_i)$$

where  $g_{M_i}$  and  $g_{M0}$  can be derived from the CAD database. Because the  $z$ -axis of  $C_f$  agrees with that of  $C_W$ , the third component of  $\psi_i^f(u_i, v_i)$  gives the height of the

home surface point and thus satisfies the height constraint,

$$h_0 = \psi'_{i,3}(u_i, v_i)$$

Since at least one of the partial derivatives of  $\psi'_{i,3}$  in terms of  $u_i$  or  $v_i$  is non-zero, we can solve from the above equation either for  $u_i$  in terms of  $v_i$  or for  $v_i$  in terms of  $u_i$ . Assume that  $u_i = u_i(v_i)$ , then, substituting the result back to the first two components of  $\psi'_i$  obtaining a parametric equation of  $x_i$  in terms of the single parameter  $v_i$ , i.e.,

$$x_i = \begin{bmatrix} \bar{\psi}_i(v_i) \\ \psi_{i,3}(v_i) \end{bmatrix}, \quad \bar{\psi}_i(v_i) \in \mathbb{R}^2.$$

On the other hand, the transformation from  $C_W$  to  $C_M$  can be expressed as

$$g_{MW} = g_{M_0} \cdot g_{0f} \cdot g_{fW}$$

where the (unknown) transformation  $g_{fW}$  is given by

$$g_{fW} = \begin{bmatrix} \bar{R}_{fW} & 0 & \bar{p}_{fW} \\ 0 & 1 & 0 \\ 0 & 0 & 1 \end{bmatrix}$$

for some  $\bar{R}_{fW} \in SO(2)$  and  $\bar{p}_{fW} \in \mathbb{R}^2$ . Since rigid transformation preserves distance, the objective function can be translated into

$$\begin{aligned} \mathcal{E} &= \sum_{i=1}^n \|g_{MW} y_i - g_{M_i} \psi'_i(v_i)\|^2 \\ &= \sum_{i=1}^n \|g_{fW} y_i - g_{0f}^{-1} g_{M_0}^{-1} g_{M_i} \psi'_i(v_i)\|^2 \\ &= \sum_{i=1}^n \|\bar{R}_{fW} \bar{y}_i + \bar{p}_{fW} - \bar{x}_i\|^2 \end{aligned}$$

for

$$\bar{x}_i = g_{0f}^{-1} g_{M_0}^{-1} g_{M_i} \psi'_i(v_i) = \bar{\psi}_i(v_i) \in \mathbb{R}^2$$

This is clearly a two-dimensional problem, with a configuration space defined by  $SE(2) \times \mathbb{R}^{2n}$ .

Therefore, the localization problem of 2.5D workpieces can be formulated to find  $\bar{R}_{fW} \in SO(2)$ ,  $\bar{p}_{fW}$  and  $\bar{x}_i$  so as to minimize

$$\mathcal{E}(\bar{R}_{fW}, \bar{p}_{fW}, \bar{x}_1, \dots, \bar{x}_n) = \sum_{i=1}^n \|\bar{R}_{fW} \bar{y}_i + \bar{p}_{fW} - \bar{x}_i\|^2 \quad (5.2)$$

subject to the surface constraints

$$S_i(\bar{x}_i) = 0, \quad i = 1, \dots, n$$

### 5.3 Geometric Algorithms

When a workpiece is 2.5 dimensional, the localization problem can be reduced to a two dimensional problem as formulated in problem (5.2). This means that the problem has less variables to be solved. Correspondingly, the algorithms solving for the problem become simpler than the 3D algorithms. The former has three unknown variables, the later has six.

Using the similar techniques in the 3D workpiece localization, we develop an iterative algorithm to solve the problem. For notation simplicity, we denote  $g_{JW} \in SE(2)$  as  $g$  in later discussions.

#### Algorithm 13. (2.5D Workpiece Localization )

**Input:** (a) Measurement data  $Y = \{y_i \in \mathbb{R}^2, i = 1, \dots, n\}$  and home surface  $S_i$  of  $y_i$ .

(b) Probe height =  $h_0$ , CAD description of a workpiece,  $g_{J0}$  and  $g_{M0}$ ;

**Output:** Optimal solution  $g_{Jw} \in SE(2)$ ;

**Step 0:** (a) Set  $k = 0$ ;

(b) Initialize  $g^0$ ;

(c) Compute  $x_i^0$ ;

(d) Compute  $\mathcal{E}^0 = \mathcal{E}(g^0, x^0)$ ;

(e)  $k = k + 1$ .

**Step 1:** (a) Solve for  $x_i^k$ ;

(b) Compute  $g^k$  using  $(x_i^k, g^{k-1})$ ;

(c) Compute  $\mathcal{E}^k = \mathcal{E}(g^k, x^k)$ ;

(d) If  $(1 - \mathcal{E}^k / \mathcal{E}^{k-1}) < \delta_1$ , exit. Else

(e) Set  $k = k + 1$  and return to Step 1(a).

A key observation in the above iterative method is that the Euclidean transformation  $g_k$  and the home surface points  $x_i^k, i = 1, \dots, n$  are optimized separately. Thus, with an initial condition  $g_0$ , this leads to a sequence  $\{g_k, x_i^k, i = 1, \dots, n\}$  which hopefully will converge to a global minimum of the objective function (5.2).

Using similar methods, all the techniques in 3D localization can be applied to solve the 2.5D localization problem.

### 5.3.1 Home Surface points

With the height constraint

$$h_0 = \psi'_{i,3}(u_i, v_i), \quad (5.3)$$

when  $\frac{\partial \psi'_{i,3}}{\partial u_i} \neq 0$ , we can solve from the above equation for  $u_i$  in terms of  $v_i$ . Assuming that  $u_i = u_i(v_i)$ , then we have

$$x_i = \begin{bmatrix} \bar{\psi}_i(v_i) \\ \psi_{i,3}(v_i) \end{bmatrix}, \quad \bar{\psi}_i(v_i) \in \mathbb{R}^2.$$

and

$$y_i = \begin{bmatrix} \bar{y}_i \\ h_0 \end{bmatrix}$$

For notation simplicity, we denote the  $\bar{y}_i \in \mathbb{R}^2$  and  $\bar{x}_i \in \mathbb{R}^2$  as  $y_i \in \mathbb{R}^2$  and  $x_i \in \mathbb{R}^2$ ,  $R_{fw}$  and  $p_{fw}$  as  $R$  and  $p$ , respectively, if there is no special explanation. Correspondingly, the objective function at the  $k^{\text{th}}$  iteration step can be rewritten as

$$\mathcal{E}_k(R_k, p_k, x_i^k) = \sum_{i=1}^n \|R_k y_i + p_k - x_i^k\|^2. \quad (5.4)$$

Then applying the Lagrangian multiplier technique to (5.4) in terms of  $v_i$ , yields

$$\langle R_k y_i + p_k - x_i^k, \bar{\psi}_{v_i}^i \rangle = 0, \quad i = 1, \dots, n \quad (5.5)$$

where  $x_i^k = \psi_i(v_i)$  is the parametric description of  $S_i$ , and  $\bar{\psi}_{v_i}^i$  are the partial derivatives of  $\psi_i$  with respect to  $v_i$ . With properly selected initial conditions for  $v_i$ , Newton's algorithm can be applied to (5.5) to solve for  $x_i^k, i = 1, \dots, n$ . With the  $v_i$  and the height constraint in (5.3), we can solve for  $u_i$ . Then the normal of the surface  $S_i$  at the point  $x_i$  is given by

$$n_i = \frac{\psi_{u_i}(u_i, v_i) \times \psi_{v_i}(u_i, v_i)}{|\psi_{u_i}(u_i, v_i) \times \psi_{v_i}(u_i, v_i)|} \in \mathbb{R}^3$$



### 5.3.2 Transformation update $g$

There are a number of ways to compute the Euclidean transformation update  $g_k$ . Corresponding to the approaches in the 3D localization, the following algorithms can be developed.

#### • The 2.5D Variational Algorithm:

Let

$$\bar{y} = \frac{1}{n} \sum_i y_i, \quad \bar{x}^k = \frac{1}{n} \sum_i x_i^k$$

and

$$\tilde{y}_i = y_i - \bar{y}, \quad \tilde{x}_i^k = x_i^k - \bar{x}^k.$$

Compute the singular value decomposition of

$$W = \sum_{i=1}^n \tilde{y}_i (\tilde{x}_i^k)^T = U \Sigma V^T,$$

where  $U, V \in \mathbf{R}^{2 \times 2}$  are unitary and  $\Sigma$  is the diagonal matrix of singular values. Then, the optimal Euclidean transformation update is given by

$$\begin{aligned} R_{k+1} &= V U^T \\ p_{k+1} &= \bar{x}^k - R_{k+1} \bar{y} \end{aligned} \quad (5.6)$$

#### • The 2.5D Tangent Algorithm:

Let

$$g_k = \begin{bmatrix} R_k & p_k \\ 0 & 1 \end{bmatrix} \in SE(2)$$

and express  $g_{k+1}$  in terms of  $g_k$  as

$$g_{k+1} = e^{\hat{\xi}} g_k \quad (5.7)$$

for a screw increment

$$\hat{\xi} = \begin{bmatrix} \hat{\omega} & v \\ 0 & 0 \end{bmatrix} \in \mathbf{R}^{3 \times 3} \quad \omega \in \mathbf{R}, \quad v \in \mathbf{R}^2,$$

where

$$\hat{\omega} = \begin{bmatrix} 0 & -\omega \\ \omega & 0 \end{bmatrix} \in SO(2).$$

For small values of  $\xi = (v, \omega) \in \mathbb{R}^3$ , (5.7) can be approximated by

$$g_{k+1} \cong (I + \hat{\xi})g_k.$$

Substituting the above expression into the objective function (5.4) and minimizing the result with respect to  $\xi$  yield a system of linear equations in terms of the unknown  $\xi \in \mathbb{R}^3$ ,

$$A\xi = b \quad (5.8)$$

where for  $y_i^k = R_k y_i + p_k$  and

$$\tilde{y}_i^k = \begin{bmatrix} 0 & -1 \\ 1 & 0 \end{bmatrix} \begin{bmatrix} (y_i^k)^1 \\ (y_i^k)^2 \end{bmatrix} = \begin{bmatrix} -(y_i^k)^2 \\ (y_i^k)^1 \end{bmatrix},$$

$$A = \begin{bmatrix} \sum_{i=1}^n (\tilde{y}_i^k)^T & \sum_{i=1}^n \langle \tilde{y}_i^k, \tilde{y}_i^k \rangle \\ nI & \sum_{i=1}^n \tilde{y}_i^k \end{bmatrix} \in \mathbb{R}^{3 \times 3}$$

and

$$b = \begin{bmatrix} \sum_{i=1}^n \langle \tilde{y}_i^k, x_i^k - y_i^k \rangle \\ \sum_{i=1}^n (x_i^k - y_i^k) \end{bmatrix} \in \mathbb{R}^3.$$

Solving for  $\xi$  from (5.8) and then substituting the results into (5.7) give the transformation  $g_{k+1}$ .

### • The 2.5D Hong-Tan Algorithm:

Assume the same form of updating the transformation  $g_k$  as in (5.7). However, the objective function, with a different form from (5.4), is the sum of squared distances to the tangent plane to  $S_i$  at  $x_i^k$ , i.e.,

$$\mathcal{E} = \sum_{i=1}^n \langle R_k y_i + p_k - x_i^k, n_i^k \rangle^2. \quad (5.9)$$

Then, the system of linear equations from which  $\xi \in \mathbb{R}^3$  is solved is given by

$$A\xi = b$$

where

$$A = \begin{bmatrix} \sum_{i=1}^n \langle \tilde{y}_i^k, n_i^k \rangle (n_i^k)^T & \sum_{i=1}^n \langle \tilde{y}_i^k, n_i^k \rangle^2 \\ \sum_{i=1}^n n_i^k (n_i^k)^T & \sum_{i=1}^n \langle \tilde{y}_i^k, n_i^k \rangle n_i^k \end{bmatrix} \in \mathbb{R}^{3 \times 3}$$

and

$$b = \begin{bmatrix} -\sum_{i=1}^n \langle y_i^k - x_i^k, n_i^k \rangle \langle \tilde{y}_i^k, n_i^k \rangle \\ -\sum_{i=1}^n \langle y_i^k - x_i^k, n_i^k \rangle n_i^k \end{bmatrix} \in \mathbb{R}^3.$$

where  $y_i^k$  and  $\tilde{y}_i^k$  are defined as in the last algorithm, and  $n_i \in \mathbb{R}^2$  is  $\bar{n}_i$ , taken from the  $\begin{bmatrix} \bar{n}_i^T & n_{i,3} \end{bmatrix}^T \in \mathbb{R}^3$ . Using Gauss elimination in the above equation to solve for  $\xi$  yields the desired transformation update  $g_{k+1}$ .

After having  $g_{Jw}$ , the  $g_{MW}$  is obtained by

$$g_{MW} = g_{M0} g_{0f} g_{Jw}$$

## 5.4 Conclusion

In this chapter, we introduced a proper procedure for reducing the localization problem from  $SE(3) \times \mathbb{R}^{3n}$  to  $SE(2) \times \mathbb{R}^{2n}$  for 2.5D workpieces. Since the set of configurations describing relative displacements of the workpiece is  $SE(2)$ , we can simplify the associated localization problem. We developed three algorithms for solving the problem. Apparently, the 2.5D workpiece localization algorithms have higher computational efficiency than the 3D localization algorithms.

## **Chapter 6**

# **A Computer-Aided Setup(CAS) System for Workpieces**

### **6.1 Introduction**

With advances in CNC technology and availability of on-machine probing sensors, it is possible to automate the process of workpiece setup. Especially, an open architecture CNC system allows users to integrate their own new algorithms and functions on it. Based on this technology, we developed a prototype of the computer-aided setup and inspection system on a 3-axis open architecture CNC milling machine tool of Hong Kong University of Science and Technology. The system consists of five parts, they are precise probing, error compensation, localization and reliability analysis, tool path modification, and dimension inspection. All these functions can be operated on an interactive end-user interface window on which CAD models can be easily displayed and manipulated. In this chapter, we first briefly describe an open architecture CNC machine tool system. Next, we introduce how to implement the CAS system on the CNC machine tools. Then, we present the structure and operational principle of the CAS system. Finally we demonstrate the validity of the localization algorithms implemented on the CAS system.

### **6.2 An Open Architecture CNC System**



Figure 6.1: Implementation of localization algorithms in a five-axis machine center environment.

An open architecture CNC system can provide hardware independent and portable software modules for CNC builders and users of machine tools. This means that the system is flexible for the users of machine tools and CNC builders to rapidly adapt various new modules and purposes. For example, the open architecture design system allows the machine tool users to be able to add control functions of sensor-based machining process and monitoring algorithm modules on it.

Figure 6.2 shows the diagram of an open architecture CNC machine system developed by the intelligent machine Lab of HKUST. The system consists of a 3-axis milling machine tool, an upper level host computer, a DSP-based controller, and an intelligent measuring and machining module. The host computer controls the DSP controller and performs user interface, communication, CAD/CAM and other functions. The DSP controller performs the control of multi-axis motion. The intelligent measuring and machining module includes sensors, adaptive control, fault diagnostic and probing system. Users can also integrate new control algorithms and functions by themselves. A CNC monitor is used to display man-machine interface information, coordinates of probing data, NC codes being executed, and tool paths that a tool cutter is passing, etc.

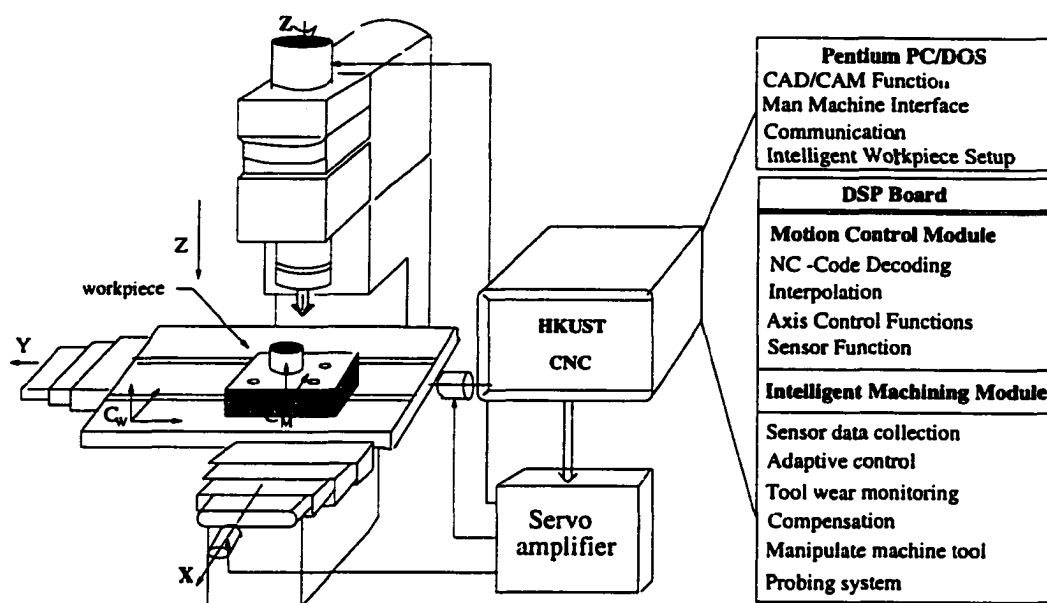


Figure 6.2: An open architecture CNC machine system

### 6.3 Composition of the CAS System

The CAS system, as a new function module integrated on the CNC machine tool, performs the following functions: probing points, data collection, localization and modification of toolpath. Correspondingly, the CAS system consists of a probing system and a software module including workpiece localization and compensation algorithms, as shown in Figure 6.3.

#### 6.3.1 Probing System

Touch trigger probes are widely used sensors for on-machine metrology on tool machines as well as on coordinate measuring machines. The probing system we choose to use consists of a MP12 touch trigger probe with an optical signal and wide angle transmission and a probing interface produced by Renishaw Ltd. The probe is a precision omni-directional trigger device consisting of a probe body and a stylus. The probe body is mounted in the machine spindle. The interface converts the probing signal and indicates the status of the probe. The panel on the probe interface has five LEDs for indicating the probe status.

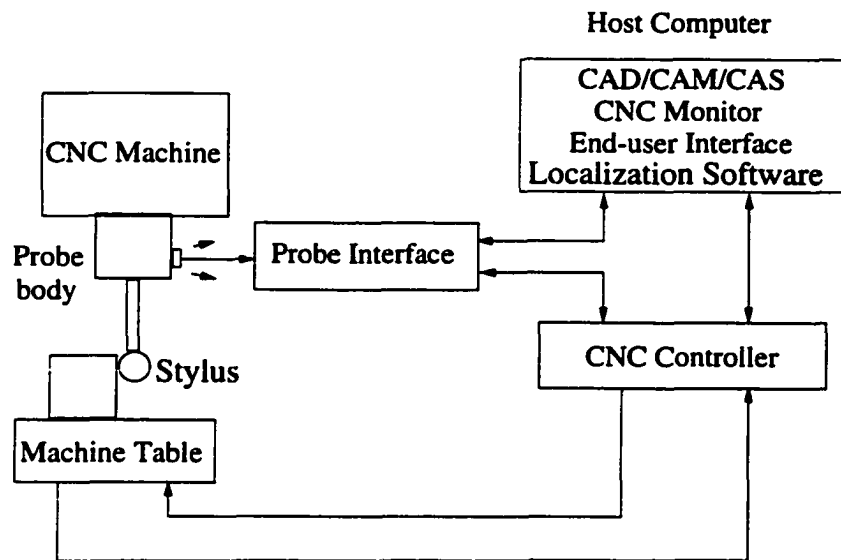


Figure 6.3: The composition diagram of CAS system

The touch trigger probing system relies on a switching principle which is based on a kinematic location to give the high repeatability required. When the stylus is touching the surface of a workpiece, the trigger signal is transmitted to the interface by optical transmission. Then the signal is converted by the probe interface into an acceptable signal form for the machine controller. When receiving the signal, the host computer records the current coordinates of the contact point. After the contact is released, the stylus support allows the stylus to return to its datum position with a very high accuracy for further measuring. The probe can achieve a high accuracy due to the probe's inherent repeatability.

A control handle is installed via the host computer and the DSP controller. It is programmed to drive the servo motors so that the machine table can move along the three axes directions. By operating the handle, we can perform measurement of points on surfaces of a workpiece.

### 6.3.2 Software System

The CAS system performs three functions: (i) measuring points on surfaces of a workpiece; (ii) using the point set and the CAD model of the workpiece to determine the transformation(position and orientation) of the workpiece and analyzing the

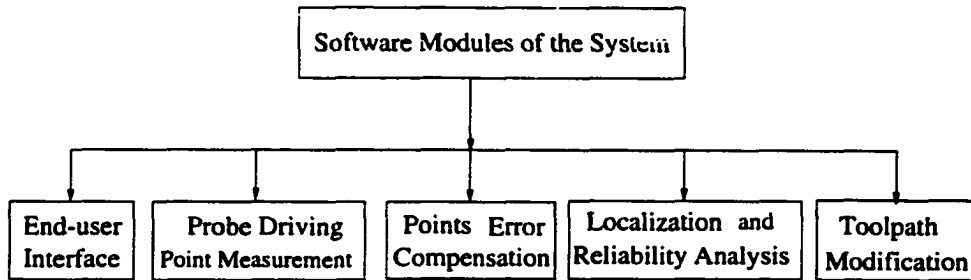


Figure 6.4: Software modules of the CAS system

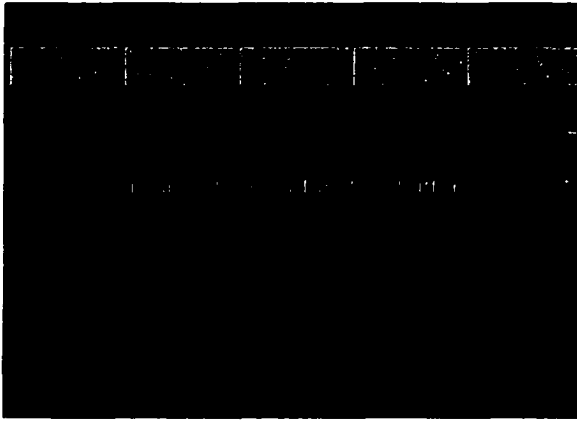
reliability of the localization result; (iii) modifying tool paths originally generated according to the determined transformation of the workpiece. Therefore, as shown in Figure 6.4, the corresponding software consists of five main modules: (i) end-user interface; (ii) measurement module; (iii) error compensation for measurement points; (iv) workpiece localization and reliability analysis; (vi) tool path modification.

Figure 6.5 displays the windows of the end-user interface showing function buttons. The functions, Homing, Probing, Localization, and Inspection are performed by pressing "H", "P", "L" and "I", respectively. After pressing any one of these function buttons, a corresponding new window appears and displays the subfunctions.

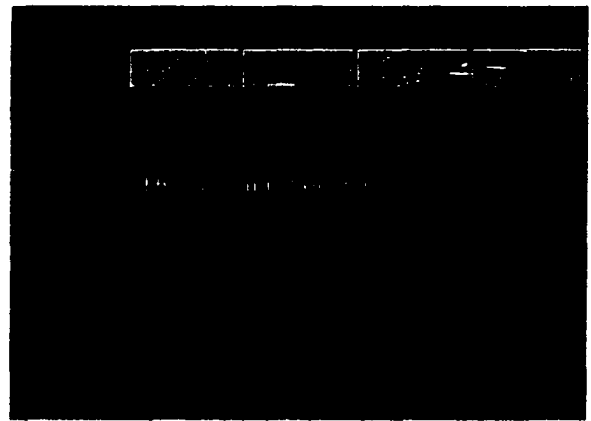
## 6.4 Operational Principle of the CAS System

The operational principle of the CAS system is as follows: First, arbitrarily fixture a workpiece on the worktable of the milling machine tool. Next install the probe tip to the machine spindle. After turning on the machine tool and entering the main end-user interface window, choose the button "Home" to find the original point of the machine tool. Then choose the button "Probing" to start the probing program. There are two choices, manual probing and auto-probing. If need to finish probing, choose the button "Finish" to save the set of measurement points in a data file. Then with these points and the CAD model of the workpiece, pressing "Localization" will automatically compensate for the measurement errors due to stylus radius and compute out the translation and orientation of the workpiece's CAD frame relative to the machine frame. Then change the probe tip into a tool

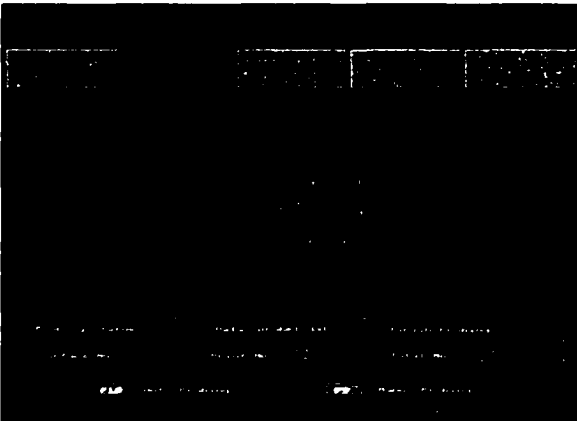




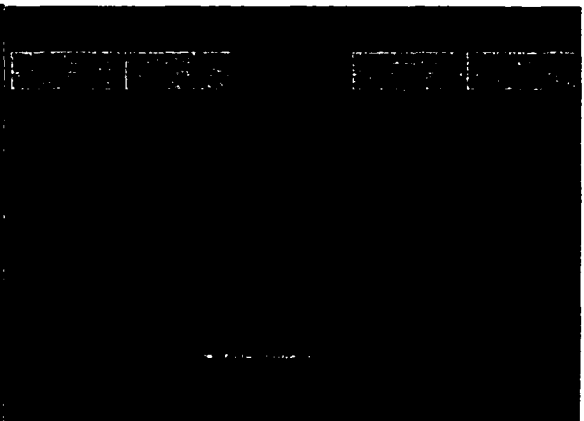
(a) After starting localization system



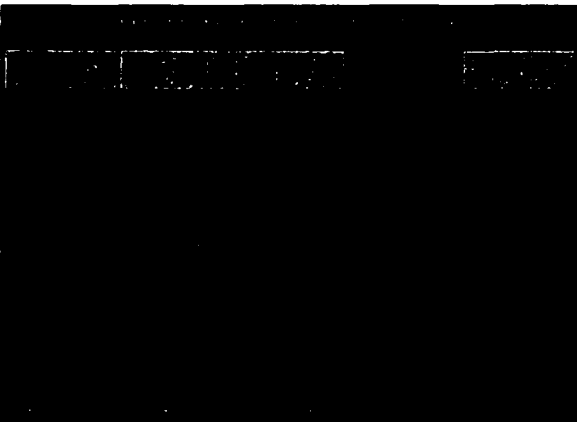
(b) Homing



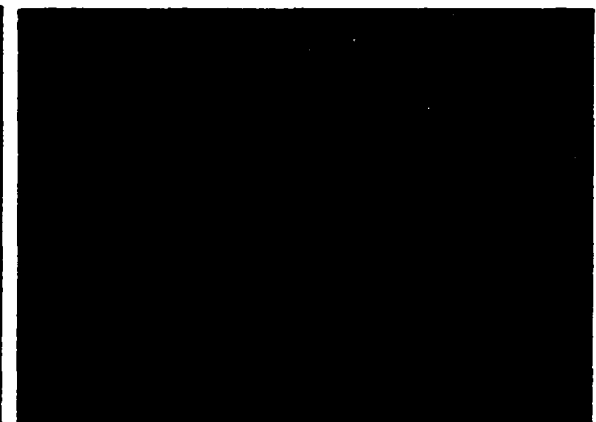
(c) Probing



(d) Localization



(e) Inspection



(f) Machining

Figure 6.5 The user-machine interface of the CAS system (Dos version)

- Input: (1) CAD model of a workpiece  
(2) Toolpath of a workpiece relative to the CAD frame
- Output: (1) Transformation of the workpiece's CAD frame relative to the machine frame  
(2) Modified tool path of the workpiece in the machine frame

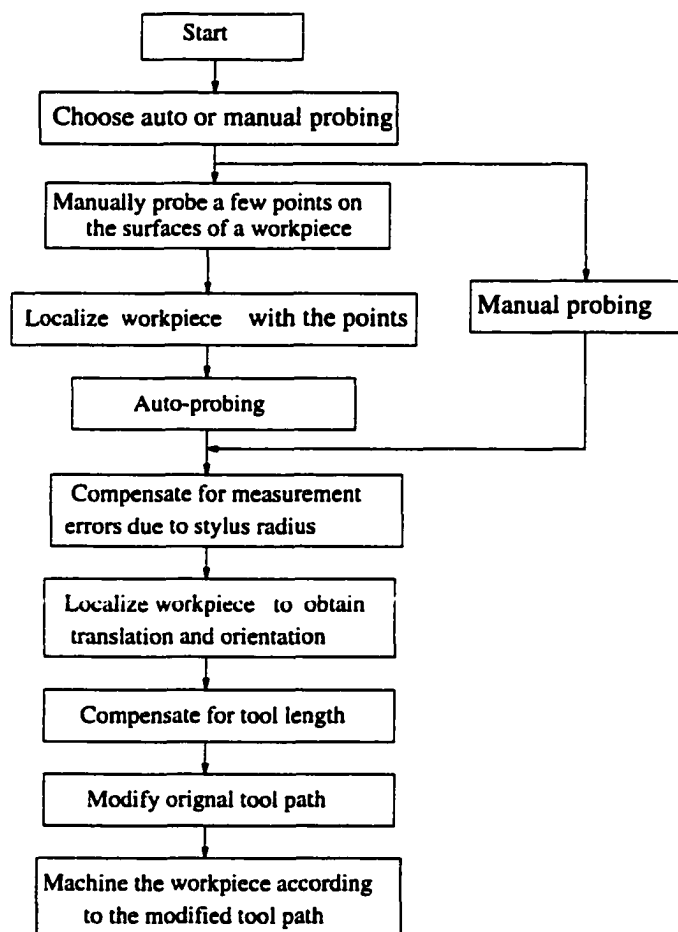


Figure 6.6: Procedure of workpiece localization

cutter and compensate for the tool length( in a machine center with tools library, it can be automatically performed). After that, modify the originally generated toolpath using the obtained transformation. The modified toolpath can then act on the workpiece as if the workpiece were accurately fixtured. Figure 6.6 summarizes the procedure of performing workpiece localization. In later sections, the functions described above will be discussed in detail.

### 6.4.1 Probing Strategy

We developed both manual probing and auto-probing methods in our CAS system as described in Figure 6.7. In the manual probing mode, we move the workpiece surface to approach the probe tip by operating the handle. The three buttons of the control handle are corresponding to the motion in  $x$ -,  $y$ - and  $z$ -axis directions, respectively. For example, the handle and top buttons control the motion of the worktable up and down in the  $z$ -axis direction, respectively. Operating the handle forward, backward, leftward and rightward, controls the motion of the worktable in the  $x$ -axis and the  $y$ -axis directions, respectively. Since the deformation of the tip's mechanism triggers the touching signal, the approaching speed of the tip to a surface affects the measurement accuracy. Therefore, we developed two touching modes so as to speed up probing and improve the accuracy of measurement. First moving the surface towards the probe tip with a high speed, when touching the surface, the worktable stops immediately and moves away from the tip in a small distance, then it moves towards the tip with lower speed until it touches the tip again. At this moment, the host computer of the machine tool records the coordinates of the touch point and the index of the surface to which the point belongs in a data file. Here, the slow approaching process is performed automatically according to the opposite motion direction away from the tip, the handle is not enabled during the process.

Usually, manual probing takes relatively longer time for measuring points than auto-probing. In addition, manual operation may cause operation errors. Therefore, we need to speed up the probing process and reduce the operation error by auto-probing. In the auto-probing process, we use two steps. Firstly, we probe a few points, usually six points on one complicated surface or three non-parallel planar

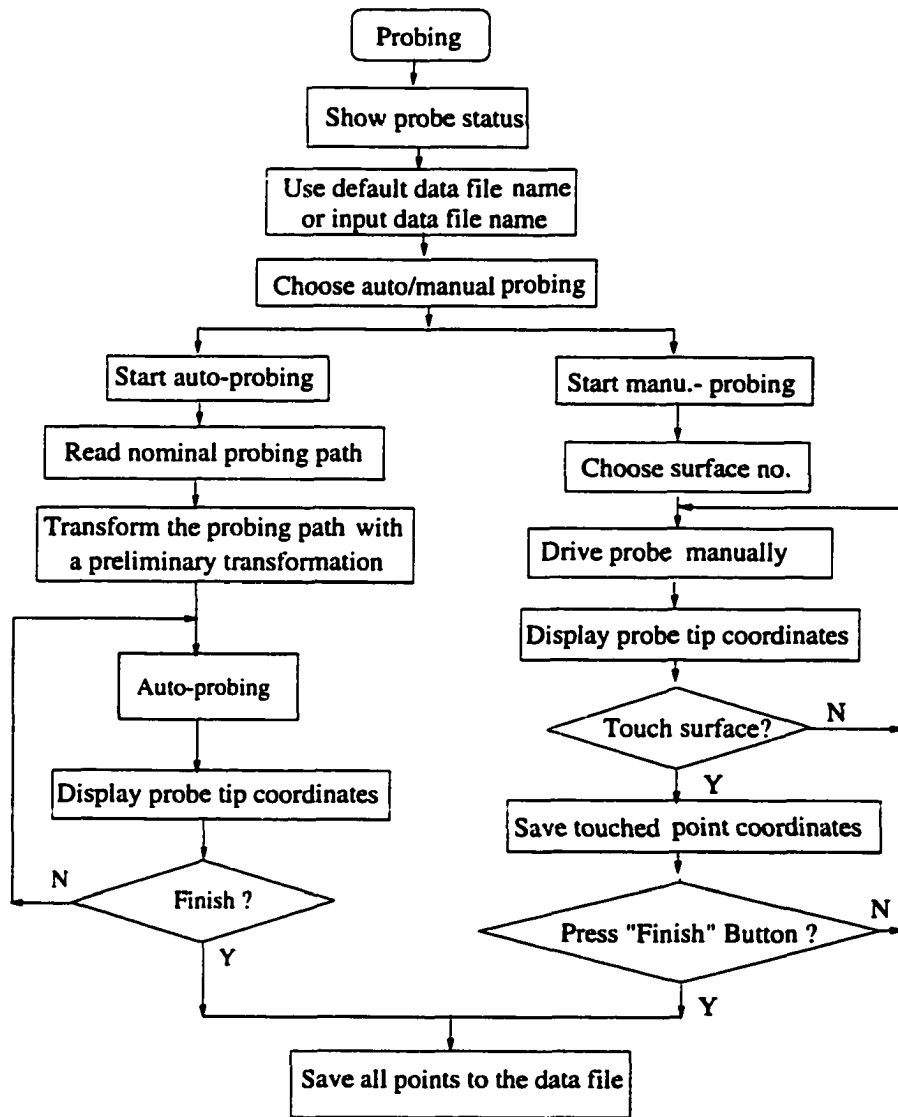


Figure 6.7: The probing process

surfaces by operating the handle manually. With these points and the CAD model of the workpiece, we can compute a preliminary transformation  $g_1$ (translation and orientation) of the workpiece's CAD frame with respect to the machine frame using the localization algorithms. In auto-probing, the key point is how to plan the probing path. Actually, with the CAD model of a workpiece we can generate in advance a probing path and points to be measured which are relative to the CAD-model frame. Then, with this preliminary transformation, we obtain the transformed probing path which is relative to the machine frame.

In our CAS system, the nominal probing points are generated in advance by the data generation module. The details are as follows: Let  $\psi_i(u, v)$ , ( $u \in [a, b]$ ,  $v \in [c, d]$ ) be the parametric representation of surface  $S_i$ , where  $(u, v)$  are surface coordinates. On the  $(u, v)$  space, values of  $(u, v)$  are selected for points to spread uniformly over the space. Assume that  $N$  points in  $u$  direction and  $M$  points in  $v$  direction are chosen, then the parameters  $(u_j, v_k)$  of  $(j \times k)^{th}$  point are computed by

$$\begin{cases} u_j = a + (b - a) * j/N, & j = 1, \dots, N \\ v_k = c + (d - c) * k/M, & k = 1, \dots, M \end{cases}$$

Correspondingly, the nominal probing points expressed in the CAD model frame are given by

$$x_i(u_j, v_k) = \psi_i(u_j, v_k)$$

where  $j = 1, \dots, N$ ,  $k = 1, \dots, M$ , and  $i = 1, \dots, M \times N$  and the normal of each point is given by

$$n_i = \frac{\psi_{u_i} \times \psi_{v_i}}{|\psi_{u_i} \times \psi_{v_i}|}$$

where  $\psi_{u_i}$  and  $\psi_{v_i}$  are partial derivative of  $\psi_i$  relative to  $u_i$  and  $v_i$ , respectively. Then, using the preliminary transformation  $g^*$  transforms these nominal points to the machine frame, i.e.  $g^*x_i, i = 1, \dots, N \times M$ . Let  $d \in \mathbb{R}$  be a given distance, we compute point  $g^*(x_i - dn_i)$  along the normal direction of each point  $g^*x_i$ . Then two sets of points  $g^*(x_i - dn_i)$  and  $g^*x_i, i = 1, \dots, N \times M$  can be obtained. With the two sets of points, the motion path of the worktable is planned as follows: starting from  $g^*x_1 - dn_1$ , the worktable moves towards the tip along the normal direction of the point  $g^*x_1$ . After touching the surface, the host computer records the coordinates of the point, and the worktable moves backward to the point  $g^*(x_1 - dn_1)$ . Then from

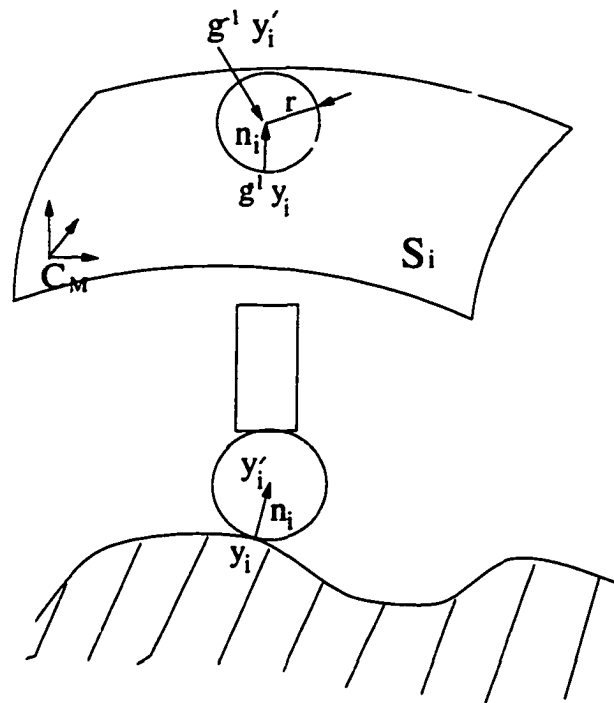


Figure 6.8: The touch location and its coordinates of a probing point

this point, it moves to the next point  $g^*(x_2 - dn_2)$ , repeating the above process until all planned points are measured automatically. In practical operation, the auto-probing is performed by pressing the auto-probing button according to the path of the generated points. After auto-probing, a new set of measured points are obtained and the new optimal transformation of the workpiece is computed with them.

We only consider the path planing of some special cases in our experiments. In the auto-probing, another important problem needs to be considered is collision avoidance when performing measurement. We hope that a general case of this problem will be studied in our future research.

#### 6.4.2 Error Compensation for Measurement Points

In the probing system, the coordinates recorded by the computer are the coordinates of the center point  $y'_i$  of the probe tip instead of the exact touch point  $y_i$ , as shown in Figure 6.8. Therefore, it is needed to compensate the bias due to the radius of the stylus. We propose an iterative process to solve this problem. First, we use the un-

compensated data set  $\{y'_i\}_{i=1}^n$  to compute out an optimal Euclidean transformation  $g_1$ . Then, we transform the point  $y'_i$  into  $x'_i = (g_1)^{-1}y'_i$ ,  $i = 1, \dots, n$  which are relative to the CAD model frame  $C_M$ . Let  $r$  be the radius of the stylus and  $n'_i$  the normal of the surface  $S_i$  at  $x'_i$ , then the points can be compensated by

$$y_i = y'_i - (g_1)^{-1}n'_i r, \quad i = 1, \dots, n.$$

Then we localize the workpiece again with the compensated data  $\{y_i\}_{i=1}^n$  to obtain a new optimal transformation  $g_2$ . Assume that  $g_k = (R_k, p_k)$  is the  $k^{th}$  transformation obtained, and define the orientational and translational errors to be

$$\mathcal{E}_R = |\theta|, \quad \text{where } e^{\hat{\omega}\theta} = R_{k-1}^T R_k, \quad \|\omega\| = 1$$

and

$$\mathcal{E}_p = \|p_{k-1} - p_k\|.$$

When  $\mathcal{E}_R \leq \epsilon_1$  and  $\mathcal{E}_p \leq \epsilon_2$ , where  $\epsilon_1 > 0$  and  $\epsilon_2 > 0$ , we obtain the compensated optimal Euclidean transformation  $g_k^*$ . Otherwise, the procedure is repeated to update the Euclidean transformation  $g_k$  until the above criteria are satisfied. The compensation process is summarized in Figure 6.9.

### 6.4.3 Reliability analysis and toolpath modification

After compensating for the measurement error due to the radius of the stylus, we have obtained the optimal transformation  $g^*$ . Next, we perform the reliability analysis to the localization result. If the result does not satisfy the specified requirements, we have to go back to measure more points or choose more proper locations of points and repeat the above procedure until the specified requirements are satisfied. If with enough points and  $m$  ( $m$  is an upper bound allowed to repeat) times repeated procedures, a satisfactory transformation still can not be obtained, then exit and report this result.

With a satisfactory transformation, we perform a toolpath modification program to transform the originally generated toolpath into a new toolpath which is relative to the machine frame. The new toolpath can act on the workpiece as if it were accurately fixtured to the machine table. Then, we have completed the whole computer-aided setup procedure till now.

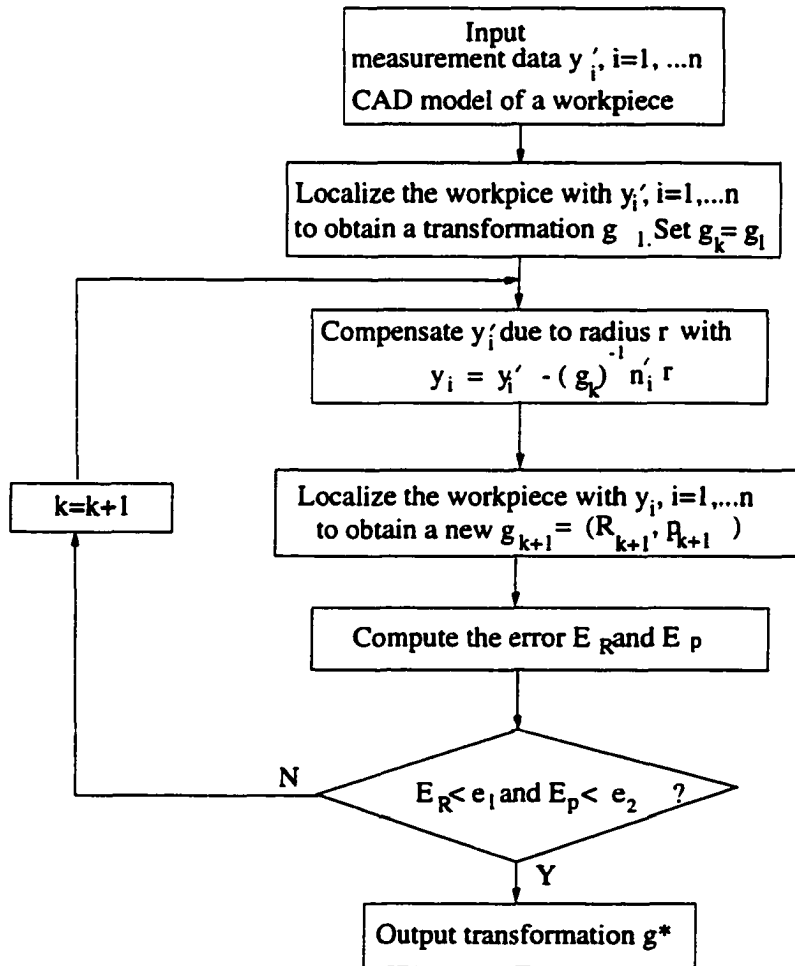


Figure 6.9: Error compensation for measurement points



## 6.5 Experimental Verification of the CAS System

We verified the CAS system through localizing and machining several workpieces. The experimental processes are as follows. First, we arbitrarily placed and fixed the workpiece on the machine table. Then, we driven the touch probe to measure 40 points on the three finished surfaces of the workpiece. The host computer automatically recorded the coordinates of the measurement points and their surface indices in a data file. Then, by pressing the button "Localization", the algorithms accomplished the probe radius compensation and computed out the position and orientation of the workpiece. At the same time, they did the reliability analysis for the localization results. In the experiments, we placed the workpiece at different positions and orientations and repeated the operation procedure, we obtained the localization results of three sets of experiments shown in Table 6.1, where  $\mathcal{E}_*$  is the minimal value of the objective function,  $\theta_*$  is the upper bound of the total orientation error,  $d_*$  is the upper bound of the displacement error. From the experimental results, we know that with the second set of measurement points, the localization results computed have the largest error upper bounds. Therefore, this set of localization results is not reliable. The other two sets of localization results have higher accuracy and reliability. Since we used in the experiments the measurement points from planar and cylinder surfaces to localize the workpiece, the three algorithms have almost the same accuracy. This is consistent with the previous simulation results.

The workpiece in Figure 6.10 is a bracket that we machined using the above localization method. Starting from the raw stock, a cube, we arbitrarily fixtured it on the machine table, then performed probing and localization processes to obtain the transformation of the workpiece between the CAD frame of the workpiece and the machine table frame. With the obtained transformation, we modified the toolpath originally generated by a CAM software and performed machining with the new modified toolpath. Figure 6.11 shows the other two finished workpieces by means of the CAS system.

Experi.	Algorithms	Transformation	$\epsilon_0$	Error bounds	
				$\theta_0$	$d_0$
1	Hong-Tan	$R = \begin{bmatrix} 0.866164 & 0.499758 & -0.001448 \\ -0.49976 & 0.866161 & -0.002313 \\ 0.000098 & 0.002727 & 0.999996 \end{bmatrix}$ $p = [ 161.4941 \quad -165.5649 \quad 44.2332 ]$	0.0205	0.0944	0.0544
	Variational	$R = \begin{bmatrix} 0.866163 & 0.499759 & -0.001448 \\ -0.499761 & 0.866160 & -0.002314 \\ 0.000098 & 0.002728 & 0.999996 \end{bmatrix}$ $p = [ 161.4936 \quad -165.5649 \quad 44.2332 ]$	0.0206	0.0945	0.0544
	Tangent	$R = \begin{bmatrix} 0.866145 & 0.499790 & -0.001447 \\ -0.499792 & 0.866142 & -0.002328 \\ 0.000090 & 0.002739 & 0.999996 \end{bmatrix}$ $p = [ 161.4870 \quad -165.5711 \quad 44.2304 ]$	0.0207	0.0945	0.0544
2	Hong-Tan	$R = \begin{bmatrix} 0.863240 & 0.437634 & -0.251581 \\ -0.504791 & 0.750090 & -0.427261 \\ 0.001725 & -0.495824 & 0.868421 \end{bmatrix}$ $p = [ 207.5641 \quad -86.744 \quad 76.977 ]$	11.904	1.035	0.6404
	Variational	$R = \begin{bmatrix} 0.862558 & 0.438645 & 0.252158 \\ -0.505956 & 0.749263 & 0.427334 \\ -0.001485 & -0.496181 & 0.868218 \end{bmatrix}$ $p = [ 207.4005 \quad -86.8942 \quad 77.0319 ]$	11.9086	1.035	0.6404
	Tangent	$R = \begin{bmatrix} 0.862520 & 0.438702 & 0.252189 \\ -0.506020 & 0.749235 & 0.427306 \\ -0.001489 & -0.496172 & 0.868223 \end{bmatrix}$ $p = [ 207.3921 \quad -86.9096 \quad 77.0310 ]$	11.9087	1.035	0.6404
3	Hong-Tan	$R = \begin{bmatrix} -0.582133 & 0.572018 & -0.577854 \\ -0.813093 & -0.409417 & 0.413832 \\ 0.000136 & 0.710755 & 0.703440 \end{bmatrix}$ $p = [ 182.0162 \quad -119.9881 \quad 84.9639 ]$	0.0855	0.2482	0.0912
	Variational	$R = \begin{bmatrix} -0.582133 & 0.572021 & -0.577852 \\ -0.813093 & -0.409419 & 0.413830 \\ 0.000136 & 0.710755 & 0.703440 \end{bmatrix}$ $p = [ 182.0166 \quad -119.9883 \quad 84.9629 ]$	0.0855	0.2482	0.0912
	Tangent	$R = \begin{bmatrix} -0.582136 & 0.57196 & -0.577905 \\ -0.813091 & -0.409381 & 0.413871 \\ 0.000136 & 0.710819 & 0.703374 \end{bmatrix}$ $p = [ 182.0081 \quad -119.9832 \quad 84.9836 ]$	0.0856	0.2482	0.0912

Table 6.1: Transformations of the workpiece computed by experimental measurement points

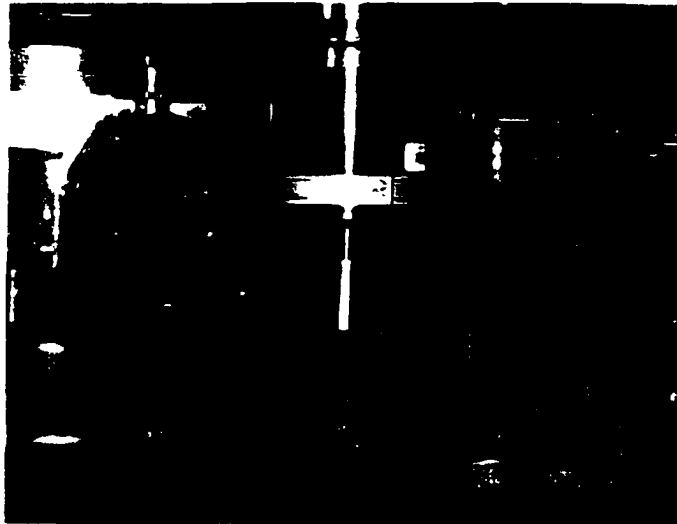


**Figure 6.10** The CAS system is measuring the workpiece bracket



**Figure 6.11** The three workpieces machined by means of the CAS system

## **6.6 Conclusion**

We developed the prototype of the CAS system and verified the localization algorithms on it. In the CAS system, two new techniques were used. The auto-probing sped up the probing process and reduced the operation error. The iterative compensation for the measurement error efficiently improved the localization accuracy. The experimental results showed that the system can localize various workpieces with simple or complicated surfaces efficiently by means of general purpose fixtures. The system can eliminate the need of having an operator fixture workpiece accurately, thus simplifying and accelerating greatly the machining cycle.



## Chapter 7

# Conclusion and Future Work

### 7.1 Conclusions

In this dissertation, we developed systematically the theory, algorithms, and implementation methods of workpiece localization. We classified the localization problem associated with each of the three types of workpieces as: (a) the general 3-dimensional localization problem; (b) the symmetric localization problem; and (c) the hybrid localization/envelopment problem. Then, we formulated these problems and focused on solving problems (a) and (c). The details can be summarized as follows:

First, we provided a geometric theory for a unified treatment to the localization algorithms of general 3-dimensional workpieces. we formulated the general 3-dimensional localization problem as a least squares problem (LSP) on the Euclidean group,  $SE(3)$ . The mathematics of LSP was analyzed in detail where necessary conditions were derived for the optimal Euclidean transformation and the optimal home surface points. We described in detail an iterative method for solving LSP and showed how different considerations in updating the Euclidean transformations lead to different algorithms. We showed the local convergence of three localization algorithms and presented a method to improve the performance of these algorithms. We gave simulation results showing convergence, accuracy and computational efficiency of the various geometric algorithms.

Next, we discussed the factors affecting the accuracy and reliability of localization results. Using the F-test method in statistics, we developed effective methods to

analyze the reliability of workpiece localization. This work allows the localization method to be applied effectively into real manufacturing tasks.

Then, with the geometric properties of the homogeneous space  $SE(3)/G_0$ , where  $G_0 \subset SE(3)$  is the symmetry subgroup defined by the set of finished surfaces, we proposed the hybrid localization/envelopment problem. We formulated the hybrid problem as a symmetric localization problem on the homogeneous space  $SE(3)/G_0$  of the Euclidean group and a minimization problem on  $G_0$  subject to inequality constraints. We solved the envelopment problem by solving a sequence of linear programming problems where the solution from the symmetric localization problem is used as an initial condition. We also addressed the issue of hybrid localization/inspection/machinability. We developed a methodology for treating localization, on-line inspection and machinability of workpieces simultaneously using the geometric properties of the homogeneous space. Simulation results showed the effectiveness of the hybrid algorithms. This method provides the transformation of a workpiece, the tolerance values of finished surfaces, and maximum machinable volumes existing on unfinished surfaces. Thus one can decide if further machining is necessary according to the results obtained. It is also possible to adaptively adjust the machining so as to improve the product quality using this method. We also defined a localization problem for workpieces with special geometry shapes and analyzed their configuration space. We showed that this localization problem can be transformed into a two-dimension problem. Thus, a set of simpler algorithms solving them can be given.

Finally, we proposed a computer-aided setup (CAS) system and implemented the system on an open architecture machining tool environment. The experimental results showed the validation of the developed localization algorithms and the CAS system. Availability of the CAS system eliminates the need of having an operator fixture workpiece accurately, thus simplifying and accelerating greatly the machining cycle.

## 7.2 Future Research

As described in Chapter 6, automating workpiece setup involves two key parts: acquisition of coordinate points and localization algorithms. This dissertation has made extensively study on the workpiece localization algorithms. And these algorithms are robust, reliable and efficient enough to apply to practice setup systems. Using a high precision touch trigger probe as the 3D coordinate measurement system, we implemented a prototype of the computer-aided setup system on a HKUST(Hong Kong University of Science and Technology) open architecture CNC milling machine tool and have demonstrated the effectiveness of these algorithms.

However, in the process of automatic workpiece setup, probing points on surfaces of a workpiece manually using a touch trigger probe takes much longer time than the computational time of the localization algorithms. Therefore, although the automatic workpiece setup is flexible for the setup of various workpieces, a conflict between taking long time to measure points on site and efficient use of machining ability of a CNC machine tool will occur. With the fast, robust and reliable algorithms, the remaining problem of affecting effective applications of the setup system will be the acquisition of high precision coordinate points.

There are many sensor technologies available for 3D coordinate acquisition. Among these sensors, three distinct technologies namely, mechanical touch trigger probes, laser scanners, and vision systems, are widely adopted. Touch trigger probes are slow, however they can have resolutions on the order of  $0.005mm$  and are very robust. Laser scanners have very high data rate, up to 2500 data points per second, and good resolutions on the order of 0.01 mm. Vision systems have resolutions on the order of 0.1 mm, however they can simultaneously acquire thousands of data points over a large spatial range.

The three measurement technologies described above have their own advantages and shortcomings, a cooperative way of them to achieve a higher performance will be possible. Based on this idea, further work can focus on studying the following three problems: (1) How to take the advantages of each measurement technology and incorporate the efficient localization algorithms to develop a rapid coordinate acquisition system? (2) How many points are needed to guarantee the localization



accuracy and how to relate the measurement accuracy to the accuracy of localization? (3) What should be taken into account when performing on-line inspection directly on a machine tool using workpiece localization methods?

#### • **Rapid acquisition of coordinate points**

A rapid coordinate acquisition system will consist of a high precision touch trigger probe, a high speed laser scanner system or a 3D vision system. With the CAD model of a workpiece and the efficient localization algorithms, the procedure of rapid coordinate acquisition is proposed as follows:

- (1) With the CAD model of a workpiece, we make a measurement plan, i.e., generate target points, normal vectors of the points on the surfaces and optimal probe angles as well as collision-free path, all of which are with respect to the CAD model's frame. This measurement plan is made off line.
- (2) With a high-speed laser scanner system or a 3D vision system, we acquire points rapidly and compute the transformation( translation and orientation) of the workpiece relative to the machine reference frame by the efficient localization algorithms we developed. This preliminary transformation is not accurate enough to localize the workpiece for machining.
- (3) With the preliminary transformation, we modify the initially generated measurement points and the path in step (1), so that the path and the measured points are with respect to the machine reference frame.
- (4) Once a surface is chosen to be measured, the high precision touch trigger probe will automatically measure points on the surface of the workpiece according to the modified measurement path, the points and the optimal measurement angles.

Since no time needs to spend on measurement planning on site, the off-line generation of the measurement path can save valuable process time. Furthermore using the above acquisition method, the measurement process will be carried out automatically in a situation where there is less pressure, thus the chances of human error will be reduced to a minimum.

**• Adaptive probing**

This problem relates closely to the first step of the procedure of the rapid coordinate acquisition. Current methods usually determine the total number of points to be measured on a feature of a workpiece by experience.

The idea here is to expand the efficient reliability analysis method to the auto-probing algorithm, so that it can diagnose whether the measurement points are enough to guarantee the localization accuracy or not. The following procedure is proposed to solve this problem:

- (1) Measure at least 6 points on three finished non-parallel planes of a workpiece;
- (2) Compute the translation and orientation of the workpiece with respect to the machine frame;
- (3) Estimate the upper bounds of the translational error and the orientational error;
- (4) Verify whether the upper bounds are less than the specified accuracy or not. If not, continue the probing process to obtain more points, together with the original points and repeat steps (2) and (3) until the accuracy requirement is satisfied.

In the probing process, since the localization and reliability analysis algorithms take the time under the order of 1 second, the reliability analysis does not affect probing speed. When the probing task is finished, the whole localization process is completed, and a satisfactory and reliable localization result is achieved, with least number of measurement points, i.e., least localization time.

The above proposed coordinate acquisition technology and algorithms will be transferable to other applications, such as automatic calibration in inspection and agile machining, coordinate metrology in dimensional control, reverse engineering in rapid product design and realization, and robotic assembly.

**• On-machine inspection**

Today, for a high precision inspection, one employs mainly CMMs to determine

if a part was made correctly or to create a set of dimensions from an existing part. This process is performed off-line and is often away from factory floors. Industry is exploring the increased use of CMMs for process control. This is creating the need to combine the measurement with the machining process. With increasing frequency, CNC machine tools are capable of exchanging the cutting tool for a measuring probe which transforms them into CMMs. This makes it possible to perform the on-machine measurement and adjustment in machining process. In this case, the function of measuring is not only to determine if the part was manufactured correctly but also to provide data to make the process adjustments necessary to keep the results within the control limits.

As described in Chapter 6, a computer-aided localization system based on open architecture CNC machine tools is possible to accomplish the function, i.e. combine the measurement and machine process, and adaptively adjust the machining. The process of inspection is similar to the one of workpiece localization. Thus the procedure of on-machine inspection just after machining can be as follows: First use the workpiece localization method to determine the position and orientation of an arbitrarily fixtured workpiece; Then modify the original generated toolpath so that the toolpath is with respect to the machine frame, and perform machining; After machining, automatically change the tool into an on-machine probe, then use it to measure points according to a measurement plan or a path which are created when doing the CAD design of the workpiece and are relative to the CAD frame. With the measurement points, inspection algorithms are chosen to perform the inspection. The dimension, form or surface finish tolerance value are obtained. If the results indicate an out-of-tolerance condition, the probe might automatically take more measurement points, which is exactly what a human operator would do in a normal course of action. By repeating the number of measurement points, the uncertainty of the data is reduced and a better decision can be made regarding the acceptability of the surface. It may be possible to repeat or adjust machining to make the surface satisfy quality requirements. If satisfied, the next machining process can proceed. Otherwise, it is not necessary to start next step machining. This process can not only save time significantly, but also improve product quality by

controlling the quality of the whole workpiece in each step.

The inspection of workpieces in situ has the significant advantage of possibly being able to immediately rework the workpiece based upon the inspection results. However, the use of machine tool as a CMM has some significant liabilities which need to be carefully considered when employing this measurement technology because of the difference between workpiece setup and inspection. In particular, the inspection is sensitive only to errors which are not common to both the production and measurement processes. Hence major sources of error such as the machine tool's geometry are not detected by the inspection. For example, if the machine tool's axes are out-of-square, the cutting process will produce an out-of-square workpiece. The inspection process, using the same out-of-square axes, will consequently measure the workpiece to be perfect. Hence the on-machine inspection process is oblivious of all error sources common to both the production and the inspection processes. These include machine geometry, thermal distortions, and errors in the thermal corrections. Sources of error which are not common to the two systems maybe detected by the inspection process. They include tool and workpiece deflection under cutting forces, tool offset errors, tool wear, and errors introduced by the probing system, e.g. by a miscalibrated probe.

Therefore, particular attention should be paid to machine tools which both produce and inspect the workpiece. If some form of an interim testing program is taken to ensure the accuracy of the system, the above problems may be overcome. This involves periodically comparing the results from the machine tool's inspection and from an independent CMM, or the inspection of calibrated artifacts directly on the machine tool.



# Bibliography

- [1] K.S. Arun, T.S. Huang, and S.D. Blostein. Least-squares fitting of two 3-d point sets. *IEEE Trans. on Pattern Analysis and Machine Intelligence*, 9(5):698–700, 1987.
- [2] P. Besl and N. McKay. A method for registration of 3-d shapes. *IEEE Trans. on Pattern Analysis and Machine Intelligence*, 14(2):239–256, 1992.
- [3] R. Booles, P. Horaud, and M. Hannah. 3DPO: Three dimensional part orientation system. In *Robotics Research: The First Symposium*, Cambridge, Mass: MIT Press, 1984.
- [4] W. Boothby. *An Introduction to Differentiable Manifolds and Riemannian Geometry*. Academic Press, 1975.
- [5] R.W. Brockett. Least square matching problems. *Linear Algebra and Its Applications*, 1222/123/124:761–777, 1989.
- [6] Z.X. Li, J.B. Gou and Y.X. Chu. Geometric Algorithms for Workpiece Localization *IEEE Transaction on Robotics and Automation*, ( to appear), 1998.
- [7] Y.X. Chu, J.B. Gou, H. Wu, and Z.X. Li. Localization algorithms: Performance evaluation and reliability analysis. In *IEEE Intl. Conf. on Robotics and Automation*, 1998.
- [8] Y.X. Chu, J.B. Gou, and Z.X. Li. On the hybrid workpiece localization/envelopment problems. In *IEEE Intl. Conf. on Robotics and Automation*, 1998.

- [9] Y.X. Chu, J.B. Gou and Z.X. Li. Performance analysis of localization algorithms In *IEEE Intl. Conf. on Robotics and Automation*, 1247–1252, 1997.
- [10] L. Conlon. *Differentiable manifolds, A first course*. Birkhauser, 1993.
- [11] I.J. Cox, J.B. Kruskal, and D.A. Wallach. Predicting and estimating the accuracy of a subpixel registration algorithm. *IEEE Trans. on PAMI*, 12(8):721–734, 1990.
- [12] O.D. Faugeras and M. Hebert. The representation, recognition, and locating of 3-D objects. *International Journal of Robotics Reseearch*, 5(3):27–52, 1986.
- [13] R. Fletcher. *Practical methods of optimization*. John Wiley & Sons, 1987.
- [14] A. B. Forbes. Least-squares best-fit geometric elements. Technical report, National Physical Laboratory, UK, 1989.
- [15] S. Gordon and W. Seering. Real-time part position sensing. *IEEE Trans. on Pattern Analysis and Machine Intelligence*, 10(3):374–386, 1988.
- [16] J.B. Gou, Y.X. Chu, and Z.X. Li. On the symmetric localization problem. *IEEE Trans. on Robotics and Automation*, 14(4):533–540, 1998.
- [17] J.B. Gou, Y.X. Chu, and Z.X. Li. A geometric theory of form, profile and orientation tolerances (to appear). *Precision Engineering*, 1998.
- [18] W. E. Grimson and T. Lozano-Perez. Model-based recognition and localization from sparse range or tactile data. *International Journal of Robotics Reseearch*, 3(3):3–35, 1984.
- [19] K. Gunnarsson and F. Prinz. CAD model-based localization of parts in manufacturing. *Computer*, 20(8):66–74, 1987.
- [20] R.J. Hanson and M.J. Norris. Analysis of measurements based on the singular value decomposition. *SIAM J. Sci. Stat. Comput.*, 2(3):363–373, 1981.
- [21] J. Hong and X. Tan. Method and apparatus for determining position and orientation of mechanical objects. *U.S. Patent No. 5208763*, 1990.

- [22] B.K. Horn. Closed-form solution of absolute orientation using unit quaternions. *J. Opt. Soc. Amer. A*, 4(4):629–642, 1987.
- [23] X.M Li, M. Yeung, and Z.X. Li. An algebraic algorithm for workpiece localization. In *IEEE Intl. Conf. on Robotics and Automation*, pages 152–158, 1996.
- [24] J. Marsden and T. Ratiu. *Mechanics and Symmetry*. Springer-Verlag, 1994.
- [25] C.H. Menq, H. Yau, and G. Lai. Automated precision measurement of surface profile in CAD-directed inspection. *IEEE Transactions on Robotics and Automation*, 8(2):268–278, 1992.
- [26] C.W. Ziemain and D.J. Medeiros. Automated feature accessibility algorithm for inspection on a coordinate measuring machine. *Int. J. PROD. RES.*, Vol.35, No.10, 2839-2856, 1997
- [27] K.C.Sahoo, C.H. Menq. Localization of 3D Objections Having Complex Sculptured Surfaces Using Tactile Sensing and Surface Description *Journal of Engineering for Industry* Vol. 113, 85–92, Feb, 1991.
- [28] R. Murray, Z.X. Li, and S. Sastry. *A Mathematical Introduction to Robotic Manipulation*. CRC Press, 1994.
- [29] A. Nadas. Least squares and maximum likelihood estimates of rigid motion. *IBM Research Report*, RC6945, 1978.
- [30] F. Park and B. Martin. Robot sensor calibration: Solving  $AX = XB$  on the EEuclidean group. *IEEE Trans. on Robotics and Automation*, 10(5):717–721, 1994.
- [31] M.J. Powell. On search directions for minimization algorithms. *Mathematical programming*, 4:193–201, 1973.
- [32] D.A. Simon and T. Kanade. Geometric constraint analysis and synthesis: Methods for improving shape-based registration accuracy. In *Proc. of 1st Joint CVRMed/MRCAS Conf*. Springer-Verlag, 1997.



- [33] H.E. Trucks. *Designing for Economic Production*. Society of Manufacturing Engineers, 2nd edition, 1987.
- [34] A.S. Wallack and J.F. Canny. Object localization using light beam sensing. Technical report, Engineering Research Center, College of Engineering, University of California at Berkeley, 1992.
- [35] H.T. Yau, C.H. Menq. An Automated dimensional inspection environment for manufactured parts using coordinate measuring machines. *International Journal of Production research*, vol. 30, no.7:1517–1536, 1992.
- [36] H.J. Pahk and W.J. Ahn. Precision Inspection System for Aircraft Parts Having Very Thin Features Based on CAD/CAI Integration. *International Journal of Advance Manufacturing Technology*, 12:442–449, 1996.
- [37] K.T. Gunnarsson. Optimal Part Localization by Data Base Matching with Sparse and Dense Data. PhD thesis, Carnegie-Mellon University, 1986.
- [38] S. Haramaki. Development of On-machine Measurement System Using Non-contact Profile Sensor. International Conference on Recent Advances in Mechatronics, Istanbul, Turkey, pp836–839, Aug. 1995.
- [39] Young Jin Kim and Kunwoo Lee Sampling of Inspection Points for Free-form Surfaces. Proc. of the 3rd International Conference, Computer Integrated Manufacturing, World Scientific, Part vol.2, pp1307–15, Singapore, 1995.
- [40] M. Sykes. Application of Touch Trigger Probe Systems in Manufacturing. Industrial and Product Engineering, March, 1985.
- [41] In-cycle gauging as a production tool. Quality Today, July, 1986.
- [42] In-cycle probes bring big rewards. Machinery and production engineering, July 1981.
- [43] Y.J. Lin and P. Murugappan. A New Algorithm for CAD-Directed CMM Dimensional Inspection. Proc. of the 1998 IEEE International Conference on Robotics and Automation, pp893–898, May 1998.

- [44] H. ASADA and A.B. BY Kinematic Analysis of Workpiece Fixturing for Flexible Assembly with Automatically Reconfigurable Fixtures. *IEEE Journal of Robotics and Automation*, vol. RA-1, No.2 June 1985.
- [45] I.J. COX, J.B. Kruskal and D.A. Wallach. Predicting and Estimating the Accuracy of a Subpixel Registration Algorithm. *IEEE Transaction on Pattern Analysis and Machine Intelligence*, vol.12, no.8,pp.721-34, Aug.1990.
- [46] P.Bourdet and Clement. A Study of Optimal;-Criteria Identification Based on the Small-Displacement Screw Model. *Annals of the CIRP*, Vol. 37/1/1998.
- [47] D.A.Simon and T. Kanade. Geometric Constraint Analysis and Synthesis: Methods for Improving Shape-Based Registration Accuracy. *CVRMed-MRCAS*, pp181-90,1997.
- [48] X. Huang and P. Gu. Tolerance Analysis in Setup and Fixture Planning for Precision Machining. *Proc. of the Fourth International Conference on Computer-Integrated Manufacturing and Automation Technology*, pp.298-305, 1994.
- [49] P.D. Lin and T.H.Liu. Machining and Dimensional Inspection of Spatial Cams on 5-Axis Machine Tools. *International Journal of Advanced Manufacturing Technology*,12:356-365, 1996.
- [50] M. Anjanappa. J.J. Dickstein and M. Subbacharay. Computer-Aided Inspection Data Analyzer *International Journal of Advanced Manufacturing Technology*,12:93-102, 1996.
- [51] T.C. Woo and R. Liang. Dimensional Measurement of Surfaces and their Sampling. *Computer Aided Design*, vol.25, no.4, pp.233-239, 1993.
- [52] F.L.Litvin, Y. Zhang and C. Kuan Computerized Inspection of Real Surfaces and Minimization of Their Deviations. *Int. J. Man. Tools Manufact.*, Vol. 32, No.1/2, pp.141-145, 1992.
- [53] H.J.Pahk and Y.H. Kim. Development of Computer Aided Inspection System with CMM for Integrated Mold Manufacturing. *Annals of the CIRP*, Vol.42, No., pp.557-560,1993.

- [54] O. P. Bojanic, D.V. Majstorovic and R.V. Milacic CAD/CAI Integration with Special Focus on Complex Surfaces *Annals of the CIRP*, Vol.41, No.1, pp.535-538, 1992.
- [55] Y. Altintas, N.Newell and M.Ito Modular CNC Design for Intelligent Machining, Part: Design of a Hierarchical Motion Control Module for CNC Machine Tools *Transactions of the ASME*, Vol.118, Nov. 1996
- [56] E.P.Zhou, D.K. Harrison and D. Link Effecting in-cycle measurement with preteritic CNC machine tools *Computers in Industry*, 28(1996)95-102
- [57] M. Mitsushi, T. Nagao, etc. An Open Architecture CNC CAD-CAM Machining System with Data-Base Sharing and Mutual Information Feedback *Annals of the CIRP* Vol.46, Jan, 1997
- [58] Y. Rong and Y.Bai Machining Accuracy Analysis for Computer-aided Fixture Design Verification *Journal of manufacturing Science and Engineering*, Vol. 118, Aug. 1996
- [59] G. Pritschow, C. Daniel and G.Junhans Open System Controllers-A Challenge for the Future of the Machine Tool Industry *Annals of the CIRP* Vol.42, Jan, 1993
- [60] D.Dumur, P.Boucher and J. Roder Advantages of an Open Architecture Structure for the Design of Predictive Controllers for Motor Drives *Annals of the CIRP*, Vol. 47, Jan. 1998
- [61] S. Sorensen Overview of a Modular, Industry Standards Based, Open Architecture Machine Controller *Proceeding of the International Robots and Vision Automation Conference, Robotic Ind, Assoc., 1993, pp11/37-38, Ann Arbor, MI, USA*
- [62] John A. Bosch *Coordinate Measuring Machines and Systems* Marcel Dekker, Inc., New York, 1995.
- [63] Paul G. Hoel. *Introduction to Mathematical Statistics*. John Wiley & Sons, Inc., 1984.

# Biography

Yunxian Chu was born in Jiansu, China. She received her BS degree and MPh degree in the Department of Automatic Control Engineering from Southeast University in Nanjing, China in 1984 and 1987, respectively. She was a lecturer in the Department of Instrumentation Science and Engineering of Southeast University from 1987 to 1995. Since Oct. 1995, she has been working toward Ph.D. degree at the Department of Electrical and Electronic Engineering, Hong Kong University of Science and Technology, Hong Kong. She has authored and coauthored more than 10 papers during her PhD study at Hong Kong University of Science and Technology. Her research interests include automated workpiece localization, dimensional inspection, manufacturing automation, intelligent measurement and control.



# Publications

- Journal Papers:

1. Y.X. Chu, J.B. Gou and Z.X. Li. On the Hybrid Localization/Envelopment Problem. *(to appear) International Journal of Robotics Research*, 1998.
2. J.B. Gou, Y.X. Chu, and Z.X. Li. On the symmetric localization problem. *IEEE Trans. on Robotics and Automation*, 14(4):533–540, 1998.
3. Y.X. Chu, J.B. Gou and Z.X. Li. Localization algorithms: Performance evaluation and reliability analysis. *(to appear) Journal of Manufacturing Systems*, 1998.
4. Z.X. Li, J.B. Gou, and Y.X. Chu. Geometric algorithms for workpiece localization. *IEEE Trans. on Robotics and Automation*, 14(6):864–878, 1998.
5. Y.X. Chu, J.B. Gou, Z.X. Li. Performance analysis of localization algorithms. *Int. J. of Intelligent Control and Systems*, 2(1):73–92, 1998.
6. J.B. Gou, Y.X. Chu, and Z.X. Li. A Geometric Theory of Form, Profile and Orientation Tolerances. *(to appear) Precision Engineering*, 1998.

- Conference Papers:

1. Y.X. Chu, J.B. Gou, and Z.X. Li. A Geometric Algorithm for Hybrid Localization/Inspection/Machinability Problem. (Accepted) in *Proc. IEEE Int. Conf. on Robotics and Automation*, 1999.
2. Y.X. Chu, J.B. Gou, and Z.X. Li. A Geometric Algorithm for the Hybrid Workpiece Localization/Envelopment Problems. In *Proc. of ASME Design*

- Engineering Technical Conferences*, Atlanta, 1998, DETC/DFM-5745, ( on the finalist for best paper award).
3. Y.X. Chu, J.B. Gou, H. Wu, and Z.X. Li. Localization Algorithms: Performance Evaluation and Reliability Analysis. In *Proc. of IEEE Int. Conf. on Robotics and Automation*, 1998, pages:3652-3657.
  4. Y.X. Chu, J.B. Gou, and Z.X. Li. On the Hybrid Workpiece Localization/Envelopment Problems. In *Proc. of IEEE Int. Conf. on Robotics and Automation*, 1998, pages:3665-3670.
  5. Y.X. Chu, J.B. Gou, B. Kang, K.T. Woo, and Z.X. Li. Performance Analysis of Localization Algorithms. In *Proc. IEEE Int. Conf. on Robotics and Automation*, 1997, pages:1247-52.
  6. J.B. Gou, Y.X. Chu, H. Wu, and Z.X. Li. A Geometric Theory for Formulation of Form, Profile and Orientation Tolerances: Problem Formulation. In *Proc. of ASME Design Engineering Technical Conferences*, Atlanta, 1998, DETC/DFM-5743.
  7. J.B. Gou, Y.X. Chu, H. Wu, and Z.X. Li. A Geometric Theory for form, profile and orientation tolerances: Evaluation Algorithms and Simulation Results. In *Proc. of ASME Design Engineering Technical Conferences*, Atlanta, 1998, DETC/DFM-5744.
  8. J.B. Gou, Y. X. Chu, H. Wu and Z.X. Li. Geometric Formulation of Orientation Tolerance and Evaluation. In *Proc. of IEEE Int. Conf. on Robotics and Automation*, 1998, pages:2728-2733.
  9. J.B. Gou, Y.X. Chu, and Z.X. Li. A Geometric Approach to Form Tolerance and Evaluation. In *Proc. of IEEE Int. Conf. on Robotics and Automation*, 1998, pages:3646-3651.
  10. Z.X. Li, J.B. Gou, and Y.X. Chu. Fundamentals of Workpiece Localization: Theory and Algorithm. In *Proc. of 2nd Asian Control Conference*, Seoul, 1997.

11. B. Kang, J.B Gou, Y.X Chu, and Z.X. Li. A CAD-based probing and localisation method for arbitrarily fixed workpiece. In *Proc. of IEEE Int. Conf. on Robotics and Automation*, 1997, pages:1247-52.